UNIVERSIDADE FEDERAL DE SANTA MARIA
CENTRO DE CIÊNCIAS RURAIS
PROGRAMA DE PÓS-GRADUAÇÃO EM CIÊNCIA DO SOLO

Alan Carlos Batistão

PROPRIEDADES REOLÓGICAS DE SOLOS AFETADAS PELA MATÉRIA ORGÂNICA, ÁREA SUPERFICIAL ESPECÍFICA E SALINIDADE

Santa Maria, RS
2018

Alan Carlos Batistão

PROPRIEDADES REOLÓGICAS DE SOLOS AFETADAS PELA MATÉRIA ORGÂNICA, ÁREA SUPERFICIAL ESPECÍFICA E SALINIDADE

Tese apresentada ao curso de Pós-Graduação em Ciência do solo, da Universidade Federal de Santa Maria (UFSM – RS) como requisito parcial para obtenção do título de **Doutor em Ciência do Solo**

Orientador: Prof. Dr. José Miguel Reichert

Santa Maria, RS
2018

1

Batistão, Alan Carlos
Propriedades reológicas de solos afetadas pela matéria orgânica, área superficial específica e salinidade / Alan Carlos Batistão.- 2018.
195 p.; 30 cm

Orientador: José Miguel Reichert
Tese (doutorado) - Universidade Federal de Santa Maria, Centro de Ciências Rurais, Programa de Pós Graduação em Ciência do Solo, RS, 2018

1. Carbono orgânico do solo 2. Terras Pretas de Índio 3. Distribuição do tamanho de partículas 4. Salinização 5. Região Semiárida I. Reichert, José Miguel II. Título.

Sistema de geração automática de ficha catalográfica da UFSM. Dados fornecidos pelo autor(a). Sob supervisão da Direção da Divisão de Processos Técnicos da Biblioteca Central. Bibliotecária responsável Paula Schoenfeldt Patta CRB 10/1728.

Endereço: Universidade Federal de Santa Maria – Centro de Ciências Rurais – Departamento de Solos, Av.Roraima, n. 1000, Cidade Universitária, Bairro Camobi, Santa Maria, RS, 97105-900.
Fone (55) 3220 8108; E-mail: alanbatistao@gmail.com

Alan Carlos Batistão

PROPRIEDADES REOLÓGICAS DE SOLOS AFETADAS PELA MATÉRIA ORGÂNICA, ÁREA SUPERFICIAL ESPECÍFICA E SALINIDADE

Tese apresentada ao curso de Pós-Graduação em Ciência do solo, da Universidade Federal de Santa Maria (UFSM – RS) como requisito parcial para obtenção do título de **Doutor em Ciência do Solo**

Aprovado em 31 de agosto de 2018:

José Miguel Reichert, Dr. (UFSM)
(Presidente/Orientador)

Dörthe Holthusen, Dra. (UFSM)

Getulio Coutinho Figueiredo, Dr. (UFRGS)

Paulo Ivonir Gubiani, Dr. (UFSM)

Ricardo Simão Diniz Dalmolin, Dr. (UFSM)

Santa Maria, RS
2018

Dedico (*in memorian*) às minhas avós Gertha Liegel e Leonilda Troni, por todos os momentos maravilhosos que passamos juntos.

AGRADECIMENTOS

Alguém já me disse que “em um coração onde mora a gratidão, também habitará sempre a felicidade”. Hoje eu entendo o significado desta frase, pois feliz é aquele que teve a ajuda de um amigo para superar os desafios impostos pela vida. Aqui, gostaria de expressar a minha gratidão a todas as pessoas que tornaram esses quatro anos mais felizes;

A Deus, pela vida e por me dares exatamente o que preciso, pois sem Ele, não teria forças e nem persistência para continuar em frente;

Aos meus pais Luiz e Noeli, por me ensinarem a caminhar, me incentivando sempre, com muito amor, a seguir meus próprios passos, não medindo esforços para que meus sonhos se concretizassem;

Às minhas irmãs Ana Paula e Sandra, que mesmo à distância, sempre se fizeram presentes, alegrando o meu dia com uma mensagem de incentivo;

À minha namorada Isabel, pelo carinho, amor e compreensão, por transformar minha vida com o seu jeito alegre e simples de viver, me ajudando a ser uma pessoa melhor a cada dia;

À minha querida amiga Patrícia Pértile, pelas horas gastas me auxiliando a operar o reômetro, por me ensinar a me organizar no laboratório e pelos puxões de orelha quando eu merecia. Acima de tudo, agradeço pelo seu coração bondoso, me ajudando dentro e fora do mundo acadêmico sempre com um sorriso no rosto;

Ao meu orientador Prof. Dr. José Miguel Reichert, por me receber como aluno de doutorado, pela confiança no meu trabalho e pela orientação prestada durante o desenvolvimento da tese;

À Dra. Dörthe Holthusen, pela simpatia e humildade no esclarecimento das várias dúvidas sobre a reologia;

Ao técnico de laboratório Flávio Fontinelli, pelas conversas no laboratório e por me auxiliar nas técnicas metodológicas que eu não dominava;

Ao meu amigo e agora doutor Luís Antônio Coutrim dos Santos, por ter cedido as Terras Pretas Arqueológicas e por me ajudar, sempre com muita disposição, nas análises no laboratório de pedologia;

À Prof. Dra Jeane Cruz Protela e ao Prof. Dr. Milton César Costa Campos, por ter enviado amostras de solo para análise reológica;

Aos companheiros do grupo de pesquisa Miguel’s Researchers, pelas discussões científicas, pelo auxílio no laboratório e pelos churrascos na casa do professor Miguel;

As bolsistas de iniciação científica Diuli, Luiza, Karina e Rafaela, pela ajuda na execução de várias tarefas durante o desenvolvimento da tese;

A todos os professores do Programa de Pós-Graduação em Ciência do Solo, por partilhar sua sabedoria, sempre estarem disponíveis e dispostos para ajudar, me incentivando na busca pelo conhecimento;

A todos os funcionários do Programa de Pós-Graduação em Ciência do Solo, em especial ao Secretário Heverton Heinz; pela cordialidade, prestatividade e agilidade no desempenho de suas atividades;

À Coordenação de Aperfeiçoamento de Pessoal de Nível Superior (CAPES) pela bolsa de estudos de Doutorado;

A todos os integrantes do movimento de Emaús, em nome dos meus padrinhos de movimento Rodrigo Pivoto Mulazzani e Janet Arnt, por terem proporcionado meu reencontro com Deus, renovando a minha fé e minha convicção;

Aos membros do grupo de vivência Pentecostes e Kerigma (Penterígma), pelas discussões sobre a Palavra e os ensinamentos de Jesus Cristo, sempre me ajudando a enxergar o mundo por uma óptica diferente;

Aos cantores de Emaús, por todos os acordes tocados em harmonia e com alegria à serviço da Igreja;

Aos meus companheiros atuais de apartamento, Jordano e Cristiano, pelas pulseadas, pelas partidas de truco, pelas conversas filosóficas e pelas conversas irracionais, por todos os momentos de descontração ao som do bom e velho Rock and Roll;

Ao meu amigo André Lavezo, pela ajuda durante meu estabelecimento em Santa Maria e por todos os bons momentos vividos enquanto dividíamos o mesmo apartamento;

A todos os usuários da Sala 3011, pelos momentos de discussão, de descontração e pelas rodas de chimarrão, em especial ao Edberto Moura Lima, por auxiliar na confecção dos mapas;

Aos integrantes do Grupo Cevas, em especial ao Patrick, Rogério, Gilmar e Betânia, pelos momentos de lazer na universidade e fora dela, tomando uma cerveja bem gelada para relaxar;

Aos funcionários da limpeza, por sempre manterem limpo e organizado o nosso local de trabalho e de estudo;

A todos os meus amigos, que não estão citados diretamente aqui, mas que contribuíram de alguma forma para que fosse possível a conclusão desta etapa em minha vida;

Meu muitíssimo obrigado!!!

“Talvez não tenha conseguido fazer o melhor, mas lutei para que o melhor fosse feito. Não sou o que deveria ser, mas Graças a Deus, não sou o que era antes”.

(Martin Luther King)

RESUMO

PROPRIEDADES REOLÓGICAS DE SOLOS AFETADAS PELA MATÉRIA ORGÂNICA, ÁREA SUPERFICIAL ESPECÍFICA E SALINIDADE

AUTOR: Alan Carlos Batistão
ORIENTADOR**:** José Miguel Reichert

A estrutura do solo consiste na disposição geométrica das partículas em agregados. É um atributo dinâmico e juntamente com textura influencia os demais processos físicos do solo. Para o início da agregação e formação da estrutura, é necessário que as partículas do solo estejam floculadas, o que depende de alguns fatores, como o teor de carbono orgânico do solo (COS), da área superficial específica (ASE) e da concentração e do tipo de cátions. Dessa forma, o objetivo do trabalho foi verificar o efeito do teor de COS, do tipo de cátion e da ASE sobre a resistência da microestrutura do solo avaliada por reometria. Para isso, foram realizados três estudos separados. No estudo I, para verificar o efeito do COS, amostras de dez Terras Pretas Arqueológicas (TPAs) foram coletadas na região amazônica. As amostras foram submetidas a quatro níveis de oxidação do COS pela aplicação de 0 (C_0), 40 (C_1), 80 (C_2) e 120 (C_3) ml de peróxido de hidrogênio concentrado a aproximadamente 100 g de solo. No estudo II, para verificar o efeito da ASE, amostras de 13 solos com diferentes composições granulométricas e grande variação na ASE foram coletadas no Rio Grande do Sul. Para verificar o efeito do tipo de cátions no estudo III, amostras de 16 horizontes de quatro perfis de solos salinizado foram coletados no Rio Grande do Norte. Os tratamentos deste estudo foram: solo saturado por capilaridade com solução salina de KCl (+K), $CaCl_2$ (+Ca) e $MgCl_2$ (+Mg) na concentração de 0.1 mol L^{-1}, lixiviação do sais soluveis (SD) por lavagens sucessivas com álcool 60% e solo não tratado (controle). Todos os tratamentos foram submetidos ao teste de varredura de amplitude com deformação controlada em um reômetro modular equipado com dispositivo de medição de placas paralelas. Como resultado dos testes foram obtidas as seguintes variáveis reológicas: deformação (γ_{LVR}) e tensão (τ_{LVR}) no final do intervalo viscoelástico linear (LVR), deformação (γ_{YP}) e valor do módulo de armazenamento (G'_{YP}) no ponto de escamento (YP), a tensão máxima de cisalhamento (τ_{max}) e a integral Z (Iz). No estudo I, a oxidação do COS afetou todas as variáveis reológicas, diminuindo a elasticidade e resistência da microestrutura. O efeito da perda de COS foi diferente entre as TPAs, de acordo com a quantidade e tipo do COS perdido. No estudo II, o aumento da ASE aumentou a elasticidade verificada pela γ_{LVR}, γ_{YP} e Iz, entretanto a formação de microagregados muito estáveis (pseudoareias) em solos com elevada ASE proporcionou redução dessas variáveis. A resistência da microestrutura avaliada pela τ_{LVR}, G'_{YP} e τ_{max} não apresentou relação com a ASE, mas foi correlacionada com a força normal atuante sobre a amostra e pela concentração de cátions. No estudo III, a lixiviação dos sais do solo provocou aumento da elasticidade da microestrutura verificada no LVR e redução da elasticidade no YP em relação ao controle enquanto a saturação por cátions, principalmente por K^+ proporcionou efeito contrário. A lixiviação dos sais e a saturação com solução salina aumentaram a resistência do solo.

Palavras chave: Reologia. Terra Preta de Índio. Carbono do solo. Teor de argila. Salinização.

ABSTRACT

PROPRIEDADES REOLÓGICAS DE SOLOS AFETADAS PELA MATÉRIA ORGÂNICA, ÁREA SUPERFICIAL ESPECÍFICA E SALINIDADE

AUTHOR: Alan Carlos Batistão
ADVISOR**:** José Miguel Reichert

Soil structure consists of the geometric arrangement of particles in aggregates. It is a dynamic property and (especially) together with texture influences several soil physical processes. For aggregation and structure formation, soil particles must be flocculated, which depends on some factors such as soil organic carbon (SOC) content, specific surface area (SSA), and concentration and type of cations. The objective of the study was to evaluate the effect of SOC, cation type, and of SSA on the resistance of soil microstructure evaluated by rheometry. Three separate studies were carried out. In study I to verify the effect of SOC, samples from ten Archaeological Black Earths (ABE) were collected in the Amazon region. The samples were submitted to four levels of SOC oxidation by the addition of 0 (C_0), 40 (C_1), 80 (C_2) and 120 (C_3) ml of concentrated hydrogen peroxide to approximately 100 g of soil. In study II, to verify the effect of ASE, samples of 13 soils with different granulometric compositions and great variation in ASE were collected in Rio Grande do Sul. To verify the effect of cation type in study III, samples of 16 horizons of four salinized soil profiles were collected in Rio Grande do Norte. The treatments in this study were: soil saturated by capillarity with saline solution KCl (+K), $CaCl_2$ (+Ca) and $MgCl_2$ (+Mg) in the concentration of 0.1 mol L^{-1}, Leaching of soluble salts (LS) by successive leaching with alcohol 60% and untreated soil (control). All the treatments were submitted to an amplitude sweep test with controlled deformation in a modular rheometer equipped with parallel plate measuring device. As a result, the following rheological variables were obtained: strain (γ_{LVR}) and shear stress (τ_{LVR}) at the end of the linear viscoelastic range (LVR), strain (γ_{YP}) and storage modulus value (G'_{YP}) in yield point, the maximum shear stress (τ_{max}) and integral Z (Iz). In study I, the SOC oxidation affected all rheological variables, reducing the elasticity and resistance of soil microstructure. The effect of SOC loss was different among ABEs, according to the amount and quality of SOC lost. In study II, the increase in SSA increased the elasticity verified by γ_{LVR}, $\gamma_{yp\ and}$ Iz, but the formation of very stable microaggregates (pseudosands) in soils with high SSA provided reduction of these variables. The microstructural stiffness, evaluated by τ_{LVR}, G'_{YP} and τ_{max}, was not correlated with SSA, but was influenced by particle size distribution, normal force acting on the sample, and cation concentration. In study III, soil desalination caused an increase in microstructural elasticity verified in LVR and reducing elasticity in YP when compared with the control, whereas the saturation by cations, mainly by K^+, provided an opposite effect, increasing the microstructural stiffness. Salt leaching and saline saturation increased soil resistance.

Keywords: Rheology. Archaeological Black Earth. Soil Carbon. Clay content. Salinization.

LISTA DE FIGURAS

Apresentação

Estudo I - Resilience and microstructural resistance of Archaeological Dark Earths with different soil organic carbon contents in western Amazonia, Brazil

LISTA DE TABELAS

Estudo I - Resilience and microstructural resistance of Archaeological Dark Earths with different soil organic carbon contents in Western Amazonia, Brazil.

Estudo II - Specific surface area effect on soil elasticity and microstructure resistance evaluated by rheometry

Estudo III - Soil solution composition affects microstructure of tropical saline alluvial soils in a semi-arid environment

SUMÁRIO

1 APRESENTAÇÃO

A estrutura do solo é caracterizada pelo arranjo e disposição das partículas minerais e orgânicas, formando o sistema poroso. A estrutura determina a intensidade dos processos físicos como a movimentação e retenção de água no solo, a transferência de calor e aeração. Além disso, influencia a atividade biológica, a ciclagem do carbono e de nutrientes e a resistência ao desenvolvimento de raízes, sendo considerada um fator chave para manutenção das funções ecológicas do solo.

As características estruturais são consequência dos fatores e processos envolvidos na formação do solo, sendo fortemente afetadas pelo clima, atividade biológica e práticas de manejo, e vulneráveis à ação degradadora de forças de natureza mecânicas e físico-químicas.

O grau de degradação estrutural provocada pelo uso intensivo e manejo inadequado do solo, dependerá então da resistência interna da estrutura e da intensidade das forças aplicadas. Geralmente, as alterações estruturais são verificadas e quantificadas pela redução da porosidade do solo, aumento da densidade e da resistência à penetração de raízes, diminuição dos fluxos de água e gases, além da diminuição do tamanho e/ou da estabilidade dos agregados.

Entretanto, a resistência da estrutura à desagregação pode ser decorrente da evolução de processos que ocorrem em escalas menores, como a floculação e dispersão, não sendo detectados pelos métodos tradicionais de avaliação estrutural. Na microescala, a resistência estrutural é dependente do tipo e intensidade de ligação entre as partículas, na qual é influenciada pela mineralogia, textura, teor de matéria orgânica, concentração e tipo de cátions, pH, conteúdo de água, ciclos de umedecimento e secagem e atividade biológica.

Portanto, torna-se essencial a realização de estudos para compreensão dos processos de estruturação em microescala e dos fatores que interferem no comportamento mecânico, em nível de partícula, de diferentes tipos de solo. Uma maneira de estudar as modificações causadas pelas práticas de manejo na rigidez estrutural do solo em escala de partículas é por meio da reologia.

Reologia é a ciência que estuda o comportamento deformacional e de fluxo de corpos sujeito a tensões externas, sendo amplamente utilizada na indústria química, farmacêutica e alimentícia. Nos últimos anos, com a adaptação de algumas técnicas,

a reologia vem sendo inserida nos estudos de mecânica do solo para avaliar elasticidade a resistência da microestrutura à deformação, fornecendo informações quantitativas sobre os efeitos dos constituintes do solo, dos organismos e das práticas de manejo nos mecanismos e na força de ligação entre partículas. Também permite realizar inferências sobre as consequências das alterações causadas pelo manejo e/ou por mudanças climáticas sobre a propriedades reológicas de solos ocorrentes nas diferentes regiões brasileiras.

Um processo atribuído tanto ao manejo inadequado do solo, bem como às mudanças climáticas e ambientais é o aumento das taxas de mineralização do carbono orgânico do solo (COS). O COS exerce papel fundamental no processo de formação e estabilidade dos agregados do solo, sendo considerado um dos principais agentes estabilizadores da estrutura de solos tropicais. Uma consequência da mineralização do carbono é a redução dos estoques de COS, afetando as propriedades físicas, químicas e biológicas do solo.

Quanto às propriedades físicas, a redução do teor de COS está relacionada com a diminuição da taxa de infiltração e da retenção de água, da porosidade, do tamanho e da estabilidade dos agregados, bem como com o aumento da argila dispersa em água e da resistência do solo à penetração. Contudo, poucos estudos têm avaliado o efeito da redução do teor de COS sobre a microestrutura. Estes estudos geralmente são realizados por meio da comparação entre solos com distribuição de tamanho de partículas e características físicas bem diferentes. Isso dificulta o entendimento de como a redução de COS influencia as propriedades reológicas do solo, se o efeito da perda de COS sobre a propriedades reológicas é semelhante em diferentes tipos de solo, ou se a mudança elasticidade e resistência da microestrutura é dependente da quantidade de COS perdida.

A distribuição do tamanho de partículas é uma considerada uma das mais estáveis propriedades físicas do solo, pois não é afetada a curto e médio prazo pelo manejo do solo ou por mudanças climáticas. Ela influência as demais características edáficas como o movimento e retenção de água, porosidade e distribuição do tamanho de poros, a compressibilidade e resistência do solo a penetração, bem como a disponibilidade de nutrientes às plantas. Essa influência está relacionada com a reatividade das partículas, que é condicionada pela área superficial específica (ASE).

Devido ao seu pequeno tamanho, as partículas de argila contribuem grandemente com a ASE. Solos argilosos geralmente apresentam maior ASE e consequentemente, grande reatividade, o que os processos físicos da agregação. Porém, diferenças na forma e rugosidade das partículas podem resultar em área superficial bastante discrepantes entre solos com teor de argila semelhante.

Além do mais, os processos físicos que governam o comportamento do solo podem mudar com pequenas diferenças na ASE. Isso poderia explicar os resultados contraditórios sobre o efeito da argila na resistência ao cisalhamento. Alguns trabalhos têm relacionado à resistência ao maior conteúdo de argila, enquanto outros observaram maior resistência em solos com maior teor de areia. Ainda, estes trabalhos comparam solos com granulometria bastante diferente, não verificando o efeito de um aumento gradual no teor de argila sobre as propriedades da microestrutura, especialmente no que diz respeito à ASE. A utilização da ASE poderia melhorar o entendimento dos processos relacionados à associação das partículas e o efeito destas sobre as propriedades reológicas do solo.

Assim como a mineralização do COS, a salinização é outro processo que ocorre naturalmente, mas pode ser intensificada pela ação antrópica devido à utilização inadequada da água de irrigação e controle da drenagem ineficiente. A salinização é definida como processo de acúmulo de sais solúveis, principalmente de sódio, no solo sob regiões de clima árido e semiárido. O excesso de sais no solo afeta negativamente a germinação e o desenvolvimento vegetativo, podendo causar a morte das plantas. Também ocasiona degradação da estrutura do solo, aumentando a dispersão das partículas de argila e a densidade, dificultando o movimento de ar e água.

Visando reduzir o efeito prejudicial do excesso de sais sobre a produção vegetal e sobre a estrutura, tem-se utilizado algumas técnicas de remediação da salinidade. Dentre essas técnicas, destacam-se a lavagem do solo, que solubiliza e lixivia os sais juntamente com água percolada para as camadas mais profundas, e também a incorporação de corretivos químicos, que substitui o Na^+ nos complexos de troca catiônica. A remediação da salinidade proporciona melhoria das propriedades químicas e físicas do solo na macroescala. No entanto, não se sabe ao certo como essas técnicas afetam as propriedades reológicas ou qual a técnica que proporciona melhoria na microestrutura.

Visto que as propriedades reológicas são influenciadas por uma multiplicidade de fatores, e as várias possibilidades de interação entre eles tornam a microestrutura do solo um assunto ainda mais complexo. Portanto, ainda há muitos desafios a serem superados para o entendimento de como a modificação dos fatores envolvidos na ligação de partículas, como o teor de COS, a ASE e a salinidade, interferem nas propriedades reológicas, e consequentemente na microestrutura dos solos tropicais.

1.1 OBJETIVOS

1.1.1 Objetivo geral

Esta tese teve como objetivo geral verificar como a redução do teor de teor de matéria orgânica, área superficial específica a e alteração do tipo de cátions na solução do solo afetam a elasticidade e resistência da microestrutura de solos de solos tropicais.

1.1.2 Objetivos específicos

Para avaliar o comportamento da microestrutura e sua relação com as propriedades edáficas, objetivou-se especificamente:

I. Determinar a elasticidade e a resistência microestrutural de Terras Pretas Arqueológicas submetidas a diferentes níveis de oxidação da matéria orgânica para saber como a redução do teor de carbono altera as propriedades reológicas do solo.
II. Determinar a elasticidade e a resistência microestrutural de solos com área superficial específica (ASE) distinta para conhecer o comportamento das propriedades reológicas em função da ASE
III. Comparar a elasticidade e a resistência microestrutural de solos salinos, de solos com sais solúveis lixiviados e de solos saturados com diferentes tipos de cátions para saber como as técnicas de remediação da salinidade afetam nas propriedades reológicas.

1.2 REVISÃO BIBLIOGRÁFICA

1.2.1 Estrutura e agregação do solo

A estrutura do solo refere-se ao arranjo espacial das partículas de areia, silte e argila e dos poros, em formas geométricas definidas e separadas por planos de fratura (HILLEL, 2004; REICHERT et al., 2010; TAVARES FILHO, 2013).

A estrutura é um atributo edáfico dinâmico, resultante dos processos de formação do solo e modificada por ações contínuas e combinadas do clima, da atividade biológica e das práticas de manejo, que alteram a disposição e a forma das unidades estruturais, modificando o espaço poroso e influenciando propriedades fundamentais para o desenvolvimento das plantas (DEXTER, 1988; HILLEL, 2004; TAVARES FILHO, 2013).

No geral, pode-se identificar três grandes categorias de estrutura: grãos simples, solo maciço e agregados. A primeira é constituída de grãos individuais, onde as partículas estão desacopladas em relação às partículas vizinhas, formando um arranjo aleatório. A estrutura maciça é formada de massa unida em grandes blocos coesos e compactados. A categoria de agregados representa uma condição intermediária, onde as partículas de solo se associam em pequenos complexos estáveis, formando agregados de tamanho e formato variável (HILLEL, 2004).

De acordo com a teoria hierárquica da agregação proposta por Tisdal e Oades (1982), os agregados podem ser agrupados em cinco classes de tamanho (< 2 µm; de 2 a 20 µm; de 20 a 250 µm, de 250 µm a 2 mm; e > 2 mm). Cada classe de agregados tem características próprias, sendo formadas pela união dos agregados das classes anteriores, seguindo uma hierarquia, cuja formação e estabilização depende do tipo e intensidade dos agentes cimentantes.

O primeiro nível hierárquico é constituído basicamente por minerais de argila interagindo com óxidos de ferro (Fe) e alumínio (Al) e ácidos orgânicos, formando aglomerados através do processo de floculação. O nível seguinte é composto pelos aglomerados ligados a partículas de silte pela ação cimentante da matéria orgânica, formando complexos maiores. Estes, por sua vez são unidos às partículas de areia fina pela ação cimentante do húmus e por interação com pelos radiculares e hifas produzidas por microrganismos, originando microagregados. O último nível hierárquico é composto por vários microagregados unidos principalmente por hifas de

fungos e raízes de plantas dando origem aos macroagregados (BRAIDA et al., 2011; DEXTER, 1988; TISDALL; OADES, 1982).

Os microagregados também podem ser formados dentro dos macroagregados. As raízes e hifas de fungos, são os agentes de agregação que mantém os macroagregados unidos. Estes agentes são temporários, permanecendo por um período curto no solo. Ao se decomporem, geram fragmentos revestidos com mucilagens, tornando-se encrustados com argila, iniciando a formação de microagregados dentro dos macroagregados (OADES, 1984; SIX et al., 2004; SIX; ELLIOTT; PAUSTIAN, 2000).

Os limites entre os níveis hierárquicos e a importância relativa dos agentes na estabilidade dos agregados variam conforme o tipo de solo. Entretanto, o limite de 250 µm tem sido utilizado e aceito para distinguir microagregados (<250 µm) e macroagregados (>250 µm) em diferentes classes de solo (BRAIDA et al., 2011; TISDALL; OADES, 1982).

Os agregados possuem uma gênese própria, controlada por diversos mecanismos, proporcionando tamanho, forma, composição e estabilidade diferentes de acordo com o tipo de solo (AZEVEDO; BONUMÁ, 2004; BRONICK; LAL, 2005). Em Latossolos, os agregados são constituídos por minerais de argila, óxidos de Al e Fe, cimentados por raízes e matéria orgânica, apresentam forma de pequenos grânulos, e possuem elevada resistência e estabilidade (AZEVEDO; BONUMÁ, 2004; OADES; WATERS, 1991; VRDOLJAK; SPOSITO, 2002). Em Argissolos, os agregados são constituídos de material orgânico e sesquióxidos não cristalinos, apresentando formato variado, desde grãos soltos a blocos angulares e subangulares, dependendo do teor de argila e de matéria orgânica (MO). Em solos salinos, os agregados são constituídos de minerais de argila ligados por ponte de cátions, com grande quantidade de sódio, o que torna a estrutura adensada quando seca e dispersa e pegajosa quando úmida (DIAS; BLANCO, 2010).

Para a formação do agregado, é necessário que as partículas do solo se encontrem floculadas a nível coloidal e que todos os constituintes do agregado sejam estabilizados por agentes cimentantes (HILLEL, 2004; TAVARES FILHO, 2013). No processo de floculação, as ligações entre os minerais de argila podem ser do tipo borda-borda, borda-face e ou face-face, que depende da densidade de carga da partícula, do pH e da composição da solução do solo (BAUMGARTEN; HORN, 2009;

LAGALY, 1989). Assim, mudanças na microestrutura do solo estão relacionadas aos vários tipos de associação de partículas.

Desta maneira, todos os fatores que influenciam a capacidade de floculação, dispersão e o contato entre partículas interferem na agregação e consequentemente na resistência estrutural do solo. Dentre estes fatores, desacatam-se: teor de argila, os minerais predominantes na fração argila, a concentração e o tipo de cátions e ânions, o conteúdo de MO, o efeito de pressão exercida pelo crescimento radicular e do deslocamento de organismos, forças capilares associadas aos meniscos de água e ciclos de umedecimento e secagem (BASTOS et al., 2005; BAUMGARTEN; HORN, 2009; DEXTER, 1988; HILLEL, 2004).

1.2.2 Fatores que interferem na agregação

Como mencionado na seção 1.2.1 a agregação é fortemente influenciada pelas características das partículas constituintes do solo e pela interação interpartículas, os quais determinam a resistência da estrutura na microescala. A seguir, serão abordados os principais fatores que interferem na agregação do solo.

1.2.2.1 Teor e tipo de argila

A agregação é bastante influenciada pela textura do solo. O teor de argila interfere fisicamente na agregação por meio da expansão e contração (BRONICK; LAL, 2005). Em solos com elevado conteúdo de argila, há maior quantidade de grupos funcionais de superfície, aumentando a reatividade do solo (KÄMPF; SCHWERTMANN, 1998), a força capilar associada aos meniscos (BAUMGARTEN; HORN, 2009; DEXTER, 1988; GHEZZEHEI; OR, 2000), e consequentemente, à expressão das forças de adesão e coesão (REICHERT et al., 2010).

O aumento do teor de argila também está associado com o aumento da estabilidade de agregados pela matéria orgânica do solo (MOS), bem como aumenta a proteção física desta contra a degradação (BRADY; WEIL, 2013; LEPSCH; SILVA; ESPIRONELO, 1982; SOLLINS; HOMANN; CALDWELL, 1996).

A agregação, em solos arenosos é determinada pela quantidade de MOS, enquanto que, em solos argilosos, é determinada principalmente pela composição da argila. O tipo de mineral da fração argila influencia a capacidade de troca de cátions

(CTC), a densidade de carga, a área superficial específica (ASE) e a floculação e dispersão do solo (BRONICK; LAL, 2005; DIMOYIANNIS; TSADILAS; VALMIS, 1998; KÄMPF; SCHWERTMANN, 1998).

Em solos formados em regiões semiáridas e subtropicais, os minerais predominantes na fração argila são do tipo 2:1 e 1:1, respectivamente (KÄMPF; SCHWERTMANN, 1998). Os argilominerais 2:1 apresentam elevada ASE e densidade de cargas, com predominância de cargas elétricas negativas, o que favorece a agregação em ambientes com elevada concentração de cátions polivalentes. Entretanto, devido a capacidade expansiva da maioria destes minerais, a estabilidade de agregados é comprometida com os ciclos de umedecimento e secagem, além de contribuir para o decréscimo do teor de MOS (BRONICK; LAL, 2005; PICCOLO; PIETRAMELLARA; MBAGWU, 1997).

De maneira contrária, os argilominerais 1:1 apresentam baixa CTC, baixa ASE e, consequentemente, quantidade limitada de sítios ativos funcionais de superfície (JOHNSTON; TOMBACZ, 2002; KÄMPF; SCHWERTMANN, 1998), o que diminui a ocorrência de pontes de cátions e de MOS unindo as partículas dos minerais, proporcionando baixa formação de agregados. (SCHULTEN; LEINWEBER, 1995; SIX; ELLIOTT; PAUSTIAN, 2000). Contudo, estes minerais apresentam elevada capacidade de floculação, pois em condição de pH natural dos solos, ocorre protonação dos grupos funcionais silanol e aluminol nas folhas tetraédricas e octaédricas respectivamente, favorecendo as ligações eletrostáticas com os grupos carboxil desprotonados dos coloides orgânicos (ANDERSON; SPOSITO, 1992).

Em solos tropicais bastante intemperizados, há predomínio de óxidos e hidróxidos de Fe e Al na fração argila (HILLEL, 2004), sendo considerados os principais agentes da floculação de partículas e formação de microagregados (OADES; WATERS, 1991). Por apresentarem elevada ASE e densidade de grupos funcionais de superfície com predominância de cargas elétricas positivas (KÄMPF; SCHWERTMANN, 1998), os óxidos agem na agregação do solo pela união, por ligações eletrostáticas, de partículas carregadas negativamente, formando pontes entre moléculas orgânicas, entre estruturas cristalinas de argilominerais ou entre material orgânico e argilominerais (BRONICK; LAL, 2005; OADES; WATERS, 1991; SIX et al., 2004). Também revestem as moléculas orgânicas e partículas primárias,

protegendo-as fisicamente, aumentando a estabilidade de agregação (BALESDENT; CHENU; BALABANE, 2000; BRADY; WEIL, 2013; SIX; ELLIOTT; PAUSTIAN, 2000).

1.2.2.2 Tipo e concentração de cátions

A capacidade de troca de cátions está estreitamente relacionada com a agregação, influenciando-a de duas maneiras: por meio pontes de cátions e pela modificação da dupla camada difusa (DCD).

Em solos com predominância de argilominerais 2:1, cátions polivalentes diminuem as forças de repulsão entre as partículas carregadas negativamente, formando pontes de ligação, mantendo-as unidas. Em solos ocorrentes em regiões semiáridas, também pode ocorrer a dissolução e re-precipitação de Ca^{+2} e Mg^{+2}, na forma de carbonatos secundários, contribuindo para a formação de complexos organometálicos com a MOS, unindo moléculas orgânicas com partículas minerais (BRONICK; LAL, 2005; OADES; WATERS, 1991; ZHANG; NORTON, 2002).

A concentração e a valência dos cátions interferem na distância entre as partículas. Cátions de maior valência, como Ca^{+2} e Mg^{+2}, em concentração elevada, tem maior poder de neutralização das cargas elétricas negativas remanescentes, diminuindo a espessura da DCD à uma distância com predominância de forças atrativas (AZEVEDO; BONUMÁ, 2004; HILLEL, 2004). Entretanto o Ca^{+2} é mais eficaz no processo de agregação, uma vez que o Mg^{+2} provoca maior expansão de argilas 2:1 saturadas em consequência do seu maior raio iônico hidratado (BRONICK; LAL, 2005) e da concentração eletrolítica do solo (ZHANG; NORTON, 2002).

Diferentemente, cátions monovalentes como o Na^{+}, são altamente dispersivos, afetando diretamente a agregação pela ruptura de agregados e indiretamente pelo efeito nocivo ao desenvolvimento das plantas. O Na^{+} trocável na solução do solo aumenta a distância da DCD, contribuindo para a repulsão das cargas elétricas, dispersando as partículas de argila, quebrando os agregados e aumentando a disponibilidade de MOS à decomposição (AZEVEDO; BONUMÁ, 2004; BRONICK; LAL, 2005; HOLTHUSEN et al., 2012a). Os efeitos do Na^{+} na desagregação são mais pronunciados em solos sódicos, os quais ocorrem principalmente em regiões áridas e semiáridas. Contudo, o manejo da fertilidade com calcário e gesso pode amenizar os efeitos adversos do Na^{+} na agregação do solo pelo incremento da concentração de Ca^{+2} nos sítios de troca de cátions (BRONICK; LAL, 2005).

1.2.2.3 Matéria orgânica do solo

O conteúdo de MOS tem correlação positiva com a resistência e estabilidade de agregados, agindo tanto na aproximação como na união das partículas do solo em todos os níveis hierárquicos da agregação (BRONICK; LAL, 2005; TISDALL; OADES, 1982), influenciando os mecanismos de formação das diferentes classes de tamanho de agregados (CASTRO; LOGAN, 1991).

A aproximação entre as partículas pode ocorrer de forma mecânica, por meio de hifas de fungos, pela pressão das raízes nos constituintes do solo ou por realinhamento das partículas realizada pela passagem de organismos presentes na fauna do solo (BRONICK; LAL, 2005). A união das partículas ocorre pela formação de complexos argilo-metal-húmicos, onde cátions metálicos polivalentes agem como ponte, fazendo ligação entre as cargas negativas de moléculas orgânicas e argilominerais (EDWARDS; BREMNER, 1967). Também promovem a agregação pela formação de complexos organometálicos, no qual a matéria orgânica é atraída eletrostaticamente pelas cargas positivas dos óxidos de Fe e Al em condição de pH ácido (ANDERSON; SPOSITO, 1992; BRONICK; LAL, 2005; KÄMPF; MARQUES; CURI, 2012).

A estabilidade de agregados é dependente da liberação de substâncias cimentantes provenientes da atividade metabólica dos microrganismos e das plantas, bem como da decomposição da MOS. Entretanto, a estabilidade da estrutura do solo é dinâmica, dependendo da intensidade da ação estabilizadora dos agentes cimentantes. Os agentes orgânicos envolvidos na estabilização dos agregados do solo podem ser divididos em três grupos quanto a sua persistência no solo, os transicionais, os temporários e os persistentes, e podem atuar individualmente ou de forma combinada (BASTOS et al., 2005).

De maneira geral, os agentes temporários são constituídos de mucilagens, exsudados radiculares, hifas de fungos e raízes, permanecendo no solo por semanas, meses ou até anos, dependendo do tipo de manejo, englobando as partículas simples na estrutura dos macroagregados (ABIVEN; MENASSERI; CHENU, 2009; VEZZANI; MIELNICZUK, 2011). Os agentes transicionais como polissacarídeos, possuem um forte efeito agregante, mas de curta duração, estando geralmente associados à estabilização dos macroagregados (BRONICK; LAL, 2005; EDWARDS; BREMNER, 1967; TISDALL; OADES, 1982).

Os materiais orgânicos humificados apresentam elevada persistência do solo, porém, menor efeito agregante, sendo importantes na formação e estabilização de microagregados pela formação de complexos com óxidos de Fe e Al de baixa cristalinidade (BRONICK; LAL, 2005; EDWARDS; BREMNER, 1967; TISDALL; OADES, 1982).

Além da persistência no solo, o COS pode ser classificado quanto a compartimentalização no solo, considerando duas frações orgânicas, o carbono orgânico particulado (CO_p) e o carbono orgânico associado aos minerais (CO_{am}). O CO_p, também denominado fração leve, está vinculado à fração areia, sendo caracterizado como partículas derivadas de resíduos de plantas e hifas com estrutura celulares reconhecíveis, sendo bastante sensível às mudanças de uso e manejo do solo (FRAZÃO et al., 2010). O CO_p possui efeito indireto sobre a resistência estrutural do solo devido à sua alta capacidade de armazenar água, garantindo ação duradoura das forças de meniscos em potenciais matriciais mais negativos (BACHMANN; ZHANG, 1991), principalmente em solos arenosos onde as forças capilares são reduzidas.

Já o CO_{am} pertence a fração média e pesada da MOS e está associado às partículas de silte e argila do solo. É a fração da MOS que interage com a superfície de partículas minerais, formando os complexos organominerais (ROSSI et al., 2012), sendo menos sensíveis à mudanças ambientais.

Como mencionado acima, todos os fatores que influenciam a interação entre as partículas, interferem na resistência da microestrutura do solo à desagregação. Uma maneira de verificar as alterações da resistência estrutural do solo em escala de partículas é por meio de técnicas reológicas, que permite investigação de características micromecânicas, fornecendo informações quantitativas sobre a energia necessária para romper as ligações interpartículas.

A seguir, serão abordados alguns conceitos e princípios importantes na caracterização dos parâmetros reológicos do solo.

1.2.3 Reologia do solo

O termo reologia é originado do grego *rheo* = fluxo e *logos* = estudo. Assim, a reologia é a ciência que estuda o comportamento deformacional e o fluxo de corpos

submetido a tensões externas (BARNES, 2000; MARKGRAF; HORN; PETH, 2006), sob determinadas condições termodinâmicas ao longo de um período de tempo

A reometria é a técnica fundamentada na reologia, que estabelece empiricamente as relações entre tensão e deformação dos materiais (MARKGRAF; HORN; PETH, 2006). Esta técnica é realizada em equipamento especializado denominando de reômetro (SCHRAMM, 2006), sendo bastante difundida em pesquisas na indústria química e farmacêutica, na engenharia de alimentos e na engenharia civil (BAUMGARTEN; DÖRNER; HORN, 2013; MARKGRAF; HORN; PETH, 2006; MEZGER, 2014).

Nos últimos anos, a reometria tem sido significativamente aplicada no estudo do comportamento mecânico do solo, na investigação dos efeitos do conteúdo de água, da textura e mineralogia, da concentração de sais e do conteúdo de matéria orgânica. Também pode ser utilizada para investigar o efeito do manejo agrícola sobre a estabilidade microestrutural, buscando melhor entendimento sobre os processos de interação entre as partículas nas interfaces sólido-sólido e sólido-líquido, e consequentemente sobre mecanismos atuantes na agregação do solo (BAUMGARTEN; DÖRNER; HORN, 2013; GHEZZEHEI; OR, 2001; HOLTHUSEN et al., 2012c; HOLTHUSEN; PETH; HORN, 2010; MARKGRAF et al., 2012; MARKGRAF; HORN; PETH, 2006).

Uma maneira de verificar esses efeitos sobre a microestrutura é através do comportamento deformacional e de fluxo de um corpo sujeito a uma tensão externa, pois a deformação dependerá das suas propriedades como a viscosidade, elasticidade e plasticidade, bem como do tipo, grau e duração da tensão aplicada (MARKGRAF; HORN; PETH, 2006).

A tensão de cisalhamento (τ) aplicada na reometria é definida pela equação 1.

$$\tau = \frac{F}{A} \tag{1}$$

Em que τ é a tensão de cisalhamento (Pa), F é a força de cisalhamento (N) e A é a área de cisalhamento (m^2).

A taxa de cisalhamento ($\dot{\gamma}$) ou taxa de deformação refere-se ao gradiente de velocidade em uma amostra (HILLEL, 2004; MEZGER, 2014; SCHRAMM, 2006), sendo calculada pela equação 2.

$$\dot{\gamma} = \frac{v}{h} \quad (2)$$

Em que $\dot{\gamma}$ é a taxa de cisalhamento (s^{-1}), v é a velocidade (m s^{-1}) e h é a altura da amostra ou distância entre as placas, também denominada de *gap* (m).

A $\dot{\gamma}$ é derivada da deformação causada pela ação da τ sobre a lâmina de um fluido. Em um sistema de medição de placas paralela, a τ conduz o fluido para um fluxo onde a velocidade máxima se encontra na camada superior e diminui linearmente atravessando o corpo até chegar a zero na camada ligada a placa inferior estacionária (SCHRAMM, 2006).

A tensão de cisalhamento também, pode ser estimada pela relação entre a taxa de cisalhamento e a viscosidade (η) de um fluido ideal, fundamentada na Lei de Newton, onde a $\dot{\gamma}$ é diretamente proporcional à τ, sendo controlada somente pela resistência devido ao atrito interno do material (Equação 3). A viscosidade é definida como o coeficiente de proporcionalidade, pois em fluidos viscosos ideais submetidos a uma τ constante ocorre aumento linear na deformação no tempo, dissipando completamente a energia aplicada e deformando-se irreversivelmente (Figura 1a) (GHEZZEHEI; OR, 2001; HILLEL, 2004; MEZGER, 2014; SCHRAMM, 2006)

$$\tau = \eta . \dot{\gamma} \quad (3)$$

Em que τ é a tensão de cisalhamento (Pa), η é a viscosidade (constante) (Pa s) e $\dot{\gamma}$ é a taxa de cisalhamento (1 s^{-1}).

Figura 1 - Representação gráfica de curvas de fluxo ideais. As setas na extremidade das retas indicam a direção da deformação e do fluxo. G = módulo de cisalhamento (Pa); τ_y = a tensão de escoamento, tensão de escoamento no ponto de Bingham; = η = viscosidade; η_B = coeficiente de fluxo de Bingham.

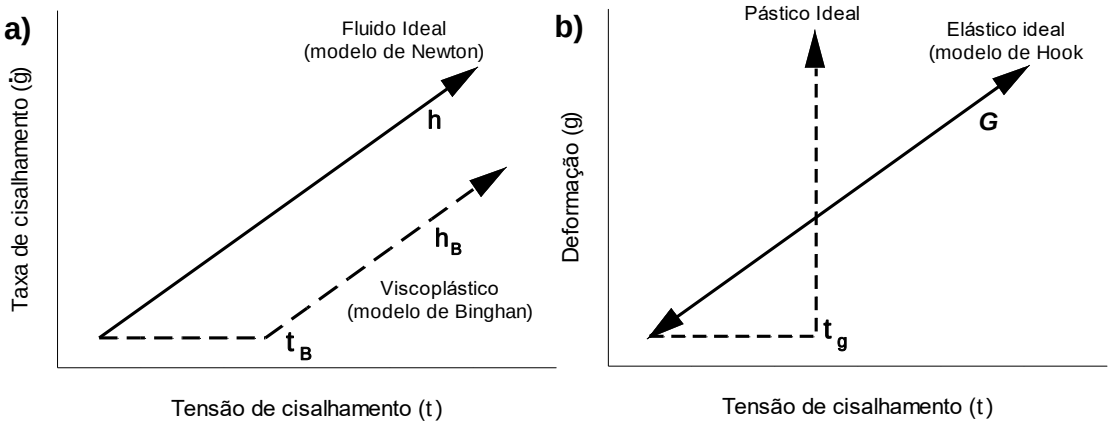

Adaptado de Barnes (2000) e Mezger (2014).

Entretanto, os materiais sólidos ideias se comportam de maneira contrária aos fluidos newtonianos. Quando uma tensão é aplicada em um sólido ideal, ocorre instantaneamente uma deformação linearmente proporcional a energia aplicada. Nestes materiais, a energia é completamente armazenada, sendo liberada após remoção da tensão, com a completa recuperação do material à sua forma original (Figura 1b) (GHEZZEHEI; OR, 2001; HILLEL, 2004; HOLTHUSEN; PETH; HORN, 2010; REICHERT et al., 2010; SCHRAMM, 2006).

Neste caso, a tensão de cisalhamento é fundamentada na lei da elasticidade de Hooke e determinada através da relação entre a deformação (γ) e o módulo de cisalhamento (G), como descrita pela equação 4 (HOLTHUSEN; PETH; HORN, 2010; MARKGRAF; HORN; PETH, 2006; MEZGER, 2014). O G, assim como a η, é uma constante de proporcionalidade, indica a rigidez da estrutura do material e define a resistência do sólido à deformação, sendo correlacionada principalmente com as propriedades físico-química do sólido (Figura 1a) (SCHRAMM, 2006).

$$\tau = G \cdot \gamma \qquad (4)$$

Em que τ é a tensão de cisalhamento (Pa), G é o módulo de cisalhamento (Pa) e γ é a deformação de cisalhamento (% ou 1), que pode ser definida pela equação 5.

$$\gamma = \frac{s}{h} = tan\,\varphi \quad (5)$$

Em que s é a deflexão (mm), h é a distância entre as placas (mm) e δ é o ângulo de deflexão (°). Quando s for igual à h (δ =45°), a deformação será igual a 100% (MARKGRAF; HORN; PETH, 2006), como visualizado na figura 2.

Já em corpos plásticos ideais, a deformação ocorre somente pós a τ atingir um valor crítico, denominado de tensão de escoamento (τ_y) como descrito na equação 6. Acima desta tensão, há uma transição de comportamento elástico para plástico (fluxo viscoso) e o corpo deforma-se progressivamente, mantendo a forma deformada quando cessada a tensão (Figura 1b) (HILLEL, 2004).

$$\tau_{máx} = \tau_y = constante \quad (6)$$

Em que $\tau_{máx}$ é a tensão de cisalhamento máxima (Pa) e τ_y a tensão de escoamento (Pa).

Figura 2 - Representação da deformação (γ) em função do quociente entre deflexão (s) e altura da amostra (h) ou tamanho gap.

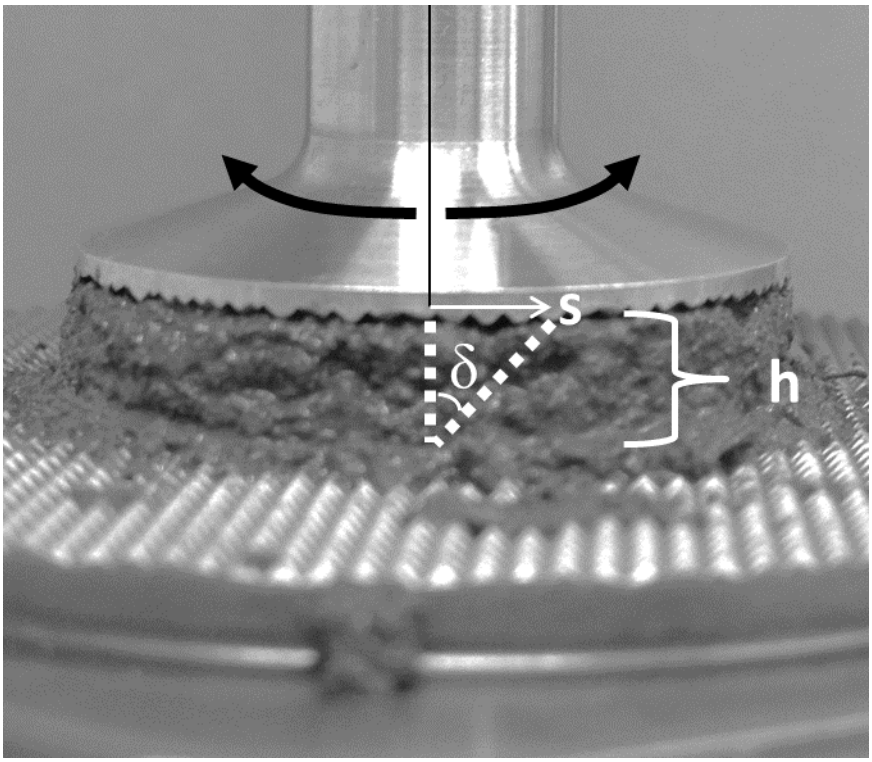

Entretanto, o solo, como a maioria dos materiais reais, exibe comportamentos de fluxo e deformação complexos, não se comportando como um sistema ideal (GHEZZEHEI; OR, 2001; SCHRAMM, 2006), podendo apresentar comportamento combinado de elasticidade, viscosidade e plasticidade. O solo sob tensão estática, exibe comportamento viscoplástico, pois o fluxo inicia apenas quando a τ excede o ponto de escoamento crítico (τ_B). Em tensões superiores, o solo flui como material viscoso, aumentando a taxa de cisalhamento linearmente ao aumento da τ superiores ao τ_B, sendo representado pelo modelo de Bingham (Figura 1a) e descrito pela equação 7.

$$\tau = \tau_B + \eta_B . \dot{\gamma} \qquad (7)$$

Em que τ é a tensão de cisalhamento (Pa), τ_B o ponto de escoamento crítico de Bingham (Pa), η_B o coeficiente de fluxo de Bingham (Pa s) e $\dot{\gamma}$ a taxa de cisalhamento (1 s^{-1}).

Contudo, quando o solo sofre uma tensão transiente, principalmente de curta duração, uma porcentagem de qualquer energia de cisalhamento gerada é temporariamente armazenada elasticamente, e somente o restante não conhecido induz o fluxo viscoso (GHEZZEHEI; OR, 2001; MARKGRAF; HORN; PETH, 2006). Quando a tensão é removida, a energia armazenada elasticamente é liberada, e parte da deformação é recuperada. Porém, a deformação do componente viscoso é permanente (GHEZZEHEI; OR, 2001). Desta forma, o solo é classificado como material viscoelástico, pois exibe simultaneamente comportamento elástico e viscoso (HOLTHUSEN; PETH; HORN, 2010; MARKGRAF; HORN, 2006; MARKGRAF; HORN; PETH, 2006; MEZGER, 2014).

Dentre os vários modelos reológicos propostos para descrição matemática do comportamento viscoelástico, destacam-se os modelos propostos por Maxwell e por Kelvin-Voight (BARNES, 2000; MARKGRAF; HORN, 2006; MEZGER, 2014). O modelo de Maxwell, que caracteriza o comportamento de um líquido viscoelástico, é análogo à um conjunto de mola e amortecedor ligados em série (Figura 3a), representando o efeito da τ na deformação plástica e no fluxo viscoso de fluidos como dispersões, onde a tensão total e as tensões de cada elemento são iguais e a deformação total é igual à soma das deformações.

Já o modelo de Kelvin-Voight, que representa um sólido viscoelástico, faz analogia à um conjunto mola e amortecedor ligados paralelamente (Figura 3b), onde a tensão total é a soma das tensões de ambos os elementos, enquanto as deformações são iguais (BARNES, 2000; MARKGRAF; HORN, 2006; MEZGER, 2014; SCHRAMM, 2006).

Contudo, o solo, como os demais materiais viscoelásticos reais, apresenta comportamento complexo, com variação no tipo e na intensidade das combinações entre os líquidos de Maxwell e os sólidos de Kelvin-Voigt de acordo com a estrutura e composição da amostra.

Uma forma para determinar as relações entre tensão e deformação em amostras viscoelásticas na reometria, sob condição de não equilíbrio, é por meio de testes oscilatórios (MEZGER, 2014). Estes têm sido utilizados para investigar as propriedades reológicas do solo, relacionando o efeito das características químicas, físicas e mineralógicas na resistência microestrutural do solo à deformação.

Figura 3 - Representação esquemática dos modelos propostos por Maxwell (a) e por Kelvin-Voight (b). τ = tensão de cisalhamento; γ = deformação.

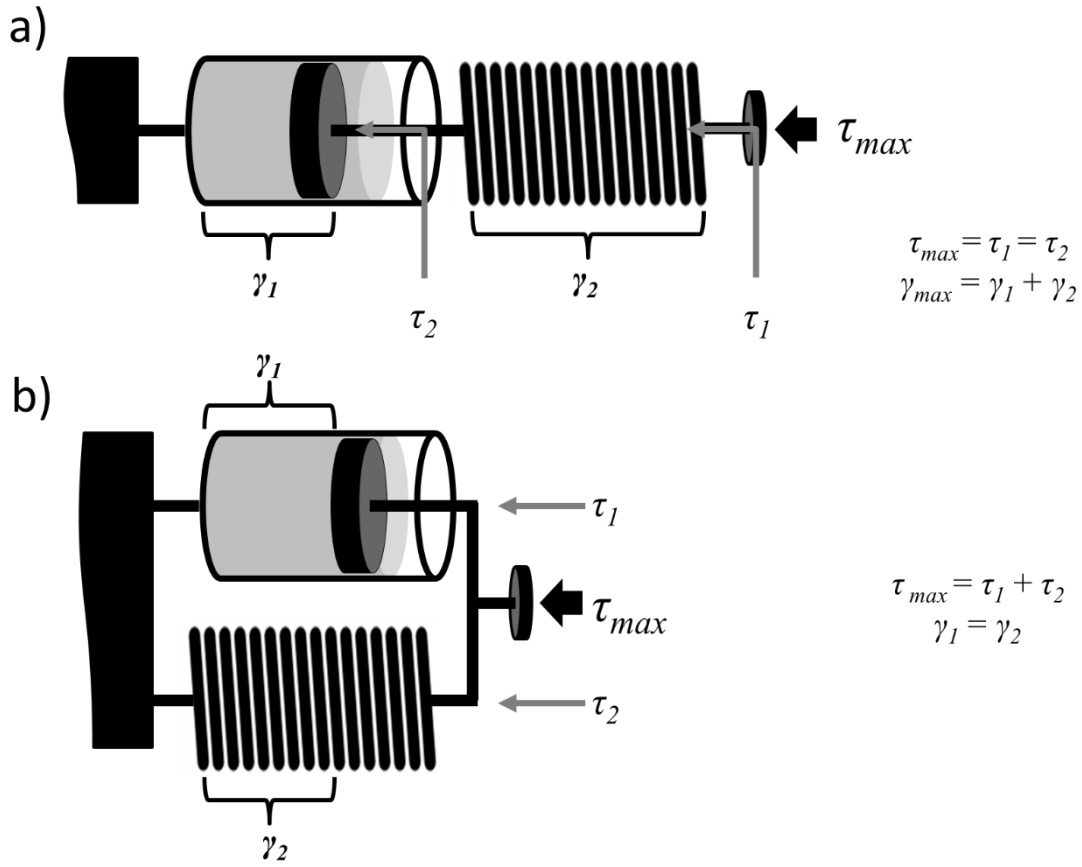

Adaptado de Mezger (2014).

Basicamente, a amostra de solo é disposta entre duas placas paralelas. A placa inferior é fixa, enquanto que a placa superior é movida para a direita e para esquerda de maneira oscilatória (Figura 4), com a deflexão (s) seguindo uma função senoidal no tempo, criando assim um fluxo laminar espiral em camadas a partir da placa inferior (s = 0) e gerando tensões de resistência na amostra (SCHRAMM, 2006). Nos testes oscilatórios, a tensão de cisalhamento é resultante da força necessária para gerar a deformação ao longo da superfície de cisalhamento (HOLTHUSEN; PETH; HORN, 2010), conforme a equação 1; com a γ calculada a partir da distância de deflexão (s) e a distância entre as placas ou altura da amostra (h), de acordo com a equação 5.

Figura 4 - Modelo esquemático de placas paralelas circulares para testes de cisalhamento oscilatório. s = distância de deflexão, δ = ângulo de deflexão; h = gap. O tamanho das setas de casa fase representa o aumento na deflexão.

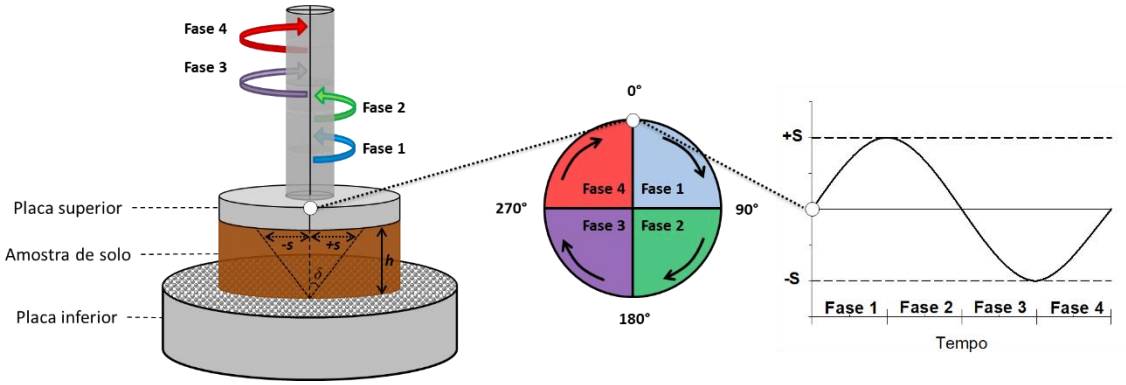

Adaptado de Holthusen; Peth; Horn, (2010); Mezger, (2014); Pértile et al., (2018) e Schramm, (2006). Na fase 1, a placa superior se movimenta da posição inicial até a extremidade direita da deflexão (+s), formando um ângulo de 90°. Na fase 2, a placa superior se movimenta para a esquerda até posição inicial, formando um ângulo de 180° (90° para a direita e 90° para esquerda). Imediatamente após o término da fase 2, a placa superior se movimenta para a extrema esquerda (-s), formando um ângulo de 270°, com uma amplitude de deformação maior que as fases anteriores (maiores setas). Por fim, ocorre o movimento da extrema esquerda a posição inicial, totalizando um ciclo de 360° em movimento oscilatório. Os ciclos são repetidos até a deformação de 100% (s = h e δ = 45°)

Dentre os testes oscilatórios, o teste de varredura de amplitude (TVA) com deformação controlada tem sido utilizado para investigar as mudanças na microestrutura do solo, obtendo informações sobre o comportamento de fluxo do mesmo (MARKGRAF; HORN, 2006). Os TVAs apresentam amplitude de oscilação variável e uma frequência constante, com o termo “varredura” representando um parâmetro variável, onde a tensão de cisalhamento ou a deformação é controlada (MARKGRAF; HORN; PETH, 2006; MEZGER, 2014; SCHRAMM, 2006).

A deformação durante o TVAs varia entre 0,0001 a 100%, com a amplitude de oscilação variando proporcionalmente ao aumento da deformação (Figura 5). A deformação de 100% ocorre quando a deflexão for igual à altura da amostra (s = h), e consequentemente, o ângulo de deflexão atinge 45° (Figura 2). Neste teste, a deformação é calculada de acordo com a equação 5. A tensão é calculada pelo quociente entre o torque requerido para gerar a deformação na superfície de cisalhamento, como explicado pela equação 8 (HOLTHUSEN; PETH; HORN, 2010; MEZGER, 2014; PÉRTILE et al., 2018).

$$\tau = \frac{2M}{\pi r^3} \quad (8)$$

Em que τ é a tensão de cisalhamento (%), *M* é o torque (Pa), e *r* é o raio da placa superior (m).

Figura 5 - Amplitude de varredura da deformação ao longo do tempo.

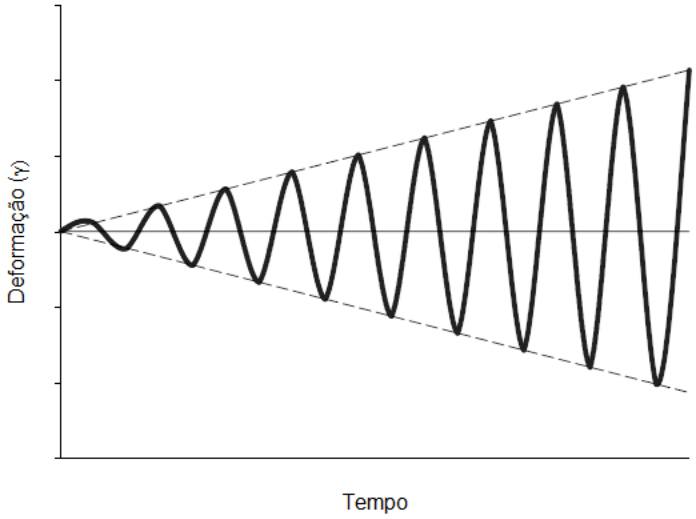

Fonte: Mezger, (2014).

A relação entre a γ predefinida e a τ resultante é dependente das características do material. Substâncias elásticas ideais reagem simultaneamente com a deformação, e, portanto, as curvas de γ e τ estão em fase, apresentando um ângulo de deslocamento de fase (δ) igual a zero (δ = 0°) (Figura 6a). Em fluídos newtonianos, ocorre um atraso de 90° na fase da curva de τ em relação à γ (Figura 6b). Já para materiais viscoelásticos, o δ varia de 0 a 90° (Figura 6c). Desta forma, o deslocamento do ângulo de perda de fase pode ser utilizado para classificar o comportamento de fluxo e a deformação do solo (HOLTHUSEN; PETH; HORN, 2010; MARKGRAF; HORN; PETH, 2006; MEZGER, 2014; SCHRAMM, 2006).

Figura 6 - Ângulo de deslocamento de fase (δ) entre curvas senoidais de deformação predefinida (linha contínua) e tensão resultante (linha pontilhada) de diferentes materiais.

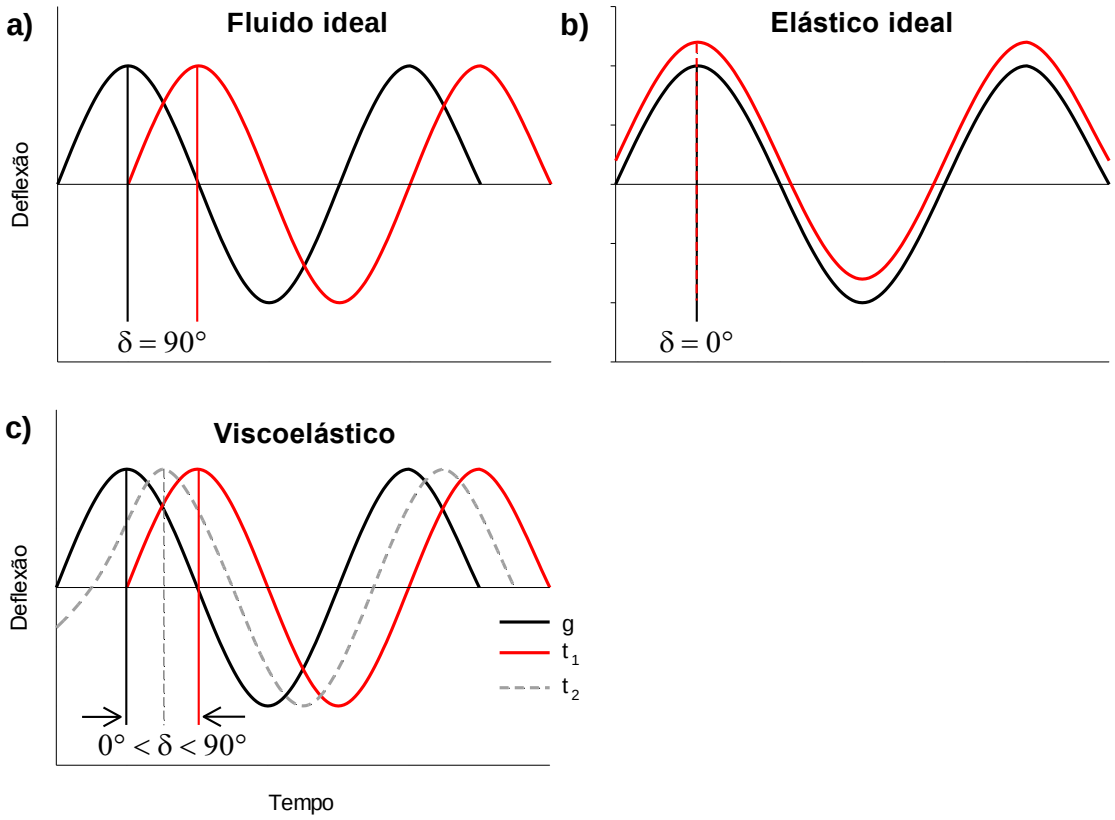

Fonte: Schramm (2006)

Entretanto, para a mensuração das propriedades reológicas de materiais viscoelásticos, é necessário adaptar os parâmetros. Pela Lei de Hooke, os materiais elásticos perfeitos apresentam módulo de cisalhamento constante quando aplicado uma tensão estática. Quando aplicada tensões oscilatórias, é adaptado um módulo de cisalhamento complexo (G*) (Equação 9), que consiste de uma parte elástica, caracterizada pelo módulo de armazenamento real (G') e de uma parte viscosa, caracterizada pelo módulo imaginário de perda (G") (HOLTHUSEN; PETH; HORN, 2010; MARKGRAF; HORN; PETH, 2006; MEZGER, 2014).

$$\tau_A = G^*.\gamma_A, \text{ em que } |G^*| = \sqrt{(G')^2 + (G'')^2} \quad (9)$$

Onde τ_A é a tensão de cisalhamento (Pa), G* o módulo de cisalhamento complexo (Pa), γ_A a deformação (%), G' o módulo de armazenamento (Pa) e G'' o módulo de perda (Pa); sendo que o índice A indica amplitude.

Dentro do módulo de cisalhamento complexo, o G' (Equação 10) representa a elasticidade do material, onde a energia da tensão é armazenada, podendo ser liberada após o teste, enquanto que o G'' (Equação 11) representa o componente viscoso, onde a parte imaginária da elasticidade é perdida, com a energia sendo liberada na forma de calor de cisalhamento para iniciar o fluxo (SCHRAMM, 2006). Tanto o G' como o G", são diretamente dependentes da tensão de cisalhamento, da deformação, e do ângulo de perda de fase (HOLTHUSEN; PETH; HORN, 2010).

$$G' = G^*.cos\delta = \frac{\tau}{\gamma}.cos\delta \quad (10)$$

$$G'' = G^*.sen\delta = \frac{\tau}{\gamma}.sen\delta \quad (11)$$

Em que G' é o módulo de armazenamento (Pa), G" o módulo de perda (Pa); G* o módulo de cisalhamento complexo (Pa), τ a tensão de cisalhamento (Pa), γ a deformação (%) e δ o ângulo de deslocamento de fase.

A relação entre G' e G'' resulta no fator de perda (tan δ) adimensional, calculado pela equação 12 e que pode ser usado para classificar o comportamento de deformação e fluxo do solo. Quando o G' é superior ao G'' ($\delta > 1$), ocorre predominância de deformações elásticas, porém, quando o G'' é maior que o G', as deformações são predominantemente plásticas, ocorrendo o fluxo viscoso do solo (BAUMGARTEN; DÖRNER; HORN, 2013; HOLTHUSEN; PETH; HORN, 2010; MARKGRAF; HORN; PETH, 2006).

$$\tan = \frac{G''}{G'} \quad (12)$$

A partir das curvas típicas de τ, tan (δ), G' e G" em função da deformação obtidas nos TVAS, são obtidos valores pontuais, que marcam mudanças no comportamento deformacional e de fluxo do solo. Esses valores pontuais são

caracterizados como parâmetros reológicos, e possibilitam comparação quantitativa da microestrutura de diferentes materiais. Os parâmetros reológicos obtidos são: o intervalo viscoelástico linear (LVR), a deformação (γ_{LVR}) e a tensão (τ_{LVR}) no final do LVR, a tensão máxima de cisalhamento (τ_{max}), bem como o valor do módulo de armazenamento (G'_{YP}) e deformação (γ_{YP}) no ponto de escoamento, como pode ser observado na figura 7 (HOLTHUSEN; PETH; HORN, 2010; MARKGRAF; HORN; PETH, 2006; SCHRAMM, 2006).

O LVR representa a faixa de deformação onde o módulo G* é constante ou seja, as curvas de G' e G'' permanecem em um valor constante de platô, não mostrando alterações significativa da estrutura da amostra não mostra em baixas deformações (MEZGER, 2014). Isso indica que a deformação é totalmente recuperável. O LVE representa fase inicial elástica dos TVAs (Fase I), de baixa deformação de cisalhamento. A amplitude do LVR começa na deformação de 0,0001% (início do teste) e termina com a $\gamma_{LVR.}$ Também é possível determinar a resistência ao cisalhamento no final do LVR (τ_{LVR}).

Deformações maiores que γ_{LVR} promovem modificações irreversíveis e cumulativas no material, porém com predomínio do comportamento elástico, representando uma fase de transição (Fase II) entre a elasticidade e o comportamento newtoniano, onde ocorre a perda da rigidez da estrutura do material e desenvolvimento de deformação plástica ou viscosa. O início da fase de transição é determinado pelo γ_{LVR}, quando a declividade do G' se torna superior à 5% (BAUMGARTEN; DÖRNER; HORN, 2013; HOLTHUSEN; PETH; HORN, 2010; MARKGRAF; HORN; PETH, 2006).

Figura 7 - Módulo de armazenamento G' (Pa) e módulo de perda G" (Pa) e do fator de perda (tan δ) em função da deformação γ (%).

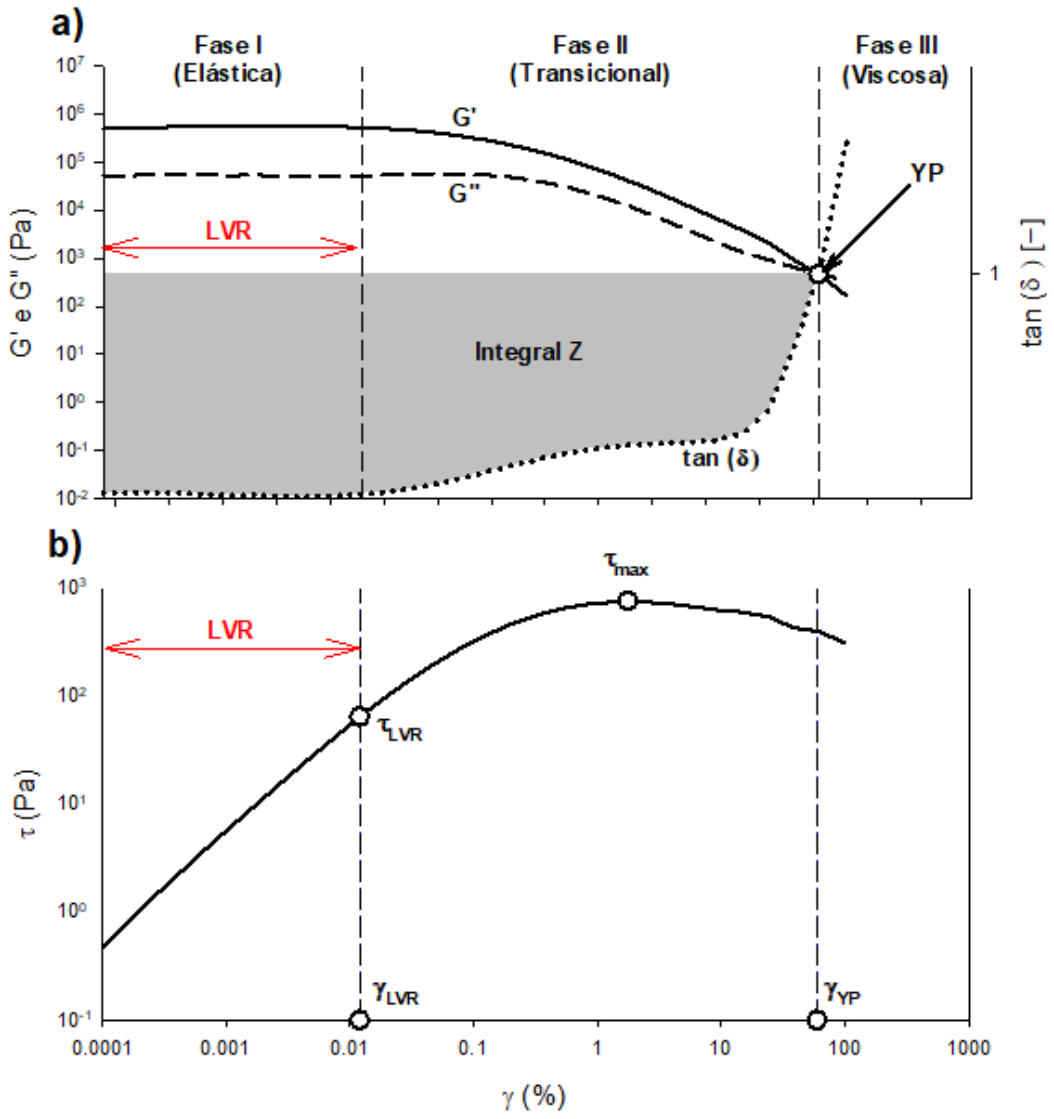

Adaptado de Pértile et al., (2016)

O limite entre a fase transicional e a fase viscosa (Fase III) é determinado pela deformação no ponto de escoamento (γ_{YP}), que ocorre quando a tan δ = 1, ou seja, quando os módulos de armazenamento e de perda se igualam (Figura 7a). Assim, o γ_{YP} de uma amostra é o nível de cisalhamento e de deformação, pois a partir deste ponto, há predomínio do comportamento viscoso, com deformação irreversível do solo (BAUMGARTEN; DÖRNER; HORN, 2013; HOLTHUSEN; PETH; HORN, 2010; MARKGRAF et al., 2012; MARKGRAF; HORN; PETH, 2006).

A integral z é outro parâmetro reológico que pode ser utilizado para caracterizar a rigidez da microestrutura do solo. É calculada pela soma da área delimitada pela curva tan δ da menor deformação aplicada até o ponto de escoamento, onde tan δ = 1 (Figura 7a), como descrito na equação 13.

$$Iz = \int_{0.0001}^{YP} \left(1 - \tan\delta\right) dx \tag{13}$$

onde Iz é a integral Z (adimensional), δ é o ângulo de deslocamento de fase e x é o valor da deformação. Quanto maior o valor da Iz, maior é o comportamento elástico e a rigidez microestrutural (MARKGRAF et al., 2012).

A tensão máxima de cisalhamento ($\tau_{máx}$) durante o teste oscilatório também pode ser utilizada como um parâmetro reológico (Figura 7b), caracterizando a máxima resistência interna que a amostra de solo oferece para resistir à ruptura da ligação entre as partículas (HOLTHUSEN et al., 2012b; HOLTHUSEN; PETH; HORN, 2010).

Assim, os testes oscilatórios com amplitude de oscilação da deformação, possibilitam investigações da influência de fatores intrínsecos e externos sobre resistência microestrutural do solo por meio da quantificação dos parâmetros reológicos descritos acima, fornecendo informações fundamentais sobre a força microestrutural do solo expressas em números absolutos (HOLTHUSEN et al., 2012b; MARKGRAF et al., 2012; MARKGRAF; HORN; PETH, 2006).

Detalhes sobre os fundamentos da reologia e a sua relação com a mecânica do solo são descritos por BARNES, 2000; GHEZZEHEI; OR, 2001; HOLTHUSEN et al., 2012a; HOLTHUSEN; PETH; HORN, 2010; MARKGRAF; HORN; PETH, 2006a; MEZGER, 2014; PÉRTILE et al., 2018; SCHRAMM, 2006.

2 RESULTADOS

2.1 ESTUDO I - RESILIENCE AND MICROSTRUCTURAL RESISTANCE OF ARCHAEOLOGICAL DARK EARTHS WITH DIFFERENT SOIL ORGANIC CARBON CONTENTS IN WESTERN AMAZONIA, BRAZIL

[2]Resilience and microstructural resistance of Archaeological Dark Earths with different soil organic carbon contents in Western Amazonia, Brazil

Alan Carlos Batistão[a,*], Dörthe Holthusen[a], José Miguel Reichert[a], Luís Antônio Coutrim dos Santos[b], Milton César Costa Campos[b]

[a]Soils Department, Federal University of Santa Maria (UFSM), Brazil.

[b]Soils Department, Federal University of Amazônia (UFAM), Brazil.

[*]Corresponding author at: Avenida Roraima 1000, prédio 42, Cidade Universitária, Camobi, Santa Maria, RS, CEP: 97105-900, Brazil. E-mail address: alanbatistao@gmail.com (A. Batistão).

Abstract - Archaeological Dark Earths (ADE) are anthropogenic soils with high fertility and excellent physical conditions due to high soil organic carbon (SOC) content. However, climate change, land use and soil management can increase SOC mineralization, resulting in microstructure damage of these soils. To verify the effect of SOC loss, we collected deformed samples from the surface horizon and simulated the reduction of C with the application of 0.2, 0.4 and 0.6 ml of hydrogen peroxide 35% per gram of soil, resulting in three treatments of different oxidation levels and untreated

[2] Artigo submetido à revista Geoderma

soil. Both original and oxidized soil were submitted to an amplitude sweep test with controlled strain and a thixotropy test, in a compact modular rheometer. To characterize the effect of soil properties on rheology and resilience of ADEs, we performed a correlation analysis with physico-chemical properties from untreated soil. Higher clay and organic matter contents increased the microstructure elasticity of ADEs. The increase in base saturation, mainly due to the high Ca^{+2} content, also favors elasticity. The soil's resilience is a result of the joint effect of particle size distribution, base saturation and SOC content. The microstructure recovers fast, regardless of the disturbance intensity. The SOC loss affected the microstructure differently in each ADE. These differences are not dependent on the amount of SOC lost and mostly labile SOC (as removed by low oxidation intensity) was responsible for soil strength.

Keywords: Indian Black Earth, rheology, organic matter, anthropogenic horizons, soil structure

1 INTRODUTION

The majority of the arable soils of the Amazon region are acidic, have low natural fertility, with reduced organic matter levels, and low cation exchange capacity (Dematthê and Dematthê, 1993; Vieira and dos Santos, 1987), being considered limiting to the productivity and sustainability of agricultural production systems (Cunha et al., 2007). Associated with these soils, there are anthropogenic surface horizons, popularly called "Archaeological Dark Earths" (ADE) or Indian Black Earth, of higher fertility and with physical properties different from the original soil (Glaser and Birk, 2012).

The ADEs occupy 0.1% to 0.3% of the Amazon basin, occurring on several soil types (Campos et al., 2011; Kämpf and Kern, 2005). They exhibit dark color and

archaeological artifacts (ceramic and/or lithic fragments, charcoal, shells) incorporated into the soil surface horizon matrix (Kern and Kämpf, 2005). This blackish color is related to the prolonged and intense incorporation of C in the form of pyrogenic charcoal (black carbon), resulting from incomplete combustion of plant residues. The black carbon is composed of chemically and biologically stable polycyclic aromatic substances (Zech et al., 1990). Its high C content is associated with humic acid and humin fractions (Campos et al., 2011) and persists in the soil for a long period of time (Kämpf and Kern, 2005), acting in aggregate formation and stabilization, and improving soil physical conditions (Cunha et al., 2007).

The soil structure of ADEs ranges from granular to angular blocks, generally of moderate to strong aggregation, presenting a friable consistency when moist and being non-plastic to slightly plastic when wet (Campos et al., 2011; Santos et al., 2013). The ADEs also have low bulk density (Santos et al., 2013), high total porosity (Barros et al., 2016) and high aggregate stability (Pantoja et al., 2015). This is due to the high organic matter levels and of the intense biological activity in the anthropogenic horizons (Cunha et al., 2007).

However, the increase in global temperature due to greenhouse gases and changes in land use and soil management may increase the mineralization rates of organic matter, reducing soil carbon levels (Bokhorst et al., 2007; Stergiadi et al., 2016). Some studies have demonstrated a detrimental effect of management practices on the physical properties of ADEs. For example, Teixeira and Martins (2002) verified that, besides the lower C content, the geometric mean diameter and the percentage of aggregates larger than 2 mm were lower in ADEs used for seed production in comparison with ADEs left under fallow. Silva et al. (2016) verified a positive correlation of soil organic carbon (SOC) content with macroporosity, total porosity and mean

diameter of aggregates, and negative correlation of SOC with bulk density and soil resistance to penetration in ADEs cultivated to cocoa.

Several other studies have characterized physical (Gomes et al., 2017, 2017), chemical (Barros et al., 2016; Campos et al., 2012, 2011; Cunha et al., 2007; Santos et al., 2013) and mineralogical properties of ADEs (Costa et al., 2004; da Costa and Kern, 1999; Kern and Kämpf, 2005; Santos et al., 2018). However, there is a lack of information on ADEs structural stability. Structural stability can be understood as the ability of soil aggregates to withstand forces without presenting breakdowns, either by rupture, fragmentation or flow (Reichert, 2010), being dependent on the factors and processes that promote the approximation of primary particles and that keep them united against the external forces that tend to separate them (Azevedo and Dalmolim, 2004). The SOC plays a fundamental role in aggregate formation and stability (Vezzani and Mielniczuk, 2011), and small changes in the amount and type of SOC can reduce aggregate stability and resilience of soil. Though it can be assumed that changes in climate and land use accelerate the loss of SOC in soils of high SOC content like ADEs, it remains widely unknown how the SOC loss affects the microstructural stability of these soils and this needs to be addressed most urgently.

However, the traditional methods of structural evaluation are not sensitive enough to detect changes in particle level interactions. As an alternative, rheological techniques have been employed in soil mechanical studies to evaluate the microstructural resistance against disturbance, allowing to know the effects of small changes in the factors and processes of aggregation on the soil microstructure resistance against external (transient) stresses. Also, with these techniques, it is possible to quantify the capacity of the soil microstructure to recover after applied stresses, returning to a condition of resistance similar to the original one.

In general, studies on the variation of physical properties of ADEs are performed by comparison of soils from distinct areas with correspondingly different grain size distribution, nutrient concentration and C content, making it it difficult to understand the role of C reduction in the alteration of soil structural strength.

Thus, the objective of this work was to analyse the rheological properties and microstructural resilience of Archaeological Dark Earths from the Southern Amazonas state, Brazil, and how these are altered by soil organic carbon reduction by means of chemical oxidation.

2 MATERIAL AND METHODS

2.1 Study area description

The studied soils are located in the municipalities of Apuí and Manicoré, in the southern region of the federal state Amazonas. The climate of the region according to the Köppen classification is Am, with tropical monsoon rain and a dry period of short duration between June and August. The average annual precipitation is approximately 2,500 mm and the average annual temperature varies between 25 and 27 °C. Relative air humidity is considered high, varying from 85% to 90% for most of the year (Alvares et al., 2013; Brasil, 1978, 1975).

The parent material in the Apuí region is sandstone of the Beneficient region (Brasil, 1975; CPRM, 2005), while the soils of Manicoré evolved from Rondonian granites (Brasil, 1978). The relief is characterized by plateaus in the highest parts that exhibit a flat topography, while the edge zone is marked by aligned hills and crests. These plateaus are combined with lower areas at the foothills, where pediplains are locally interrupted by flat top hills (Brasil, 1978; CPRM, 2001). The vegetation is

124 characterized as Dense Tropical Forest, consisting of densified and multi-stratified
125 trees, with heights varying between 20 and 50 m (Brasil, 1978).
126 The A horizons of ten profiles were chosen to be researched in agreement with
127 previous investigations on these soils conducted by Aquino et al. (2016) and Santos
128 et al. (2018, 2013). The ADEs 1, 2, 3 and 4 correspond to horizon Au_1 of soil profiles
129 1, 2, 3 and 4 studied by Santos et al. (2018), respectively. The ADEs 5 and 6 match
130 with horizon Ap1 of soil profiles 1 an 2 evaluated by Aquino et al. (2016). Furthermore,
131 the ADEs 7, 8, 9 and 10 correspond to the horizons Aup_1 of soil profiles 5, 1, 4 and 3
132 analyzed by Santos et al. (2013).
133 The samples were previously air-dried, the clods were broken and sieved in a 2
134 mm mesh, resulting in the air-dried soil, used for the rheological characterization of
135 ADEs. Information about the physical and chemical characteristics of the analyzed
136 ADEs are given in detail in table 1.
137
138 **2.2 Experimental design**
139 Each ADE was analyzed separately in a completely randomized design with
140 four treatments, consisting of the untreated soil (OX_0), i.e. soil analyzed in natural
141 condition and three levels of soil organic carbon (SOC) oxidation (OX_1, OX_2 and OX_3),
142 with each three replicates. For each oxidation treatment, about 200 g of air-dried soil
143 were placed in glass containers together with 100 ml of distilled water. Then repeatedly
144 5 ml of concentrated hydrogen peroxide (H_2O_2 35%) were added, stirred with a glass
145 rod and allowed to stand at room temperature for 48 hours until completing the volumes
146 of 40 ml (OX_1), 80 ml (OX_2) e 120 ml (OX_3) of H_2O_2, corresponding to 0.2, 0.4 and 0.4
147 ml H_2O_2 per g of soil, respectively. Eventually, the soil-solution mixture remained
148 unaltered until no reaction was observed anymore. The soil was then dried in a

149 ventilated oven at 50°C, the clods were broken and sieved in a 2.0 mm mesh and
150 prepared for rheometry. An aliquot of approximately 2 g of each treatment was ground
151 in an agate mortar and analyzed in an elementary CHNS autoanalyzer (model Flash
152 EA 1112, Thermo Finigan) to determine the total soil organic carbon (SOC) content by
153 dry combustion.
154
155 **2.3 Samples preparation for analysis on the rheometer**
156 The samples were moistened with distilled water to a gravimetric water content
157 between 0.1 e 0.3 g g^{-1}, according to the texture of each ADE (sandy to clayey soil
158 texture, respectively), and left in air-tight sealed containers for approximately 24 hours.
159 Consequently, the moistened soil was compacted in metallic rings of approximately
160 3.6 cm in diameter and 1.0 cm in height to their corresponding field density (Table 1).
161 From all three oxidation treatments as well as from the untreated soil, each three
162 samples were mounted for amplitude sweep tests. Additionally, nine samples were
163 packed of the untreated soil to conduct the resilience tests (thixotropy), i.e. three
164 samples per strain level applied.
165 The samples were saturated with distilled water for approximately 24 h and
166 analyzed in a compact modular rheometer (Anton Paar MCR 102), with a parallel plate
167 measuring device, a fixed roughened lower plate of 50 mm in diameter and a
168 roughened upper rotary plate of 25 mm in diameter (PP25 / P2 model) according to
169 Markgraf et al. (2006). Samples were placed on the bottom plate, liberated from the
170 metal rings, cut in height of 4 mm and diameter 25 mm for analysis in the apparatus
171 (Pértile et al., 2018) and submitted to the oscillatory test with amplitude sweep and
172 controlled strain.
173

2.4 Amplitude sweep test

The rheometric analyses were controlled and executed automatically by the software Rheoplus/32 V3.62 Anton Paar under the following conditions: plate distance (gap) = 4 mm; rest period before the start of the test = 30 s; strain amplitude = continuous ramp from 0.0001 to 100%; angular frequency = 0.5 Hz; temperature = 20 °C; normal force = between 0 e 12 N; number of measurement points = 30; test duration = about 14 min.

In oscillatory amplitude sweep tests, the shear stress (τ, Pa) is a result of the force required to generate shear strain (γ, %) along the shear surface (Holthusen et al., 2010), being calculated from the torque (M, mN) measured at each γ level and the corresponding upper plate radius (r, m), according to equation 1, while γ is determined by the ratio of deflection distance (s, m) at the sample's outer edge and gap size (h, m), as given by equation 2.

$$\tau = \frac{2M}{\pi r^3} \quad (1)$$

$$\gamma = \frac{s}{h} * 100 \quad (2)$$

From these parameters, we calculate the storage modulus (*G'*, Pa), the loss modulus (*G"*, Pa) and the loss factor (tan δ, dimensionless) (Figure 1a) with equations 3, 4 and 5 respectively. This adjustment derives from the presence of viscoelastic behavior under oscillatory shear and the thus complex shear modulus G*, which accounts for both elastic (*G'*) and plastic/viscous behavior (*G"*) (Holthusen et al., 2010a; Markgraf et al., 2006b; Mezger, 2014a; Pértile et al., 2016, 2018).

$$G' = \frac{\tau}{\gamma} cos\delta \quad (3)$$

$$G'' = \frac{\tau}{\gamma} sen\delta \quad (4)$$

$$\tan\delta = \frac{G''}{G'} \quad (5)$$

193

194 The *G'* represents the of the elasticity material, where the stress energy is stored
195 and can be released after the test, while *G"* represents the viscous component, where
196 the imaginary part of the elasticity is lost, with the energy being released in the form of
197 shear heat to start the flow (Schramm, 2006). When *G'* is greater than *G"* ($\delta < 1$), elastic
198 strain predominates, but when *G"* is greater than *G'*, namely after cross over (Figure
199 1a), the strains are predominantly plastic, and viscous flow of the soil occurs

200 The linear viscoelastic range (LVR) is the interval of fully reversible strain,
201 starting with the lowest strain and being limited by *G'* deviating more than 5 % from a
202 linear curve (Holthusen et al., 2012b). The end of the LVR is delimited by strain limit
203 (γ_{LVR}). Strains greater than γ_{LVR} promote irreversible and cumulative modifications in
204 the soil microstructure, though initially with predominance of the elastic behavior,
205 resulting in a transition phase of both decreasing *G'* and *G"*. This phase ends with the
206 crossover (or yield point, YP), where *G'* = *G"*, denoted by the strain (γ_{YP}) (Figure 1b).
207 Besides the strain values, it is also possible to determine the shear stress at the end
208 of the LVR range and at the YP.

209 Other two important rheological properties are the integral z (I_z) and the
210 maximum shear stress (τ_{max}). The I_z is calculated by the area in between the actual tan
211 δ during the amplitude sweep test until the YP (where tan δ = 1) and a horizontal line
212 of tan δ = 1 (Equation (1)6, Figure 1a). The higher its value, the greater the elastic
213 behavior of the soil and the greater is its microstructural rigidity (Baumgarten et al.,
214 2013; Stoppe and Horn, 2018). The τ_{max} (Figure 1b) characterizes the maximum

internal resistance that the soil sample offers to resist the rupture of its microstructure (Holthusen et al., 2010, 2012b).

$$\int_{0.0001}^{YP} (1 - \tan\delta)\, dx \tag{6}$$

Further details of the rheology fundamentals related to soil mechanics are described by Barnes, (2000); Holthusen et al., (2012a,b, 2010); Markgraf et al., (2006); Schramm, (2006).

2.5 Resilience analysis

Resilience analysis aims at detecting a sample's time-dependent structural regeneration or resilience, i.e. ability to recover from a high shear or high strain impact (Mezger, 2014). This behavior is also called thixotropy. As in the amplitude sweep test, we used controlled strain, but different strain levels to simulate different shear intensity.

The thixotropy test was performed as a three-step-strain of 1) low, 2) high and 3) again low strain (Figure 2a). In step 1, we applied for 300 s a strain of 0.002 %, which is within the linear viscoelastic range. In step 2, we apply a presumably destructive strain of 0.01, 1 or 100 % for 300 s sand in step 3, we return the initially applied strain (0.002 %) 900 s.

The recovery after the high strain (step 2) was determined as the ratio of the storage modulus (*G'*) at each time interval of step 3 in relation to the average initial value *G'* exhibited at step 1(low strain), as demonstrated in the equation 7 and seen in the figure 2b.

$$R(\%) = \frac{G'_{t_{2}+i}}{\frac{1}{n}\sum_{i=1}^{t_1} G'_i} * 100 \quad (7)$$

236

237 where R is the structural recover (%), *G'* is the storage modulus (Pa) and t is
238 the time interval of each step (Figure 2).

239 The configurations used in each step of the thixotropic analysis were controlled
240 and executed automatically by the software Rheoplus (version 3.62, Anton Paar)
241 under the following conditions: plate distance (gap) = 4 mm; rest period before the start
242 of the test = 30 s; angular frequency = 0.5 Hz; temperature = 20 °C; normal force =
243 between 0 e 12 N.

244

245 **2.6 Statistical analysis**

246 To characterize the microstructural resilience and resistance in natural condition
247 (untreated soil) of the ADEs, we performed descriptive statistics of rheological
248 variables, and Pearson's correlation analysis to verify the possible effects of physico-
249 chemical properties on soil rheology.

250 To verify the effect of the C content reduction on the microstructural resistance,
251 we tested for normality (Shapiro and Wilk, 1965) and homoscedasticity (Levene, 1960),
252 transforming the data if necessary for $\sqrt{x+1}$. Afterwards, we performed analysis of
253 variance by means of the F test, and, when significant, we compared the mean values
254 by the Scott Knott test at 5% of significance. All data were analyzed using the R
255 statistical environment, version 3.5.0. (R Development Core Team, 2017).

256

3 RESULTS

3.1 Rheology of Archaeological Dark Earths (ADEs)

The strain at the end of the linear viscoelastic interval limit (γ_{LVR}) of the ADEs ranged from 0.008 to 0.04% (Figure 3a). The ADE 9 was the soil with the highest γ_{LVR}, with a value three times higher than the overall average of all ADEs analyzed. On the other hand, ADEs 1, 5 and 8 exhibited lower reversible strain, with values of γ_{LVR} remaining below 0.01%. The stress at the end of the linear viscoelastic range (τ_{LVR}) was the rheological variable with the greatest variability, ranging from 33 to 268 Pa, where the latter, as observed in ADE 9, was 8 times higher than the minimum value observed in ADE 2 (Figure 3b).

The maximum shear stress (τ_{max}) exhibited a similar pattern as τ_{LVR}. The highest values of τ_{max} were found in the ADEs 9 e 8, being 123 and 68% higher than the average, respectively. The lowest values were observed in ADEs 2 and 10, being 56 and 45% lower than the average, respectively (Figure 3c).

The parameters strain at the yield point (YP, i.e. transition to flow behavior), γ_{YP}, and the integral Iz presented a similar pattern among themselves, but different from previous rheological variables. The highest value was verified in ADE 6, followed by ADEs 1 e 4, who supported 94, 82 e 81% of strain until flow (Figure 3d) and showed Iz of 35.9, 34.1 e 33.3 respectively (Figure 3e). However, the lowest values were observed in ADEs 7 e 8, that with only 46 and 45% of strain already exhibited predominantly viscous behavior (i.e. after the YP), at Iz of 19,6 and 17,6 respectively. The ADEs 2, 3, 9 e 10 presented intermediate values, close to the overall averages of all ADEs of 70% for γ_{YP} and of 28.5 for Iz.

The pattern of γ_{YP} found in the ADEs was not repeated in the stress at yield point, G'_{YP}. Instead, the highest resistance of 420 Pa was verified in ADE 9, followed

282 by ADEs 5 and 8, with 243 and 228 Pa respectively, while the lowest values were 70
283 and 90 Pa, observed in ADEs 10 and 7 (Figure 3f).

284 When analyzing the effect of texture and SOC content on γ_{LVR}, we verified that
285 an increase of SOC/clay ratio increased γ_{LVR} as seen in table 2. Similarly to γ_{LVR}, the
286 τ_{LVR} also showed a significant positive correlation with the SOC/clay ratio, as well as
287 with the silt/clay ratio. Similar to γ_{LVR} and τ_{LVR}, the increase of SOC/clay ratio also
288 increased τ_{max}. Increase of the silt/clay ratio and a higher soil bulk density also provided
289 increase of these parameters. The ADE 9, besides the high SOC content, also has the
290 highest silt content and a high density.

291 Correlating γ_{YP} and Iz with the physical and chemical properties of ADEs, they
292 exhibited similar correlations as seen in table 2. We verified an influence of the
293 parameters linked to soil texture, bulk density, and cations concentration and type. The
294 increase in sand content, sand/clay ratio and bulk density reduced γ_{YP}, as can be
295 observed for ADEs 7 e 8, which are the soils with the highest sand content and bulk
296 density (Table 1) and reduced values of γ_{YP} and Iz. However, the increase in the
297 SOC/sand ratio or greater clay content caused an opposite effect. There was also a
298 negative correlation between the ratio of monovalent to bivalent cations (K/[Ca+Mg]),
299 as well as the Al saturation (m) with γ_{YP} and Iz (Table 2).

300

301 **3.2 Resilience of Archaeological Dark Earths (ADEs)**

302 We verified different microstructural resilience for the ADEs for all strains
303 applied in the thixotropy test (Figure 4). When we apply the strain of 0.01%, all ADEs,
304 except for ADE 8, presented total recovery within the given time interval. The ADEs 2,
305 6, 9 and 10 even presented microstructural resistance at the end of the test (Figure

306 2b) higher than the initial, (reference) condition (step 1, Figure 2b), reaching values
307 above 105% of resilience (Figure 4).

308 When subjected to 1% strain, the ADEs exhibited less ability to recover, ranging
309 from 16 to 49% in the ADE 8 and ADE 9, respectively. With 100% strain, all ADEs lost
310 their ability to recover, reestablishing no more than 3.5% of the initial microstructural
311 stiffness, as seen in ADE 2. In some ADEs, the resilience was less than 1% (ADEs 3,
312 5, 7, 8 and 10). The greatest difference between resilience after strain of 1 and 100%
313 was observed in ADE 10, with a 72-fold reduction in the recovery of the microstructural
314 stiffness.

315 When analyzing the resilience in time, we found that the recovery of
316 microstructure strength is fast (Figure 5). Regardless of the intensity of the strain
317 applied or the physical-chemical properties of the ADEs, more than 75% of total
318 recovery occurred in the first 100 s. However, small differences in recovery time
319 occurred between the strain intensities. For samples that received strain of 0.01% in
320 step 2, more than 90% of the recovery occurred within the first 10 s. When the strain
321 intensities of 1 and 100% were applied, the samples took on average 300 and 200 s,
322 respectively, to reach 90% of the total recovery.

323 When comparing the relative resilience between strain intensities of 1 and
324 100%, we found faster recovery for ADEs 1, 2, 3, 4 and 6 subjected to strain of 100%.
325 However, the difference was very low after 100s (Figure 5). While the ADEs 7 and 8
326 showed a faster recovery at strain intensity of 1% compared to 100%, for the ADEs 5,
327 9 and 10, we did not find differences in the recovery speed.

328 Correlating the resilience with the rheological properties of the ADEs, we verified
329 positive correlation with strain at the yield point (γ_{YP}) and with integral z (Iz) when we
330 applied strain intensity of 0.01% to the samples, and with the strain (γ_{LVR}) and stress

331 (τ_{LVR}) at the end of viscoelastic linear range, storage modulus value (G'_{YP}) and
332 maximum shear stress(τ) when we submitted the samples to a strain intensity of 1%.
333 Considering the physical and chemical properties of the soil, there was a
334 positive and significant correlation of soil recovery capacity with the silt, SOC, Ca^{+2} and
335 K^{+} contents and with base saturation when we applied 0.01% strain to the samples, as
336 seen in table 3. At the same strain intensity, there was also negative correlation with
337 sand content, Al concentration, and ratios of Mg/Ca, K/Ca, K/(Mg+Ca), sand/clay and
338 sand/silt ratios. For the samples subjected to the strain intensity of 1%, we verified a
339 positive correlation with silt and SOC contents, and with the SOC/sand ratio and a
340 negative correlation with flocculation degree. There was no significant correlation
341 between the resilience and soil rheological, physical and chemical properties at the
342 strain intensity of 100% (Table 3).
343
344 **3.3 Soil organic carbon (SOC) reduction and effect on microstructure**
345 In general, the oxidation resulted in reduced SOC content, as demonstrated in
346 table 4. The SOC content reduction occurred in a differentiated way between ADEs.
347 Comparing the control (OX_0) with the highest level of oxidation (OX_3), the reduction in
348 SOC content ranged from 25% (ADE 5) to 71% (ADE 10), but this variation was not
349 related to the initial SOC content.
350 The reduction in SOC content followed a linear trend in the ADEs 1, 5, 6 and
351 10. However, for the ADEs 4 and 7, we found on average 60% reduction of the SOC
352 content with the first 80 ml of H_2O_2 added (OX_2), while adding further 40 ml (OX_3) did
353 only decrease the value by 5 %, following a trend of exponential decrease. On the
354 contrary, for the ADEs 3 and 9, we observed a considerable reduction only for OX_3,
355 with losses of 38 and 45% in the SOC content in relation to level OX_2.

356 Overall, SOC content reduction decreased the rheological variables of ADEs
357 (Figure 6 to 12). The γ_{LVR} decreased on average 62%, with the greatest reductions
358 observed in ADEs 9 (85%), 6 (78%) and 3 (72%) and the smallest in ADE 5 (25%)
359 (Figure 6). However, the impact of the SOC reduction over γ_{LVR} was different between
360 the ADEs. In ADEs 3 and 9, only reduction of SOC greater than 45% in OX_3 caused a
361 significant decrease in γ_{LVR}, while in the ADE 1, 6 and 10, an average reduction of only
362 8% SOC in OX_1, caused the same effect. Already for ADE 7, a reduction of 24% in
363 SOC content in OX_1 caused so much impact to the γ_{LVR} that even with successive
364 losses of 54% (OX_2) and 14% (OX_3) in SOC, there was no significant reduction of γ_{LVR}
365 (Figure 6).

366 The stress at the end of the linear viscoelastic range τ_{LVR} was affected more by
367 the loss of carbon than the corresponding strain γ_{LVR} (Figure 7). Comparing OX_0 and
368 OX_3, we found an average reduction of around 75% in τ_{LVR}, with values reaching
369 approximately 90% in ADEs 4 and 6. ADEs 1, 3, 4, 6 and 10 were strongly affected by
370 SOC loss, that a comparatively small loss of 12% of SOC in OX_1 already caused a
371 decrease of 82% in τ_{LVR}. Further oxidation of SOC did not cause significant decrease
372 in τ_{LVR} despite a more pronounced SOC loss from OX_1 to the other oxidation levels
373 than from OX_0 to OX_1. While τ_{LVR} decreased by 87% from OX_0 to OX_1, it increased 3-
374 fold from OX_1 to OX_2 and OX_3.

375 The behavior of τ_{max} was very similar to that of τ_{LVR} (Figure 8). In ADEs 1, 3, 4,
376 6 and 10 there was a significant difference already in the first oxidation level, which
377 itself did not differ from OX_2 and OX_3. The average reduction from OX_0 to OX_3 was
378 86%. Similarly, the SOC loss in ADE 7 in OX_1 caused a reduction of 85% in τ_{max}.
379 However, in the more intense SOC oxidation in OX_2 and OX_3 provided a significant
380 increase in τ_{max}.

Except for ADE 10, SOC oxidation at all levels caused a significant decrease of *G'* at the yield point (G'_{YP}) in relation to OX_0 as seen in figure 9. In ADEs 1, 4, 5, 6, 7, and 9, an average loss of 15% in SOC caused a significant reduction of 76% in G'_{YP} from OX_0 to OX_1. When we compared OX_1 with OX_2 and OX_3, we did not observe a significant effect of SOC reduction on G'_{YP}. The G'_{YP} decreased on average 75%.

The γ_{YP} and Iz of ADE 9 decreased linearly with SOC reduction, with values in in OX_3 51 and 53% lower than in OX_0, respectively. For ADEs 3 and 6, there was a drastic reduction of more than 35 and 50%, respectively, for these variables from OX_0 to OX_1, while additional SOC losses did not cause any further effect. For ADEs 1, 4, 7 and 10, SOC oxidation caused a reduction of γ_{YP} and Iz in OX_1, but at high SOC oxidation levels (OX_2 and OX_3), these rheological variables increased again, reaching values equal to and even higher than the control (Figure 1 and 11).

To relate the reduction in rheological parameters to the loss of SOC, we divided the relative decrease in a given rheological parameter (in %) by the loss of SOC (in g) between OX_0 and OX_3. In figure 12it is possible to observe that the SOC loss of only 1 g kg^{-1} of soil (0.1%) decreased the γ_{LVR} of ADEs by approximately 1.3%. In addition, the effect of SOC reduction was more severe in ADE 1, where the SOC loss of 1 g kg^{-1} of soil decreased 1.96% the γ_{LVR}.

The τ_{LVR} and τ_{max} showed very similar reduction pattern, with very close values among all ADEs. They reduced on average 1.6% per g of SOC loss, with the highest reduction verified in ADEs 1, which reduced approximately 2.6% g^{-1} of SOC lost (Figure 12), which corresponds to a loss of 1.56 and 13.3 Pa in shear stress for τ_{LVR} and τ_{max} respectively.

The SOC loss caused largest reduction on G'_{YP}, where each gram of carbon lost reduced this rheological variable, in average, by 1.8%. The greatest reductions

406 occurred for ADES 1 and 5, with decreasing of 2.8 and 2.7% in G'_{YP}. Furthermore, γ_{YP}
407 and Iz presented average reduction of only 0.45%. Differently from the previous
408 rheological variables, there was increase in the γ_{YP} of the ADEs 4 and 10 as well as in
409 the Iz of the ADE 4 with the reduction of the carbon content (Figure 12).
410
411 **4 DISCUSSION**
412 **4.1 Rheology of Archaeological Dark Earths**
413 The rheological variables obtained by an amplitude sweep test, according to
414 their characteristics and determination, indicate different conditions in the
415 microstructural rigidity within the same soil (Pértile et al., 2018). The microstructural
416 stiffness can be defined as the ability of microstructure to withstand tension and
417 bending. One the one hand, a rigid microstructure presents greater resistance to strain.
418 On the other hand, it can have a higher elasticity, that is a larger linear viscoelastic
419 range and, furthermore, can withstand greater strain before collapse or shear at yield
420 point.
421 The variables τ_{LVR}, τ_{max} and G'_{YP} express the resistance mobilized in
422 correspondence to a given strain at the end of linear viscoelastic range (LVR), at the
423 maximum shear stress and at the yield point (YP), respectively. On the other hand,
424 γ_{LVR} and γ_{YP} inform the strain amplitude supported by the microstructure to reach the
425 limit of viscoelastic strain (LVR) and the yield point (YP), respectively. The integral z is
426 highly correlated to the γ_{YP} due to the calculation based upon the yield point and the
427 relatively large share of larger strains close to the YP instead of the smaller strains
428 closer to the LVR.
429 A soil property can induce, simultaneously, increase of resistance evaluated by
430 the rheological variables τ_{LVR}, τ_{max} and G'_{YP} and decrease of elasticity verified by the

variables γ_{LVR}, a γ_{YP} and Iz, or vice versa, leading to erroneous interpretations on microstructural stiffness when considering parameters separately. For this reason, τ_{LVR}, τ_{max} and G'_{YP} will be treated as rheological resistance variables, and γ_{LVR}, a γ_{YP} and Iz as elasticity variables, according to the proposed division by Holthusen et al. (2019).

In this study, particle size distribution and bulk density caused this apparently contradictory effect, increasing resistance and reducing elasticity of microstructure. The high values of τ_{LVR} , G'_{YP} P and τ_{max} observed in the silty and sandy ADEs (ADEs 5, 6, 8 and 9) are the result of increased friction due to increased contact area between coarse particles (Reichert, 2010), which restricts the particles' movement in their predetermined positions (Holthusen et al., 2010a).

The ADEs with higher bulk density (ADEs 5, 8 and 9) also showed high resistance and, in the case of ADEs 5 and 8, also lower elasticity. The soil bulk density also acts on the shear stress increase by means of a higher number of contact points between particles (Braida et al., 2007). In addition, the movements related to shear, in oscillatory tests, provide a reorganization of packing of these particles (Cho et al., 2006), enabling a compact arrangement, which is energetically more stable (Stoppe and Horn, 2018), increasing the microstructure strength during the shear test until the complete collapse of the sample, which occurs after the maximum shear stress.

Differently from ADEs 5 and 8, the ADE 9 has a SOC content 12 to 70% greater than all the other ADEs, which probably resulted in a strongly different γ_{LVR} in comparison with them, even with larger particles associated with the loamy texture. As clay and SOC contents increase, larger (i. e. predominantly sand) particles, previously in direct contact, are now interconnected by clay particles and clay-humus-colloids (Vallejo and Mawby, 2000). The loss of direct contact points between these large

456 particles results in hence lower friction, providing greater slippage between sand
457 particles and lower shear strength. However, at the same time, this phenomenon gives
458 greater elasticity to microstructure of ADEs with higher clay and/or SOC content, like
459 ADEs 4, 6 and 9, due to the electrostatic forces between clay and SOC.

460 These different directions of elasticity and resistance parameters corroborate
461 with those of Stoppe and Horn (2018). When investigating the microstructural stability
462 of riparian soils along the Elbe estuary in northern Germany, these authors found a
463 decrease in elasticity and increase in resistance of microstructure with increment of
464 sand and silt contents, mainly in saturated soil conditions. Similarly, Holthusen et al.
465 (2012b), when studying the flow behavior and strain of soil microstructure, observed
466 high shear stresses in soils with lower clay content. Our results agree with those found
467 by Rocha et al. (2002), who observed that the increase of clay content decreases the
468 shear strength of soil at low water tension (1 kPa) when submitted to direct shear test
469 in a quasi-saturated condition.

470 However, divergent results were found by Pértile et al. (2016), who verified
471 higher microstructural strength in drained soils with high clay content. These authors
472 attributed the greater resistance to cohesion and menisci contraction force, especially
473 in soils with higher water stresses. Our study was conducted with saturated soil, where
474 capillary forces and cohesion are substantially reduced, which would explain the
475 difference in the impact of texture.

476 The concentration and type of cations in soil solution also affected the
477 microstructure elasticity of ADEs by the interaction among ions and electric charges
478 on mineral and organic particles surface. Higher base saturation (V) increased γ_{YP} and
479 Iz, mainly due to a higher proportion of Ca^{+2} in relation to other cations, since the
480 increase in K/Ca and Mg/Ca ratios showed a negative correlation with these variables.

481 This reflects the lower values of γ_{YP} and Iz in ADEs 7 and 8, which among the analyzed
482 soils were those with lowest V and m, lower Ca^{+2} content and high Al saturation.
483 The Ca^{+2} acted as stabilizing agent of elastic component of microstructure,
484 delaying the flow (yield point) of ADEs and, consequently providing greater Iz. The
485 Ca^{+2} effect on soil particles flocculation and in structure stabilization is well known
486 (Chorom and Rengasamy, 1995; Holthusen et al., 2012; Lee et al., 2012; Paradelo et
487 al., 2013). This stabilization can occur through the formation of organometallic
488 complexes, with Ca^{+2} acting in polycationic bridges between organic molecules,
489 improving the microaggregates stability (Bronick and Lal, 2005; Tisdall and Oades,
490 1982). Also, it might have reduced the diffuse double layer, decreasing the repulsive
491 forces of particles with similar electrical charges (Hillel, 2004; Mahanta et al., 2012),
492 increasing stable associations between particles (Brandenburg and Lagaly, 1988).
493 However, there was no Ca^{+2} stabilizing effect on the microstructural strength
494 parameters of the ADEs.
495 The increase in proportion of K^+ in relation to polyvalent cations reduced the
496 ADEs microstructure stability, similar to those results found by Paradelo et al. (2013).
497 The authors verified a destabilizing effect on clay particles caused by salts containing
498 K^+, adversely affecting soil structure after 80 years of continuous fertilizer application.
499 Holthusen et al. (2012b) also observed a decrease in the structural resistance on the
500 microscale of clayey soils with increasing K^+ content in long-term potassium fertilization
501 experiments in Germany. The monovalent ions like K^+ and Na^+, in soil solution,
502 increase the double electric layer thickness, causing rupture of associations between
503 particles (Brandenburg and Lagaly, 1988), favoring dispersion (Mahanta et al., 2012).
504 As a consequence, particle separation occurs, making SOC available for degradation
505 (Bronick and Lal, 2005).

4.1 Resilience of Archaeological Dark Earths

Thixotropy denotes the regeneration capacity of a material to, more or less fast, recover structural strength after high shear strain (Mezger, 2014; Schramm, 2006). The three-step test was effective in evaluating microstructure recovery and can be used to determine resilience of soil on the particle scale when subjected to transient stresses. It also allows establishing relationships of other soil properties with resilience, being very sensitive to modifications in physicochemical properties.

In this study, we verified complete recovery of microstructural resistance of ADE only for samples submitted to strain intensity of 0.01%. Furthermore, some ADEs even presented resilience greater than 100%. This strain intensity was not enough to cause damage to the soil recovery capacity. However, it may have caused a small reorganization in the microstructure, providing a condition of greater stability microstructural resistance with respect to the initial condition.

At the other strain intensities, the recovery of the microstructure was strongly compromised. This is because the intensity of disturbance was higher than the critical level supported by the soil microstructure. According to Lal (1993), resilience is a feature based on the restoration process, where degradations above the critical level compromise the structure and functionality of ecosystem processes, with loss of recovery capacity. For microstructure, this critical limit occurs at the end of linear viscoelastic (LVR) range. The strain intensity of 0.01% remained within the linear viscoelastic range and very close to the average of the strain limit (γ_{LVR}) of ADEs, explaining the complete recovery of the microstructure. But the increase of strain beyond this interval causes irreversible and cumulative changes in soil microstructure (Mezger, 2014).

530 Noteworthy, also the maximum shear stress (τ_{max}) was reached before 1%
531 strain. The τ_{max} can be defined as the maximum resistance of soil microstructure
532 against oscillatory movement (Holthusen et al., 2010a; Markgraf et al., 2006b), where
533 additional strain above τ_{max} causes rupture of the bonds among soil particles. Thus,
534 being both beyond the strain limit (LVR) and the strain at maximum shear strength, a
535 strain of 1 % used in the resilience tests compromised the ADEs microstructural
536 resilience.

537 Furthermore, resilience depends on the magnitude of degrading action. By
538 increasing the disturbance intensity to 100% strain, the resilience was further
539 pronouncedly reduced. All ADEs submitted to thixotropic analysis presented flow
540 (yielding) before a strain of 100%. Beyond the yield point, the particles irreversibly alter
541 their positions and arrangement (Schram, 2006), irreversibly deforming the bulk soil
542 (Holthusen et al., 2012, 2010; Markgraf et al., 2012).

543 Even if small, there is a recovery of microstructure resistance after flow, which
544 can be a result of soil particle reorganization, which provided new
545 connections/links/bonds after the rupture of previous bonds. Already with 1 % strain, a
546 recovery of resistance (by means *G'*) occurred, partly by reestablishing the pre-existing
547 links that were broken by disturbance, as well as by new interactions after the particles'
548 partial reorganization.

549 Regardless of disturbance intensity, the recovery of the microstructure
550 happened quite fast. Arthur et al. (2012), when analyzing the structural resilience at
551 the mesoscale after uniaxial compression of soils under different managements, also
552 verified fast elastic reorganization of soil structure. This can be due to the reactivity of
553 soil colloids, which perform almost instantaneous exchanges with the ions in soil

554 solution (Brady and Weil, 2013) and with adjacent particles, mainly in saturated soil
555 conditions.

556 When we correlate the resilience of the microstructure with the rheological
557 variables, we observed that the ADEs with a more elastic microstructure, i.e. higher
558 γ_{LVR} and higher strain range before flow (γ_{YP}), and ADEs with higher microstructural
559 resistance, ie, higher τ_{LVR}, τ_{max} and $G'_{YP,}$ are more resilient. This can be explained by
560 the viscoelasticity theory of soil microstructure: When the soil undergoes transient
561 tension, especially of short duration, a percentage of any generated shear energy is
562 temporarily and elastically stored, and the rest induces the viscous flow, i.e. permanent
563 disturbances in the microstructure (Ghezzehei and Or, 2001; Markgraf et al., 2006).

564 The more elastic the soil, the greater was the microstructural capacity to
565 dissipate the energy stored during the disturbance, resulting in a greater recovery, i.e.
566 greater soil resilience. Furthermore, the greater the linkage strength between soil
567 particles, the smaller is their breakage during a disturbance and the smaller is the
568 damage to soil microstructure, leading to greater resilience.

569 Similar to the rheological variables obtained with the amplitude sweep test,
570 resilience was also correlated to soil physical and chemical properties. This leads us
571 to believe that the factors involved in the resistance and elasticity of the microstructure
572 are the same ones that act on the microstructural resilience. Seybold et al. (1999) state
573 that factors and processes that interfere with resilience are the same ones that act in
574 soil formation, acting in a continuous, simultaneous and interdependent manner.

575 Among the factors favoring resilience stand out high SOC content (Ajayi and
576 Horn, 2017; Arthur et al., 2012), higher proportion of particles in the clay fraction
577 (Bonetti et al., 2017), and higher cation concentration, mainly of Ca^{+2}. These factors

578 favor the increase of soil reactivity, improving its recovery capacity (Blanco-Canqui and
579 Lal, 2010; Bonetti et al., 2017; Seybold et al., 1999).

580 Although the thixotropic analysis showed promising results in evaluation of soil
581 microstructure resilience, we do not advise to apply strain intensities below γ_{LVR} during
582 step 2 (high strain), since per definition a deformation below the limit of the linear
583 viscoelastic range is supposed to result in fully recoverable strain and thus does not
584 provide additional information. Instead, the strain intensity of 1% in our soils can be
585 considered high, because it is greater than the strain at the maximum shear stress.
586 Thus, future studies should focus on the strain intensities beyond the LVR but below
587 the one causing maximum shear stress. In addition, it is also necessary to evaluate
588 the effect of disturbance time, water content, and changes in physical-chemical
589 properties on soil recovery capacity.

590

591 **4.2 Influence of SOC removal on soil microstructure**

592 The results presented in this paper show that a loss of only 0.1% (1 g kg^{-1}) in
593 SOC content was sufficient to significantly reduce the resistance and elasticity of ADE
594 microstructure. Markgraf and Horn (2007), studying the effect of Fe-(hydr)oxides and
595 of SOC on soil microaggregation stability in southern Brazil, also verified a reduction
596 of the strain limit (γ_{LVR}) and maximum shear stress in H_2O_2-treated soils, evidencing
597 the stabilizing effect of SOC on microstructure stiffness.

598 The SOC influences the aggregation process by the linkage of soil particles
599 favored by microbial activity and by the cementing effect on mineral components (Six
600 et al., 2004). The SOC molecules have a high specific surface and a large number of
601 organic radicals. These radicals interact with the surface of the mineral particles by
602 cation bridges, electrostatic and coordination links, hydrogen bridges and van der

603 Waals forces (Kleber et al., 2007), contributing to soil aggregation (Tisdall and Oades,
604 1982).

605 However, different organic compounds act differently in aggregation; thus, the
606 SOC content reduction can cause different effects on soil structure. The results of this
607 work showed that for some ADEs, a small reduction in SOC content caused great
608 impact on the microstructure, mainly in the elasticity rheological variables. However, in
609 others, the significant effect occurred only with a large loss of SOC content. This is
610 probably related to the quality of SOC in ADEs. The quality of the SOC is related to its
611 composition. The SOC of ADEs is composed mainly of polysaccharides, carboxylic
612 groups, phenols, starch, esters and high content of aromatic structures (Santos, 2018;
613 Schellekens et al., 2017; Zech et al., 1990). According to their composition, these
614 compounds present different resistance to decomposition (i. e. they are more or less
615 labile), remaining in the soil for different periods of time (Essington, 2004; Sposito,
616 2008). Thus, the same perturbation intensity (in this case, H_2O_2 oxidation levels) can
617 cause pronounced losses of SOC in soils with high labile SOC content. The different
618 compositions and lability would explain the difference in the amount of SOC lost in
619 each level of ADEs oxidation.

620 Furthermore, the large destabilizing impact in the first oxidation level, as
621 observed in ADEs 1, 3, 4, 6, 7 and 10, could be explained by oxidation of more simple
622 and labile molecules, such as carbohydrates. These compounds play different roles in
623 aggregation of ADEs, providing great stability of aggregates to the soil for a short
624 period of time (Abiven et al., 2009). On the other hand Kleber et al. (2007) point out
625 that some SOC components, like proteins, are capable of attaching irreversibly to
626 minerals surface by means of covalent chemical bonds. Due to this feature and
627 relatively high abundance in soils, they play a predominant role in structure of organo-

628 mineral complexes, with high resistance to disaggregation and might be present in
629 ADEs 5 and 9. For these ADEs, significant changes in most rheological variables
630 occurred at more intense oxidation levels.

631 For the ADES 1, 2, 3 and 4 the SOC had been chemically fractionated in the
632 fractions fulvic acid (FA), humic acid (HA) and humin (HUM) by Santos et al. (2018),
633 based on solubility in acid and alkaline medium. These authors observed a great
634 variation in the composition of the SOC among these ADEs and found indicatives of
635 different degrees of SOC stability and of different mechanisms of interaction with the
636 soil minerals. Associating this with our results, we observed that ADE 4 shows a high
637 abundance of labile SOC (FA) and a large loss of SOC with low oxidation intensity,
638 while ADE 1 show high proportion of more stable SOC (HUM) and low loss of SOC at
639 high oxidation intensities.

640 Using the data of the chemical fractionation of the SOC and correlating it to the
641 rheological variables for the ADEs 1 to 4, we observed a significant and positive
642 correlation of the rheological variables τ_{LVR} and τ_{max} with the ratio of the alkaline extract
643 carbon content (i.e. sum of fulvic acid (FA) and humic acid (HA)) and the humin fraction
644 carbon content (HUM) [(FA+HA)/HUM)]. In addition, we also observed a positive
645 correlation with τ_{max} and fraction of FA. The FA and HA are quite effective in soil
646 aggregation (Fortun et al., 1990) and demonstrate great effects on the stability of soil
647 aggregates in a short time period (Abiven et al., 2009). The FA can form stronger
648 complexes with the mineral fraction because of its size, solubility and reactivity, and
649 constitute one of the main agents of formation and stability of aggregates in weathered
650 soils (Mendonça and Rowell, 1996) and in soils associated with ADEs (Glaser and
651 Birk, 2012; Kämpf and Kern, 2005).

652 Therefore, the reduction of FA due to oxidation can cause rupture of bonds
653 between particles, dispersing them. In addition, the FA is more labile in soil and
654 susceptible to degradation (Sposito, 2008). Thus, a small loss of this fraction of the
655 SOC already in the first level of oxidation (OX_1), possibly greatly reduced the stability
656 of the ADEs microstructure, mainly of the rheological variables of resistance.
657 The HA also plays an important role in aggregation because it forms organo-
658 mineral complexes with the soil particles more persistent over time than with FA
659 (Abiven et al., 2009; Chilom et al., 2009; Tisdall and Oades, 1982). In addition, there
660 is great variation in the proportions of the humic substances between and among the
661 ADEs (Glaser et al., 2000; Santos et al., 2018; Schellekens et al., 2017). Thus, the
662 same intensity of disturbance (e.g. same SOC oxidation levels) can cause different
663 effects on the ADEs microstructure, with the smallest reduction in the rheological
664 variables of the ADEs with greater proportion of HA. This could explain the great impact
665 of the loss of SOC on the microstructure of ADEs 1, 4 ,6 and 10 already at the first
666 level of oxidation, while in ADEs 3 and 9, significant impacts occurred only at higher
667 levels of SOC oxidation (OX_2 and OX_3). This strengthens the evidence that the SOC
668 quality has greater effect on the ADEs microstructural stability than SOC amount.
669 Despite the evident negative effect of the SOC content decrease on the
670 microstructure, the reduction of the resistance and elasticity of ADEs' microstructure
671 could be mitigated by release of inorganic compounds during the oxidation of SOC.
672 This because, differently from the standard for the other ADEs, the reduction of the
673 SOC content increase γ_{YP} and Iz of ADE 4. This increase can be due to the release of
674 cations, mainly of Ca^{+2}, trapped within the organic molecules, being available to act in
675 the aggregation process that during the SOC oxidation. Once released from the
676 molecular structure of SOC, these cations act in the aggregation by the formation of

677 bridges between particles with negative electric charge and by the reduction of the
678 diffuse double layer, as previously discussed.
679 Thereby, it is essential to carry out studies to understand the effect of different
680 amounts of SOC on the ADEs microstructure, as well as of the chemical SOC
681 composition and release of compounds resulting from SOC oxidation on the resistance
682 and microstructural elasticity of these soils.
683
684 **5 CONCLUSIONS**
685 We analyzed the rheological behavior of Archaeological Dark Earths (ADE)
686 under oscillating stress in an amplitude sweep test. We observed that the
687 microstructural resistance (stress at the end of viscoelastic linear range τ_{LVR}, maximum
688 shear stress τ_{max} and storage modulus at yield point G'_{YP}) of ADE was affected by SOC
689 content, particle size distribution, and cation type and concentration. The
690 microstructural resistance of sandy ADEs was higher due to friction among particles,
691 while the microstructural elasticity (strain at the end of viscoelastic linear range γ_{LVR}
692 and at yield point γ_{LVR} and integral z) was reduced. However, the increase in SOC
693 causes lubrication, reducing friction between particles, and consequently increasing
694 microstructural elasticity. The elasticity of microstructure increases with the saturation
695 of bases, being Ca^{+2} the main element involved in microstructural stabilization of ADEs,
696 due to its effect on diffuse double layer reduction, and to act as a bridge between
697 particles with negative electric charge.
698 In a three-interval thixotropy test, we observed evident effect of SOC, clay
699 content and Ca^{+2} concentration on the microstructural resilience of ADEs after intense
700 disturbance. Besides, soil properties that interfered in the rheological variables of the
701 amplitude sweep test were the same that affected the microstructural resilience of

ADEs. In addition, the increase in perturbation intensity decreases the microstructure resilience of ADEs. We recommend using as intense strain in the three-interval test a strain between the linear viscoelastic strain limit (γ_{LVR}) and strain at the maximum shear stress. Regardless of the disturbance and/or amplitude of the resilience, the recovery of the microstructure is quite rapid, with the main portion occurring within 100 seconds.

After reducing the SOC content of ADEs by oxidation with concentrated hydrogen peroxide and submitting them to oscillatory shear tests, we verified that the SOC is a very important factor for the microstructural stability of ADEs. The SOC loss resulted in decreased resistance and elasticity at the particle level, and affected the microstructure differently in each ADE, and these differences are not dependent on the amount of SOC lost.

Acknowledgements

This study was supported by the Federal University of Santa Maria (UFSM) and the Coordination for the Improvement of Higher Education Personnel (Capes) in the form of a doctoral scholarship to the first author. The third and fourth author thank the National Council for Scientific and Technological Development (CNPq) for research fellowships.

6 REFERENCES

Abiven, S., Menasseri, S., Chenu, C., 2009. The effects of organic inputs over time on soil aggregate stability – A literature analysis. Soil Biology and Biochemistry 41, 1–12. https://doi.org/10.1016/j.soilbio.2008.09.015

Ajayi, A.E., Horn, R., 2017. Biochar-Induced Changes in Soil Resilience: Effects of Soil Texture and Biochar Dosage. Pedosphere 27, 236–247. https://doi.org/10.1016/S1002-0160(17)60313-8

Alvares, C.A., Stape, J.L., Sentelhas, P.C., de Moraes Gonçalves, J.L., Sparovek, G., 2013. Köppen's climate classification map for Brazil. Meteorologische Zeitschrift 22, 711–728. https://doi.org/10.1127/0941-2948/2013/0507

Aquino, R.E. de, Marques, J., Campos, M.C.C., Oliveira, I.A. de, Bahia, A.S.R. de S., Santos, L.A.C. dos, 2016. Characteristics of color and iron oxides of clay fraction in Archeological Dark Earth in Apuí region, southern Amazonas. Geoderma 262, 35–44. https://doi.org/10.1016/j.geoderma.2015.07.010

Arthur, E., Schjønning, P., Moldrup, P., de Jonge, L.W., 2012. Soil resistance and resilience to mechanical stresses for three differently managed sandy loam soils. Geoderma 173–174, 50–60. https://doi.org/10.1016/j.geoderma.2012.01.007

Azevedo, A.C. de, Dalmolim, R.S.D., 2004. Soils and environment: an introduction. Pallotti.

Barnes, H. a, 2000. A Handbook of Elementary Rheology. University of Wales Institute of Non-Newtonian Fluid, Aberystwyth. https://doi.org/10.1126/science.1201543

Barros, T.R.M., Lima, H.V. de, Rodrigues, S., Kern, D.C., 2016. Distribution of textural and structural porosity in soils of Archaeological Dark Earth. Ciência Agronômica 47. https://doi.org/10.5935/1806-6690.20160073

Baumgarten, W., Dörner, J., Horn, R., 2013. Microstructural development in volcanic ash soils from South Chile. Soil and Tillage Research 129, 48–60. https://doi.org/10.1016/j.still.2013.01.007

Blanco-Canqui, H., Lal, R., 2010. Soil Resilience and Conservation, in: Principles of Soil Conservation and Management. Springer Netherlands, Dordrecht, pp. 425–447. https://doi.org/10.1007/978-1-4020-8709-7_16

Bokhorst, S., Huiskes, A., Convey, P., Aerts, R., 2007. Climate change effects on organic matter decomposition rates in ecosystems from the Maritime Antarctic and Falkland Islands. Global Change Biology 13, 2642–2653. https://doi.org/10.1111/j.1365-2486.2007.01468.x

Bonetti, J. de A., Anghinoni, I., de Moraes, M.T., Fink, J.R., 2017. Resilience of soils with different texture, mineralogy and organic matter under long-term conservation systems. Soil and Tillage Research 174, 104–112. https://doi.org/10.1016/j.still.2017.06.008

Brady, N.C., Weil, R.R., 2013. Elements of Nature and Soil Properties, 3rd ed. Bookman, Porto Alegre.

Braida, J.A., Reichert, J.M., Reinert, D.J., Soares, J.M.D., 2007. Cohesion and angle of internal friction associated with soil organic carbon and water content in Hapludult. Ciência Rural 37, 1646–1653. https://doi.org/10.1590/S0103-84782007000600022

Brandenburg, U., Lagaly, G., 1988. Rheological properties of sodium montmorillonite dispersions. Applied Clay Science 3, 263–279. https://doi.org/10.1016/0169-1317(88)90033-6

Brasil, 1978. Folha SB. 20 Purus; geologia, geomorfologia, pedologia, vegetação, uso potencial da terra. Projeto RADAMBRASIL, Rio de Janeiro.

Brasil, 1975. Folha SB. 21 Tapajós; geologia, geomorfologia, solos, vegetação e uso potencial da terra. Projeto RADAMBRASIL, Rio de Janeiro.

774 Brito, W.B.M., Campos, M.C.C., Mantovanelli, B.C., da Cunha, J.M., Franciscon, U.,
775 Rodrigues Soares, M.D., 2018. Spatial variability of soil physical properties in
776 Archeological Dark Earths under different uses in southern Amazon. Soil and
777 Tillage Research 182, 103–111. https://doi.org/10.1016/j.still.2018.05.008
778 Bronick, C.J., Lal, R., 2005. Soil structure and management: a review. Geoderma 124,
779 3–22. https://doi.org/10.1016/j.geoderma.2004.03.005
780 Campos, M.C.C., Ribeiro, M.R., Souza Júnior, V.S., Ribeiro Filho, M.R., Souza,
781 R.V.C.C., Almeida, M.C., 2011. Characterization and classification of
782 archaeological dark earths from the Middle Madeira River Region. Bragantia
783 70, 598–609. https://doi.org/10.1590/S0006-87052011000300016
784 Campos, M.C.C., Santos, L.A.C. dos, Silva, D.M.P. da, Mantovanelli, B.C., Soares,
785 M.D.R., 2012. Physical and chemical characterization of archaeological dark
786 earths and nonanthropogenic soils the Manicore, region, Amazon. Revista
787 Agroambiente 6, 102. https://doi.org/10.18227/1982-8470ragro.v6i2.682
788 Chilom, G., Bruns, A.S., Rice, J.A., 2009. Aggregation of humic acid in solution:
789 Contributions of different fractions. Organic Geochemistry 40, 455–460.
790 https://doi.org/10.1016/j.orggeochem.2009.01.010
791 Cho, G.-C., Dodds, J., Santamarina, J.C., 2006. Particle Shape Effects on Packing
792 Density, Stiffness, and Strength: Natural and Crushed Sands. Journal of
793 Geotechnical and Geoenvironmental Engineering 132, 591–602.
794 https://doi.org/10.1061/(ASCE)1090-0241(2006)132:5(591)
795 Chorom, M., Rengasamy, P., 1995. Dispersion and zeta potential of pure clays as
796 related to net particle charge under varying pH, electrolyte concentration and
797 cation type. European Journal of Soil Science 46, 657–665.
798 https://doi.org/10.1111/j.1365-2389.1995.tb01362.x

Costa, M.L. da, Kern, D.C., Pinto, A.H.E., Souza, J.R. da T., 2004. The ceramic artifacts in archaeological black earth (terra preta) from Lower Amazon Region, Brazil: chemistry and geochemical evolution. Acta Amazônica 34, 375–386. https://doi.org/10.1590/S0044-59672004000300004

CPRM, C.D.P.D.R.M., 2005. Base cartográfica digital obtida pela CPRM, a partir da base cartográfica integrada digital do Brasil ao milionésimo elaborada pelo IBGE.

CPRM, C.D.P.D.R.M., 2001. Hidroclimatologia, geologia, recursos minerais, geomorfologia e unidades de paisagens (Técnico No. 30), (Relatório Técnico). Ministério de Agricultura, Manaus.

Cunha, T.J.F., Madari, B.E., Benites, V. de M., Canellas, L.P., Novotny, E.H., Moutta, R. de O., Trompowsky, P.M., Santos, G. de A., 2007. Chemical fractionation of organic matter and humic acid characteristic in anthropogenic dark earth soils of brazilian amazonic region. Acta Amazônica 37, 91–98. https://doi.org/10.1590/S0044-59672007000100010

da Costa, M.L., Kern, D.C., 1999. Geochemical signatures of tropical soils with archaeological black earth in the Amazon, Brazil. Journal of Geochemical Exploration 66, 369–385. https://doi.org/10.1016/S0375-6742(99)00038-2

Demattê, J.L.I., Demattê, J.A.M., 1993. Comparisons of chemical properties of forest (Amazon region) and savanna soils (central region) of Brazil. Scientia Agricola 50, 272–286. https://doi.org/10.1590/S0103-90161993000200016

Essington, M.E., 2004. Soil and water chemistry: an integrative approach. CRC Press, Boca Raton, Fla.

822 Fortun, A., Benayas, J., Fortun, C., 1990. The effects of fulvic and humic acids on soil
823 aggregation: a micromorphological study. Journal of Soil Science 41, 563–572.
824 https://doi.org/10.1111/j.1365-2389.1990.tb00226.x
825 Ghezzehei, T. a., Or, D., 2001. Rheological Properties of Wet Soils and Clays under
826 Steady and Oscillatory Stresses. Soil Science Society of America Journal 65,
827 624–624. https://doi.org/10.2136/sssaj2001.653624x
828 Ghezzehei, T. a, Or, D., 2000. Dynamics of soil aggregate coalescence and theological
829 processes. Water Resources Research 36, 367–379.
830 Glaser, B., Balashov, E., Haumaier, L., Guggenberger, G., Zech, W., 2000. Black
831 carbon in density fractions of anthropogenic soils of the Brazilian Amazon
832 region. Organic Geochemistry 31, 669–678. https://doi.org/10.1016/S0146-
833 6380(00)00044-9
834 Glaser, B., Birk, J.J., 2012. State of the scientific knowledge on properties and genesis
835 of Anthropogenic Dark Earths in Central Amazonia (terra preta de Índio).
836 Geochimica et Cosmochimica Acta 82, 39–51.
837 https://doi.org/10.1016/j.gca.2010.11.029
838 Gomes, R.P., Campos, M.C.C., Soares, M.D.R., Silva, D.M.P., Cunha, J.M.,
839 Franciscon, U., Silva, L.S., Oliveira, I.A., Brito, W.B.M., 2017. Spatial variability
840 of aggregates and organic carbon under three different uses of indian black
841 earth in southern Amazonas. Bioscience Journal 1513–1522.
842 https://doi.org/10.14393/BJ-v33n6a2017-37142
843 Hillel, D., 2004. Introdution to environmental soil physics. Academic Press, San Diego.
844 Holthusen, D., Haas, C., Peth, S., Horn, R., 2012a. Are standard values the best
845 choice? A critical statement on rheological soil fluid properties viscosity and

surface tension. Soil and Tillage Research 125, 61–71. https://doi.org/10.1016/j.still.2012.07.007

Holthusen, D., Jänicke, M., Peth, S., Horn, R., 2012c. Physical properties of a Luvisol for different long-term fertilization treatments: II. Microscale behavior and its relation to the mesoscale. Journal of Plant Nutrition and Soil Science 175, 14–23. https://doi.org/10.1002/jpln.201100076

Holthusen, D., Pértile, P., Reichert, J.M., Horn, R., 2019. Viscoelasticity and shear resistance at the microscale of naturally structured and homogenized subtropical soils under undefined and defined normal stress conditions. Soil and Tillage Research 191, 282–293. https://doi.org/10.1016/j.still.2019.04.014

Holthusen, D., Peth, S., Horn, R., 2010. Impact of potassium concentration and matric potential on soil stability derived from rheological parameters. Soil and Tillage Research 111, 75–85. https://doi.org/10.1016/j.still.2010.08.002

Holthusen, D., Peth, S., Horn, R., Kühn, T., 2012b. Flow and deformation behavior at the microscale of soils from several long-term potassium fertilization trials in Germany. Journal of Plant Nutrition and Soil Science 175, 535–547. https://doi.org/10.1002/jpln.201100073

Holthusen, D., Reeb, D., Horn, R., 2012c. Influence of potassium fertilization, water and salt stress, and their interference on rheological soil parameters in planted containers. Soil and Tillage Research 125, 72–79. https://doi.org/10.1016/j.still.2012.05.003

Kämpf, N., Kern, D.C., 2005. Soil as a record of prehistoric human occupation in the Amazon, in: Topics in soil science, Tópicos. Brazilian Society of Soil Science, Viçosa, pp. 277–320.

870 Kern, D.C., Kämpf, N., 2005. Anthropc and pedogenic processes of Terra Preta soils
871 in Cachoeira-Porteira, Pará State, Brazil. Bulletin of the Museu Paraense
872 Emílio Goeldi 1, 187–201.
873 Kleber, M., Sollins, P., Sutton, R., 2007. A conceptual model of organo-mineral
874 interactions in soils: self-assembly of organic molecular fragments into zonal
875 structures on mineral surfaces. Biogeochemistry 85, 9–24.
876 https://doi.org/10.1007/s10533-007-9103-5
877 Lal, R., 1993. Tillage effects on soil degradation, soil resilience, soil quality, and
878 sustainability. Soil and Tillage Research 27, 1–8. https://doi.org/10.1016/0167-
879 1987(93)90059-X
880 Lee, B.J., Schlautman, M.A., Toorman, E., Fettweis, M., 2012. Competition between
881 kaolinite flocculation and stabilization in divalent cation solutions dosed with
882 anionic polyacrylamides. Water Research 46, 5696–5706.
883 https://doi.org/10.1016/j.watres.2012.07.056
884 Levene, H., 1960. Robust tests for equality of variances, in: Olkin, I., Ghurye, S.G.,
885 Hoeffding, W., Madow, W.G., Mann, H.B. (Eds.), Contributions to Probability
886 and Statistics: Essays in Honor of Harold Hotelling (Ingram Olkin, Sudhist G.
887 Ghurye, Wassily Hoeffding, William G. Madow, and Henry B. Mann, Eds.).
888 Stanford University Press, Menlo Park, pp. 278–292.
889 https://doi.org/10.1137/1003016
890 Mahanta, K.K., Mishra, G.C., Kansal, M.L., 2012. Estimation of electric double layer
891 thickness from linearized and nonlinear solutions of Poisson–Boltzman
892 equation for single type of ions. Applied Clay Science 59–60, 1–7.
893 https://doi.org/10.1016/j.clay.2012.02.014

894 Markgraf, W., Horn, R., 2007. Scanning Electron Microscopy–Energy Dispersive Scan
895 Analyses and Rheological Investigations of South-Brazilian Soils. Soil Science
896 Society of America Journal 71, 851–851.
897 https://doi.org/10.2136/sssaj2006.0231
898 Markgraf, W., Horn, R., Peth, S., 2006. An approach to rheometry in soil mechanics—
899 Structural changes in bentonite, clayey and silty soils. Soil and Tillage
900 Research 91, 1–14. https://doi.org/10.1016/j.still.2006.01.007
901 Markgraf, W., Moreno, F., Horn, R., 2012. Quantification of Microstructural Changes in
902 Salorthidic Fluvaquents Using Rheological and Particle Charge Techniques.
903 Vadose Zone Journal 11, 0. https://doi.org/10.2136/vzj2011.0061
904 Mendonça, E.S., Rowell, D.L., 1996. Mineral and Organic Fractions of Two Oxisols
905 and Their Influence on Effective Cation-Exchange Capacity. Soil Science
906 Society of America Journal 60, 1888–1992.
907 https://doi.org/10.2136/sssaj1996.03615995006000060038x
908 Mezger, T.G., 2014. The Rheology Handbook, 4th ed. Vincentz Network, Hanover.
909 Pantoja, J.C.M., Cunha, J.M., Campos, M.C.C., Silva, L.F.D., Mendonça Júnior, A.F.,
910 2015. Distribuição dos agregados em terra preta arqueológica de áreas
911 cultivadas no município de Novo Aripuanã, Amazonas. Revista Verde de
912 Agroecologia e Desenvolvimento Sustentável 10, 91.
913 https://doi.org/10.18378/rvads.v10i4.4425
914 Paradelo, R., van Oort, F., Chenu, C., 2013. Water-dispersible clay in bare fallow soils
915 after 80 years of continuous fertilizer addition. Geoderma 200–201, 40–44.
916 https://doi.org/10.1016/j.geoderma.2013.01.014
917 Pértile, P., Holthusen, D., Gubiani, P.I., Reichert, J.M., 2018. Microstructural strength
918 of four subtropical soils evaluated by rheometry: properties, difficulties and

opportunities. Scientia Agricola 75, 154–162. https://doi.org/10.1590/1678-992x-2016-0267

Pértile, P., Reichert, J.M., Gubiani, P.I., Holthusen, D., Costa, A. da, 2016. Rheological parameters as affected by water tension in subtropical soils. Revista Brasileira de Ciência do Solo 40, 1–14. https://doi.org/10.1590/18069657rbcs20150286

R Development Core Team, 2017. R: A Language and Environment for Statistical Computing.

Reichert, J.M., 2010. Mecânica do solo, in: Física Do Solo. Sociedade Brasileira de Ciência do solo, p. 298.

Rocha, W.W., Dias Junior, M.S., Lima, J.M., Miranda, E.E.V., Silva, A.R., 2002. Resistência ao cisalhamento e grau de intemperismo de cinco solos na região de Lavras (MG). Revista Brasileira de Ciência do Solo 26, 297–303. https://doi.org/10.1590/S0100-06832002000200002

Santos, L.A.C. dos, 2018. Mineralogia e matéria orgânica de Terra Preta Arqueológica e solos adjacentes não antrópicos na região do Apuí Amazonas (Tese). Universidade Federal de Santa Maria, Santa Maria.

Santos, L.A.C. dos, Araujo, J.K.S., Souza Júnior, V.S. de, Campos, M.C.C., Corrêa, M.M., Souza, R.A. da S., 2018. Pedogenesis in an archaeological Dark Earth – Mulatto Earth Catena over Volcanic Rocks in Western Amazonia, Brazil. Revista Brasileira de Ciência do Solo 42, 1–18.

Santos, L.A.C. dos, Campos, M.C.C., Aquino, R.E. de, Bergamin, A.C., Silva, D.M.P. da, Marques Junior, J., França, A.B.C., 2013. Characterization of Archaeological Dark Earth from the southern Amazon region. Revista Brasileira de Ciência do Solo 37, 825–836. https://doi.org/10.1590/S0100-06832013000400001

Schellekens, J., Almeida-Santos, T., Macedo, R.S., Buurman, P., Kuyper, T.W., Vidal-Torrado, P., 2017. Molecular composition of several soil organic matter fractions from anthropogenic black soils (Terra Preta de Índio) in Amazonia — A pyrolysis-GC/MS study. Geoderma 288, 154–165. https://doi.org/10.1016/j.geoderma.2016.11.001

Schramm, G., 2006. Rheology and Rheometry: theoretical and practical fundamentals. Artliber.

Seybold, C.A., Herrick, J.E., Brejda, J.J., 1999. Soil resilience: a fundamental component of soil quality. Soil Science 164, 224–234. https://doi.org/10.1097/00010694-199904000-00002

Shapiro, S.S., Wilk, M.B., 1965. An Analysis of Variance Test for Normality (Complete Samples). Biometrika 52, 591. https://doi.org/10.2307/2333709

Silva, D.M.P. da, Campos, M.C.C., Franciscon, U., Alho, L.C., Santos, L.A.C. dos, Paula Neto, P. de, Bergamin, A.C., Souza, Z.M. de, 2016. Spatial variability of soil properties in Archeological Dark Earth sites under cacao cultivation. Revista Brasileira de Ciência do Solo 40. https://doi.org/10.1590/18069657rbcs20140816

Six, J., Bossuyt, H., Degryze, S., Denef, K., 2004. A history of research on the link between (micro)aggregates, soil biota, and soil organic matter dynamics. Soil and Tillage Research 79, 7–31. https://doi.org/10.1016/j.still.2004.03.008

Sposito, G., 2008. The Chemistry of Soils, 2nd ed. Oxford University Press, NewYork.

Stergiadi, M., van der Perk, M., de Nijs, T.C.M., Bierkens, M.F.P., 2016. Effects of climate change and land management on soil organic carbon dynamics and carbon leaching in northwestern Europe. Biogeosciences 13, 1519–1536. https://doi.org/10.5194/bg-13-1519-2016

969 Stoppe, N., Horn, R., 2018. Microstructural strength of tidal soils – a rheometric
970 approach to develop pedotransfer functions. Journal of Hydrology and
971 Hydromechanics 66, 87–96. https://doi.org/10.1515/johh-2017-0031
972 Teixeira, W.G., Martins, G.C., 2002. Aggregate stability as an indicator of the soil
973 physical quality of Terra Preta de Índio (Técnico No. Circular Técnico).
974 Embrapa Amazônia Ocidental, Manaus.
975 Tisdall, J.M., Oades, J.M., 1982. Organic matter and water-stable aggregates in soils.
976 Journal of Soil Science 33, 141–163. https://doi.org/10.1111/j.1365-
977 2389.1982.tb01755.x
978 Vallejo, L.E., Mawby, R., 2000. Porosity influence on the shear strength of granular
979 material–clay mixtures. Engineering Geology 58, 125–136.
980 https://doi.org/10.1016/S0013-7952(00)00051-X
981 Vezzani, F.M., Mielniczuk, J., 2011. Soil aggregation and carbon stock of a paleudult
982 under different agricultural managaments. Revista Brasileira de Ciência do
983 Solo 35, 213–223. https://doi.org/10.1590/S0100-06832011000100020
984 Vieira, L.S., dos Santos, P.C.T.C., 1987. Amazon: its soils and other natural resources,
985 Edição Ceres. Editora Agronômica Ceres.
986 Zech, W., Haumaier, L., Reinhold, H., 1990. Ecological Aspects of Soil Organic Matter
987 in Tropical Land Use, in: Humic Substances in Soil and Crop Sciences:
988 Selected Readings. Soil Science Society of America, Madison, pp. 187–202.
989 https://doi.org/10.2136/1990.humicsubstances.c8
990
991

992 **FIGURES**

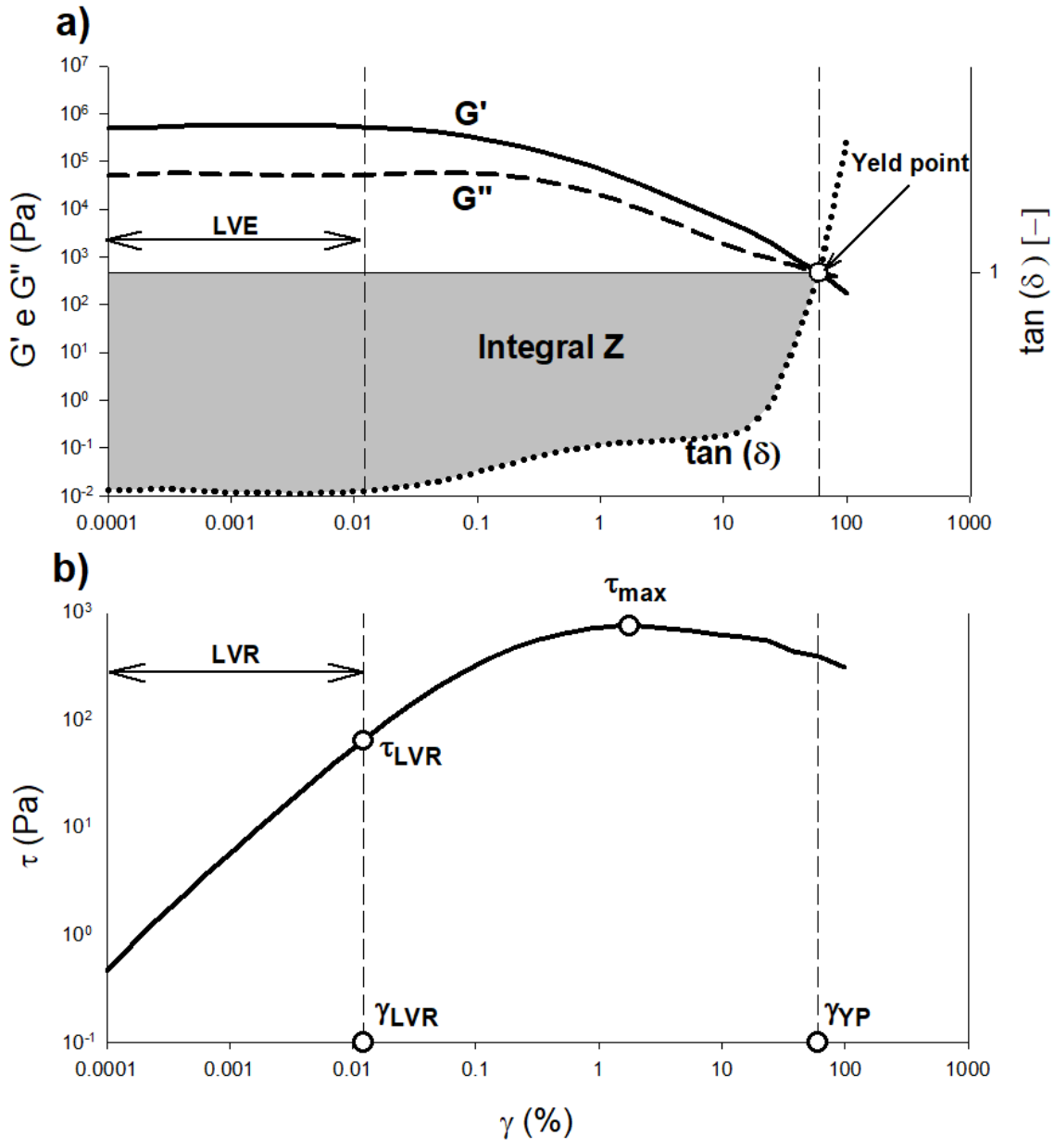

993

994 Figure 1**.** Overview of rheological properties obtained from amplitude sweep test with
995 controlled strain: a) storage (*G'*) and loss (*G"*) modulus, loss factor (tan δ), yield point
996 (YP) and integral z, calculated by sum of area between the actual tan δ and tan δ = 1;
997 b) shear stress (τ), linear viscoelastic range (LVR), strain limit (γ_{LVR}), stress at end of
998 the LVR (τ_{LVR}), maximum shear stress (τ_{max}), strain (γ_{YP}).

999

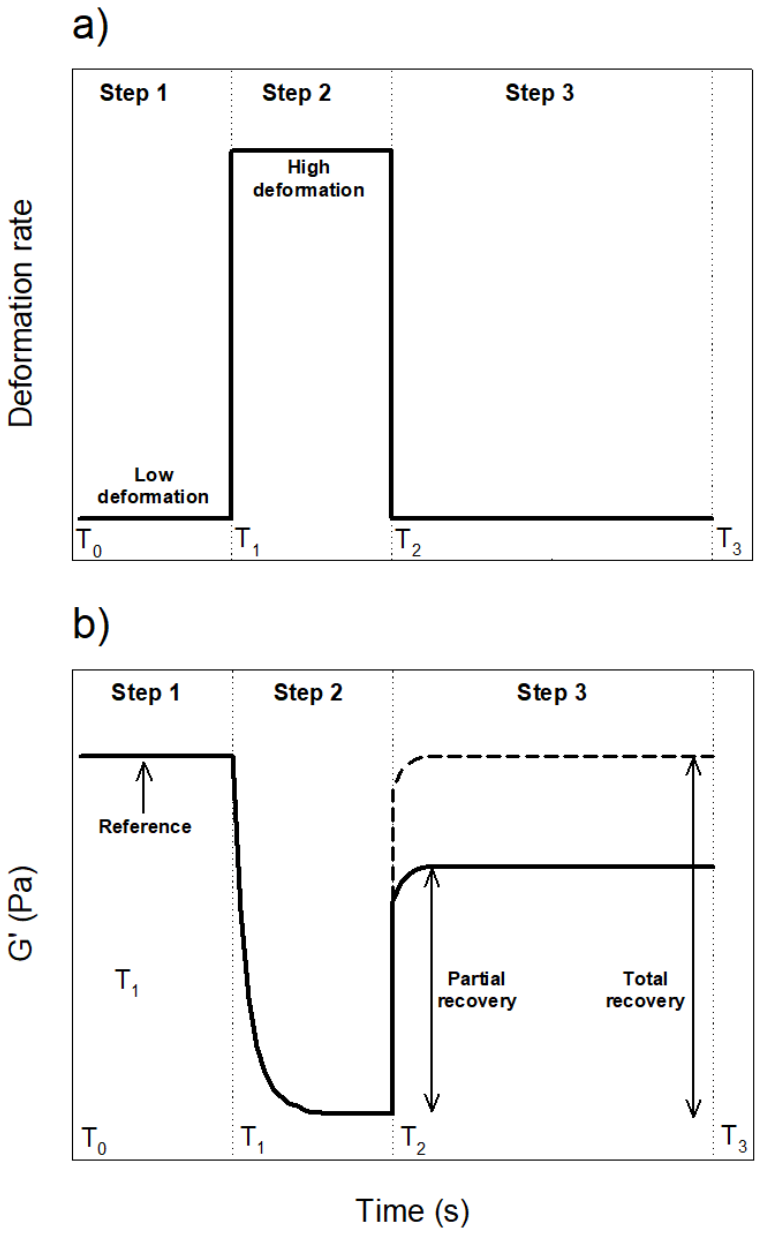

1000

1001 Figure 2 - Predetermined steps of the thixotropy test (a) and storage modulus behavior

1002 (G ') over time (b). Adapted from (MEZGER, 2014).

1003

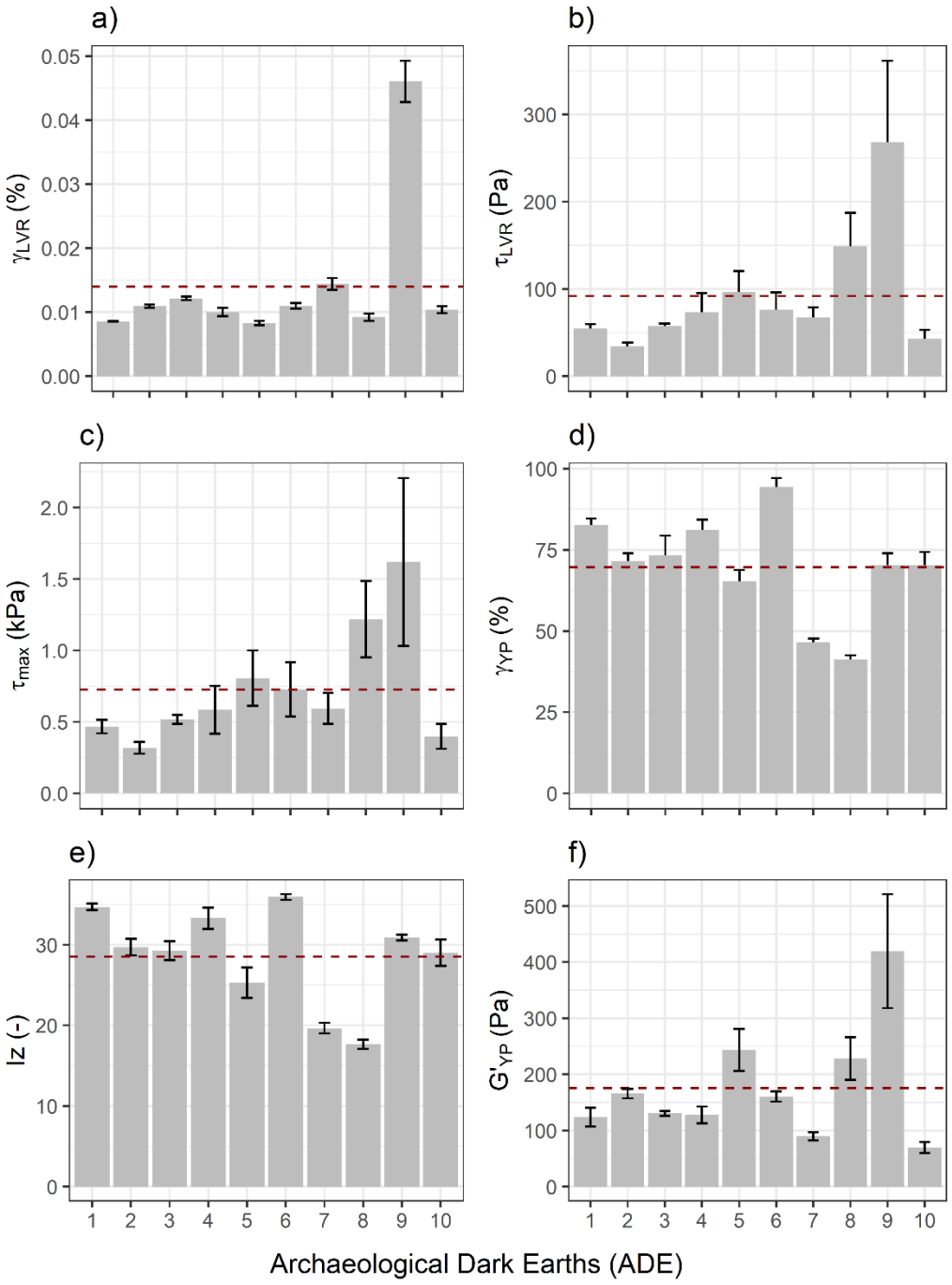

1004

1005 Figure 3 - Microstructural resistance of Archaeological Dark Earths (ADE) represented
1006 by the strain and (γ_{LVR}, a), shear stress (τ_{LVR}, b) at the end of the linear viscoelastic
1007 range, strain (c) and storage modulus value (G'_{YP}, d) at the yield point, maximum shear
1008 stress (τ_{max}, e), integral z (Iz, f) analyzed in saturated soil conditions. The dashed line
1009 represents the mean of all ADEs.

1010

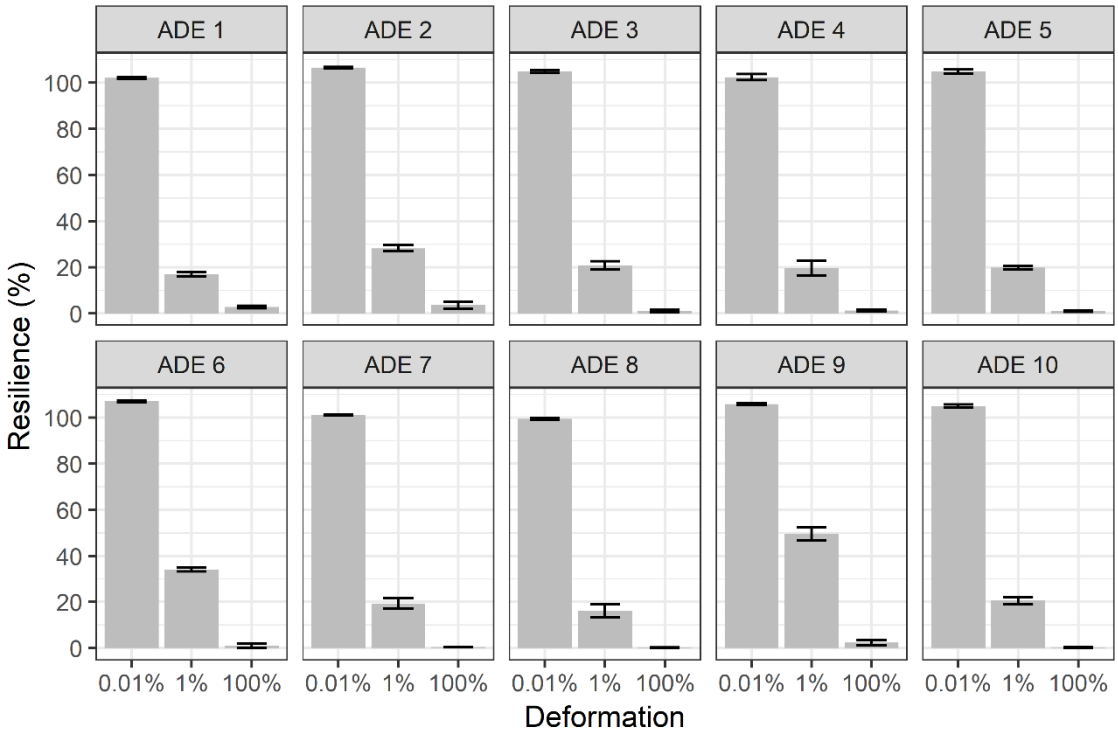

1011

1012 Figure 4 Resilience of Archaeological Dark Earths (ADE), evaluated by recovery of

1013 storage modulus (*G'*), as function of strain intensity applied during the test thixotropy.

1014

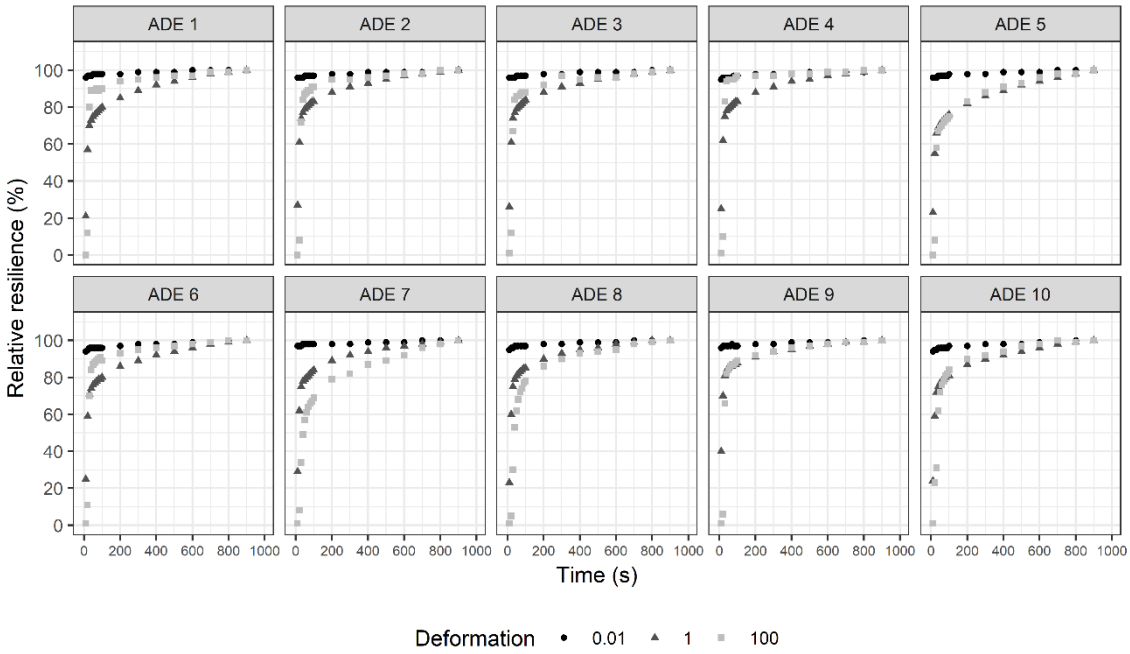

1015

1016 Figure 5. Relative resilience of Archaeological Dark Earth (ADE) in time. At each time
1017 interval, the recovery of the storage modulus (G ') was divided by the maximum
1018 recovery achieved at each applied strain intensity.

1019

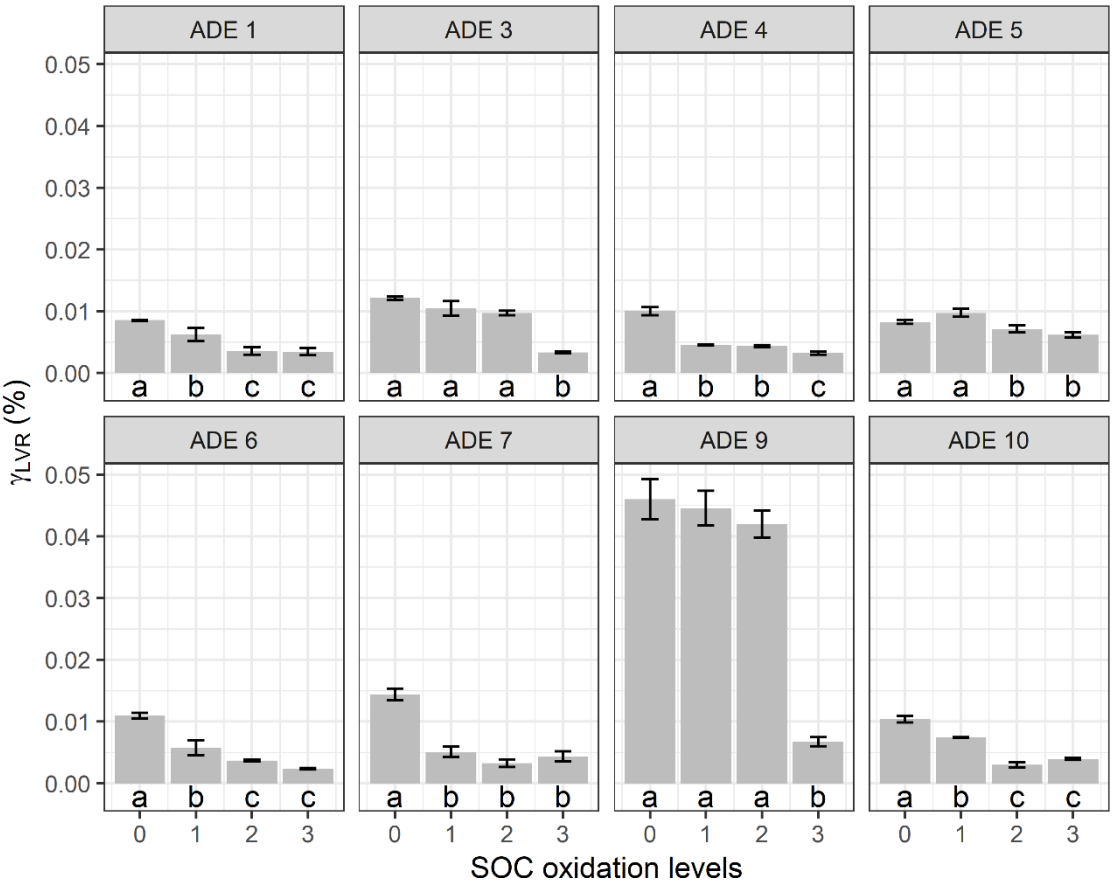

1020

1021 Figure 6. Strain limit at the end of the linear viscoelastic range (γ_{LVR}) of Archaeological
1022 Dark Earths (ADE) submitted at different oxidation levels of soil organic carbon. The
1023 SOC oxidation levels 0 (OX_0), 1 (OX_1), 2 (OX_2) and 3 (OX_3) correspond to the
1024 application of 0, 0.2, 0.4 and 0.6 ml of concentrated H_2O_2 (35%) per gram of soil. Error
1025 bars denote standard error. Means followed by lower case letters do not differ
1026 statistically by the Scott Knott test at 5% significance level.

1027

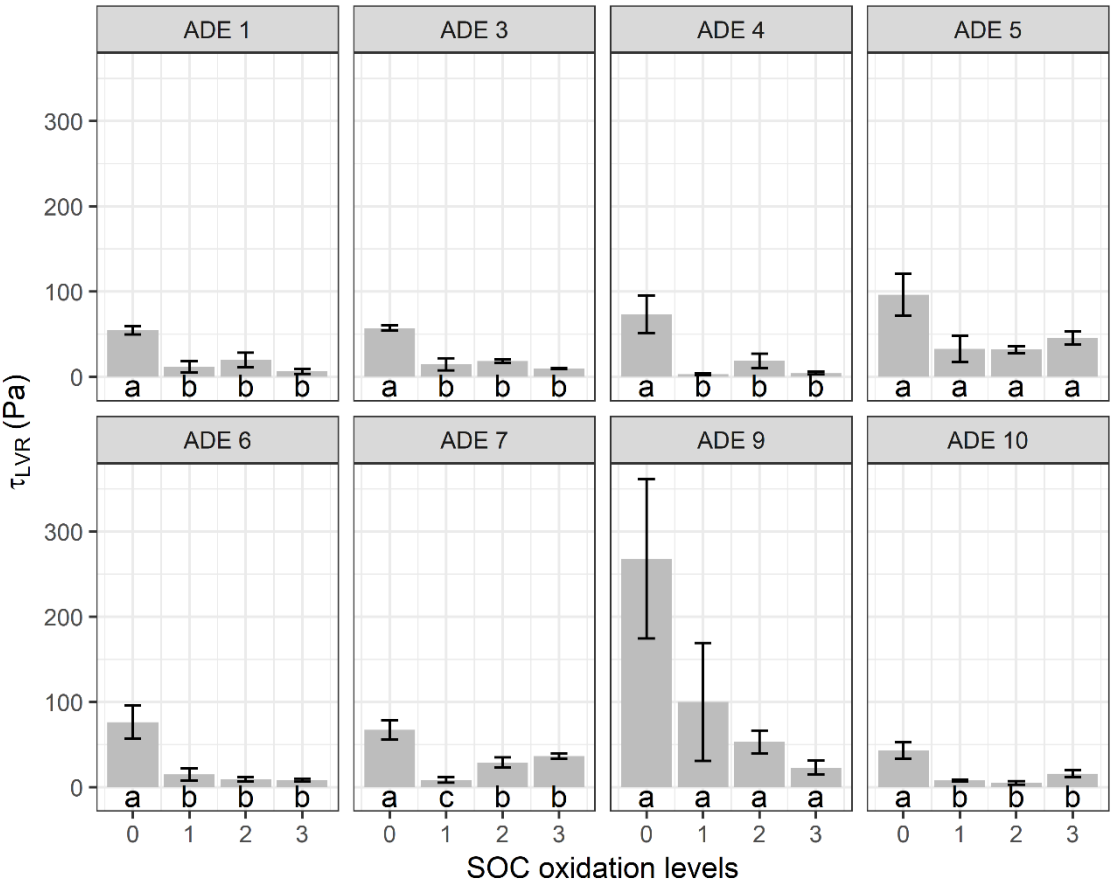

1028

1029

1030 Figure 7. Stress limit at the end of the linear viscoelastic range (τ_{LVR}) of Archaeological
1031 Dark earths (ADE) submitted at different oxidation levels of soil organic carbon. The
1032 SOC oxidation levels 0 (OX_0), 1 (OX_1), 2 (OX_2) and 3 (OX_3) correspond to the
1033 application of 0, 0.2, 0.4 and 0.6 ml of concentrated H_2O_2 (35%) per gram of soil. Error
1034 bars denote standard error. Means followed by lower case letters do not differ
1035 statistically by the Scott Knott test at 5% significance level.

1036

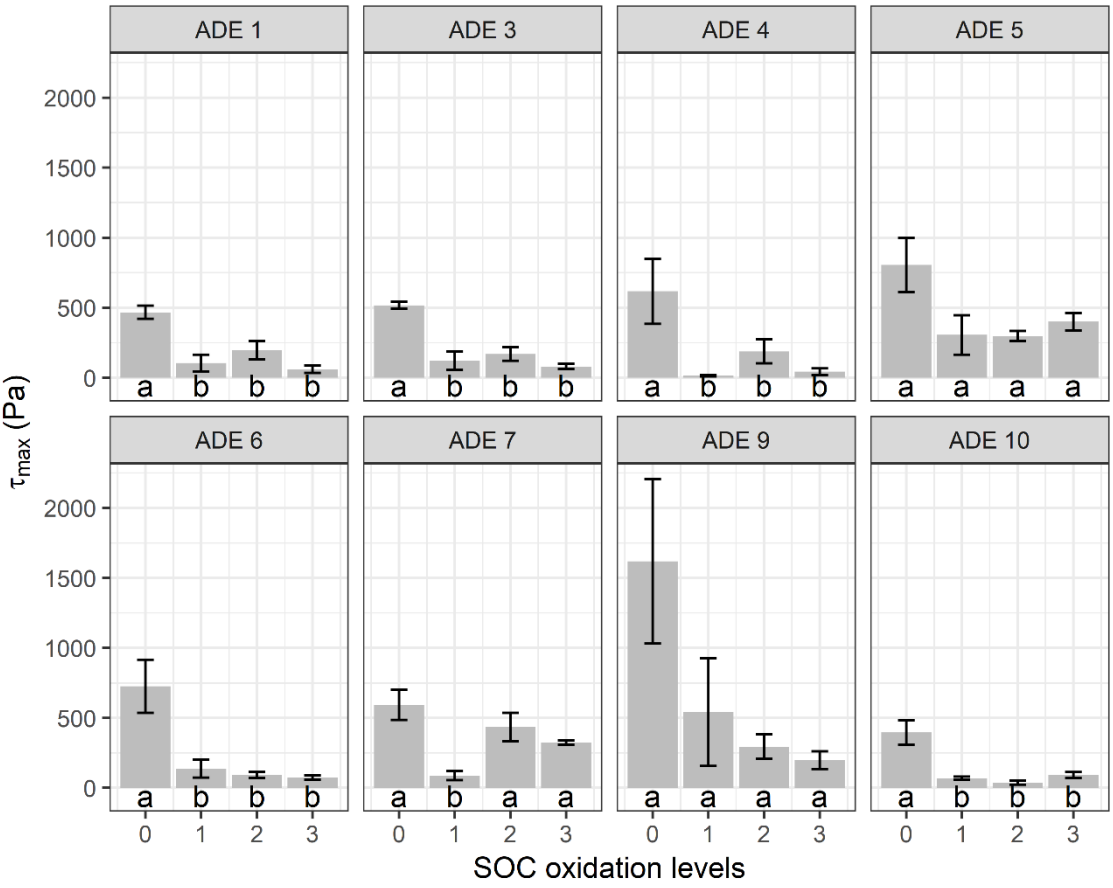

1037

1038 Figure 8. Maximum shear stress (τ_{max}) of Archaeological Dark Earths (ADE) submitted
1039 at different oxidation levels of soil organic carbon. The SOC oxidation levels 0 (OX_0),
1040 1 (OX_1), 2 (OX_2) and 3 (OX_3) correspond to the application of 0, 0.2, 0.4 and 0.6 ml of
1041 concentrated H_2O_2 (35%) per gram of soil. Error bars denote standard error. Means
1042 followed by lower case letters do not differ statistically by the Scott Knott test at 5%
1043 significance level.

1044

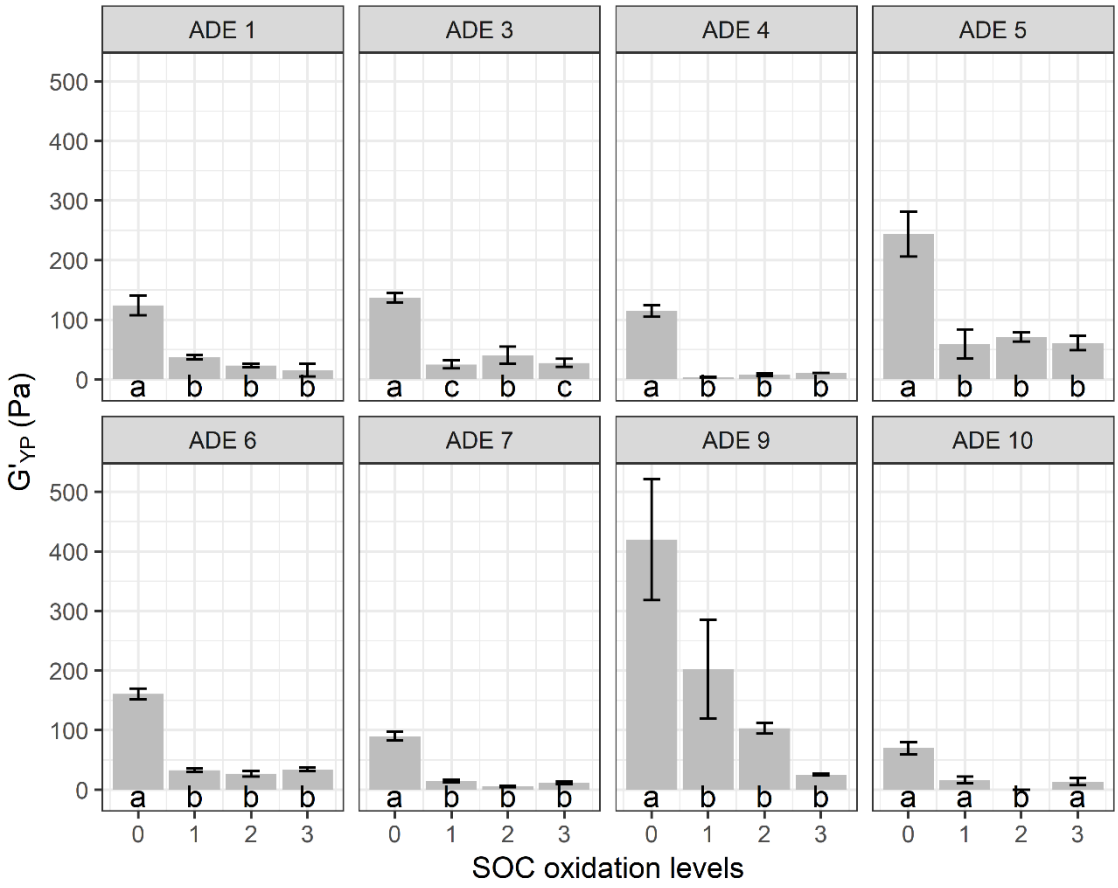

Figure 9. Storage modulus (*G'*$_{YP}$) at the yield point of Archaeological Dark Earths (ADE) submitted at different oxidation levels of soil organic carbon. The SOC oxidation levels 0 (OX_0), 1 (OX_1), 2 (OX_2) and 3 (OX_3) correspond to the application of 0, 0.2, 0.4 and 0.6 ml of concentrated H_2O_2 (35%) per gram of soil. Error bars denote standard error. Means followed by lower case letters do not differ statistically by the Scott Knott test at 5% significance level.

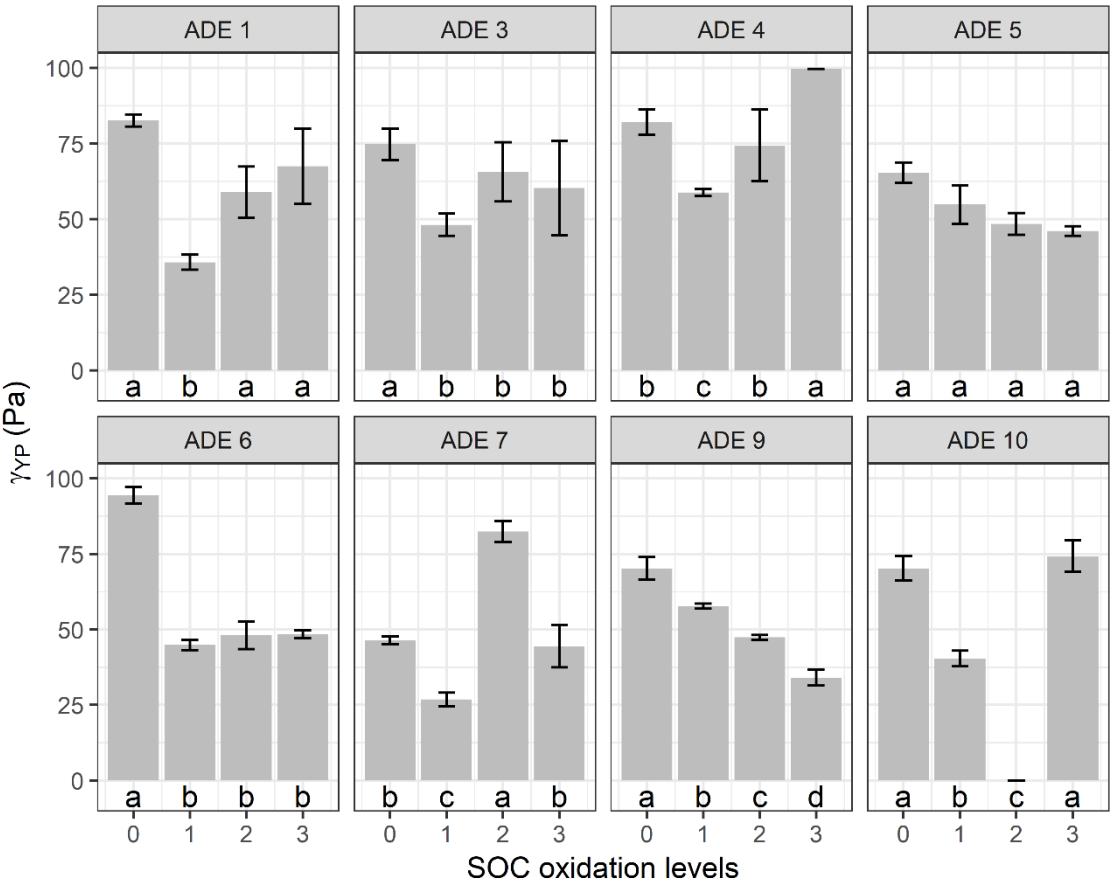

1053

1054 Figure 10. Strain (γ_{YP}) at the yield point of Archaeological Dark Earths (ADE) submitted
1055 at different oxidation levels of soil organic carbon. The levels 0, 1, 2 and 3 represent
1056 the application of 0, 0.2, 0.4 and 0.6 ml of concentrated H_2O_2 (35%) per gram of soil.
1057 Means followed by lower case letters do not differ statistically by the Scott Knott test
1058 at 5% significance level.

1059

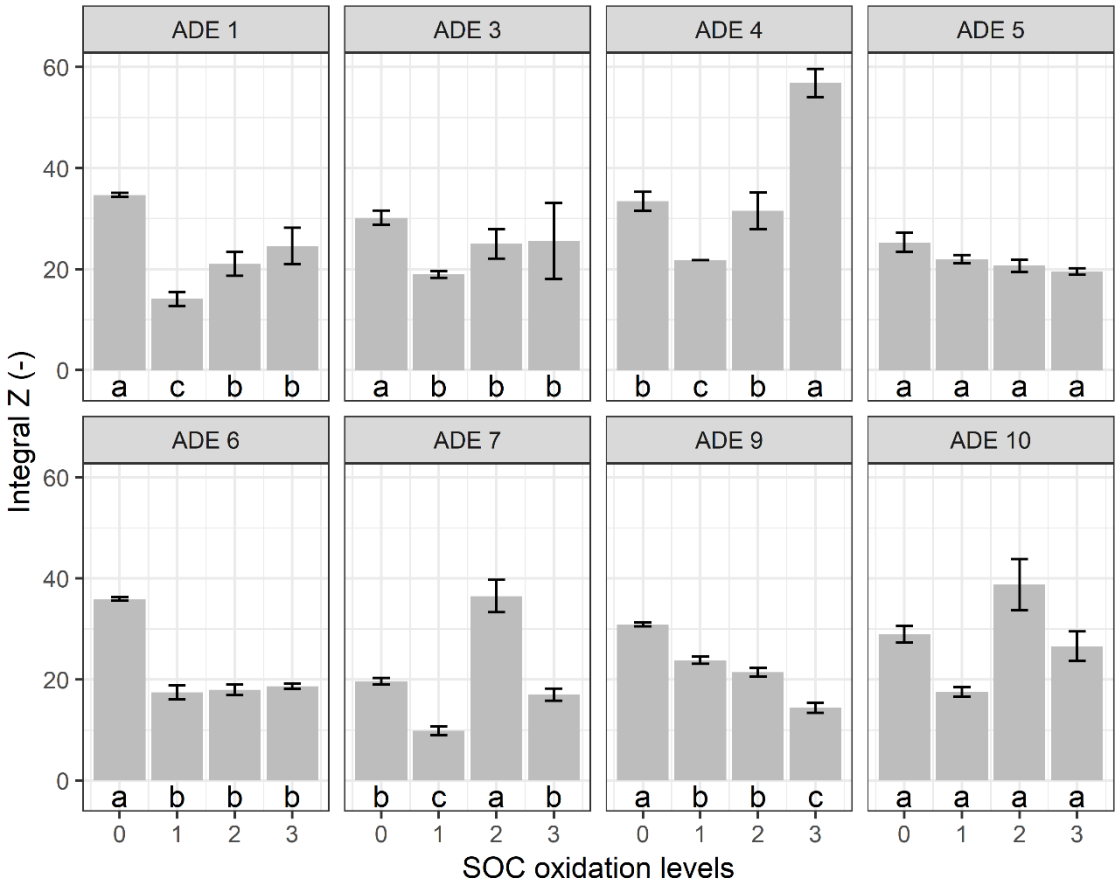

1060

1061 Figure 11. Integral z (Iz) (± standard error) of Archaeological Dark Earths (ADE)
1062 submitted at different oxidation levels of soil organic carbon. The SOC oxidation levels
1063 0 (OX_0), 1 (OX_1), 2 (OX_2) and 3 (OX_3) correspond to the application of 0, 0.2, 0.4 and
1064 0.6 ml of concentrated H_2O_2 (35%) per gram of soil. Error bars denote standard error.
1065 Means followed by lower case letters do not differ statistically by the Scott Knott test
1066 at 5% significance level.

1067

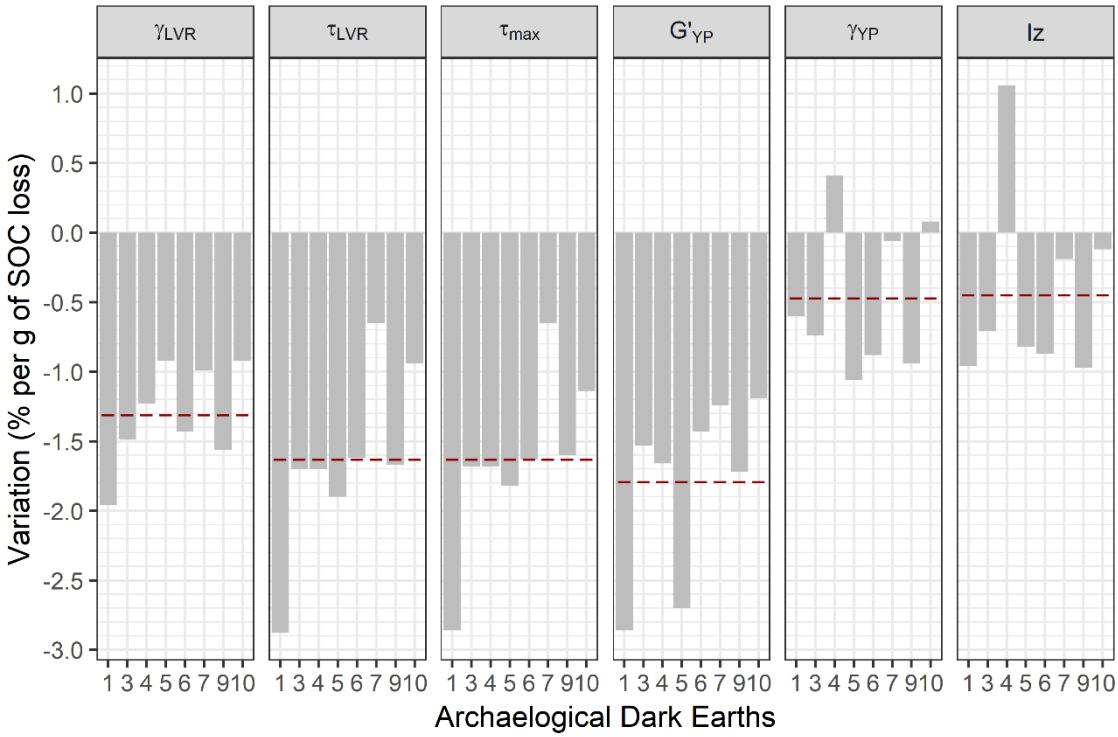

1068

1069 Figure 12. Percentage loss in rheological parameters of Archaeological Dark Earths
1070 per gram of soil organic carbon lost (comparison of OX_0 and OX_3 as there are strain
1071 (γ_{LVR}) and shear stress (τ_{LVR}) at the end of the linear viscoelastic range, strain (γ_{YP}) and
1072 storage modulus value (G'_{YP}) at the yield point, maximum shear stress (τ_{max}), integral
1073 z (Iz). The dashed line represents the average variation of all ADEs.

1074

Table 1. Physical and chemical properties of Archaeological Dark Earths (ADE) occurring in the Western Amazonia, Brazil. Data compiled from Aquino et al. (2016) and Santos et al. (2018, 2013).

Property/Sites	**ADE 1**	**ADE 2**	**ADE 3**	**ADE 4**	**ADE 5**	**ADE 6**	**ADE 7**	**ADE 8**	**ADE 9**	**ADE 10**
Depth (cm)	**0-20**	**0-16**	**0-11**	**0-23**	**0-15**	**0-15**	**0 - 16**	**0-19**	**0-22**	**0-22**
Physical properties										
Sand (g kg^{-1})	158	153	184	143	156	97	312	711	150	214
Silt (g kg^{-1})	451	454	380	352	513	520	450	196	608	504
Clay (g kg^{-1})	391	393	436	505	331	383	238	93	242	281
ρ (g cm^{-3})	0.7	0.9	0.8	0.8	1.0	0.9	1.0	1.4	1.0	0.7
CDW (g kg^{-1})	43	109	13	229	170	229	3.5	2.4	9.6	16
DF (%)	89	72	68	55	48	40	54	64	18	28
Chemical properties										
pH	5.5	6.3	6.0	5.0	4.5	5.2	5.0	5.5	6.4	6.6
P (mg kg^{-1})	206	227	236	162	166	144	94	95	432	425
Ca^{+2} ($cmol_c$ kg^{-1})	23	21	18	11	48	122	1.3	0.7	13	16
Mg^{+2} ($cmol_c$ kg^{-1})	4.1	1.9	2.9	0.4	7.0	15	0.5	0.4	1.4	2.5
K^{+} ($cmol_c$ kg^{-1})	0.2	0.5	0.5	0.3	1.3	1.3	0.1	0.1	0.4	0.4
Na^{+} ($cmol_c$ kg^{-1})	0.1	0.1	0.2	0.2	-	-	-	-	-	-
Al ($cmol_c$ kg^{-1})	0.6	0.8	0.0	0.6	0.4	0.0	1.2	1.0	0.2	0.4
H+Al ($cmol_c$ kg^{-1})	15	8.5	12	19	109	58	17	9.3	9.9	6.3
BS ($cmol_c$ kg^{-1})	28	24	22	11	56	138	1.9	1.2	14	18
CEC ($cmol_c$ kg^{-1})	43	32	33	31	165	196	19	10	24	25
V (%)	65	74	66	37	34	70	9.9	11	59	73
m (%)	2.0	3.0	0.0	5.0	2.3	0.0	38	45	1.4	1.8
SOC (g kg^{-1})	81	104	96	86	109	105	99	36	123	95

ρ: bulk density; CDW: clay dispersible in water; DF: degree of flocculation; BS: sum of bases; CEC: cation exchange capacity; V: base saturation; m: aluminum saturation.

Table 2 - Pearson correlation coefficient between strain limit (γ_{LVR}), shear stress at the end of the linear viscoelastic range (τ_{LVR}), strain (γ_{YP}) and storage modulus value (G'_{YP}) at the yield point, maximum shear stress (τ_{max}), integral zone (Iz) and different physical and chemical characteristics of Archaeological Dark Earths.

Soil property	γ_{LVR}	τ_{LVR}	γ_{YP}	G'_{YP}	τ_{max}	**Iz**
Sand	-0.16	0.21	-0.81**	0.05	0.35	-0.81**
Clay	-0.26	-0.51	0.79**	-0.35	-0.59	0.76**
ρ	0.12	0.51	-0.69*	0.47	0.65*	-0.72**
Al	-0.24	-0.13	-0.72**	-0.22	-0.09	-0.67*
V	0.11	-0.22	0.77**	-0.06	-0.33	0.80**
m	-0.15	0.12	-0.84**	-0.06	0.23	-0.81**
SOC	0.49	0.11	0.45	0.24	-0.02	0.46
Ca^{+2}	-0.16	0.14	0.64**	-0.01	0.07	0.51
Mg / Ca	-0.16	0.16	-0.83**	-0.03	0.30	-0.85**
K / Ca	0.04	0.27	-0.94**	0.07	0.37	-0.93**
K / Mg	0.18	0.12	0.07	0.09	0.05	0.13
K / (Ca + Mg)	0.12	0.30	-0.93**	-0.10	-0.37	-0.93**
Ca / (K + Mg)	0.01	-0.12	0.65*	0.02	-0.21	0.68*
SOC / Clay	0.68*	0.73**	-0.59	0.61	0.73**	-0.53
SOC / Sand	0.30	0.09	0.80**	0.28	0.03	0.76**
Sand / Clay	-0.12	0.29	-0.71**	0.15	0.43	-0.71**
Silt / Clay	0.62	0.73**	-0.56	0.59	0.74**	0.50

ρ: bulk density; m: aluminium saturation; V: bases saturation; SOC: soil organic carbon.

** and * indicate significant correlation at p ≤ 0.01 and 0.05, respectively.

Table 3. Pearson correlation coefficient of soil storage module recovery (*G'*) wich soil rheological, physical and chemical properties in each strain intensity applied in step 2 of thixotropy analysis.

Soil property	Strain intensity			Soil property	Strain intensity		
	0.01%	1%	100%		0.01%	1%	100%
γ_{LVR}	0.27	0.86**	0.28	Al^{+3}	-0.72*	-0.46	-0.03
τ_{LVR}	-0.03	0.67*	0.05	SB	0.58*	0.28	0.01
γ_{YP}	0.66*	0.31	0.41	V	0.80**	0.40	0.53
G'_{YP}	0.20	0.72*	0.29	m	-0.80**	-0.37	-0.33
τ_{max}	-0.11	0.58*	-0.08	SOC	0.78*	0.64*	0.35
Iz	0.62*	0.38	0.50	SOC/Sand	0.85**	0.67*	0.41
Sand	-0.75**	-0.39	-0.46	Mg/Ca	-0.76**	-0.39	-0.51
Silt	0.73**	0.66*	0.35	K/Ca	-0.71*	-0.25	-0.51
DF	-0.40	-0.63*	0.31	K/(Ca+Mg)	-0.65*	-0.18	-0.48
Ca^{+2}	0.58*	0.29	0.02	Sand/Clay	-0.68*	-0.30	-0.40
K^{+}	0.70*	0.28	0.00	Sand/Silt	-0.70**	-0.36	-0.40

γ_{LVR}: Strain limit, τ_{LVR}: shear stress at the end of the linear viscoelastic range; γ_{YP}: strain at yield point; G'_{YP}: storage modulus value at the yield point: τ_{max}: maximum shear stress; Iz: integral z; DF: flocculation degree; SB: sum of bases; V: bases saturation; m: Al^{+3} saturation; SOC: soil organic carbon; SOC/Sand: ratio of SOC content by sand content; Mg/Ca: ratio of Mg^{+2} concentration by Ca^{+2} concentration; K/Ca, ratio of K^{+} concentration by Ca^{+2} concentration; K/(Ca+Mg): ratio between monovalent and bivalent cations concentration; Sand/Clay: ratio of sand content by clay content; Sand/Silt: ratio of sand content by silt content. n = 10.

Table 4. Soil organic carbon content (SOC) of Archaeological Dark Earths (ADE) in each organic matter oxidation levels (OX_0, OX_1, OX_2 and OX_3) and reduction (in gram and percentage) in relation to initial amount of SOC (OX_0).

ADE	Oxidation levels	SOC ($g\ kg^{-1}$)	Reduction		ADE	Oxidation levels	SOC ($g\ kg^{-1}$)	Reduction	
			g	%				g	%
ADE 1	OX_0	81	-	-	ADE 6	OX_0	105	-	-
	OX_1	74	-6.9	8.5		OX_1	-97	-8.7	-8.3
	OX_2	61	-19	24		OX_2	-78	-28	-26.5
	OX_3	50	-30	38		OX_3	-50	-55	-52.1
ADE 2	OX_0	103	-	-	ADE 7	OX_0	100	-	-
	OX_1	105	1.3	1.2		OX_1	75	-24	-25
	OX_2	108	4.3	4.1		OX_2	34	-65	-65
	OX_3	98	-5.1	-4.9		OX_3	30	-70	-70
ADE 3	OX_0	96	-	-	ADE 8	OX_0	36	-	-
	OX_1	92	-3.1	-3.3		OX_1	44	7.7	21
	OX_2	87	-8.4	-8.7		OX_2	38	1.8	5.0
	OX_3	47	-48	-51		OX_3	17	-19	-53
ADE 4	OX_0	86	-	-	ADE 9	OX_0	124	-	-
	OX_1	53	-32	-38		OX_1	124	-0.1	-0.1
	OX_2	33	-52	-61		OX_2	113	-11	-8.7
	OX_3	31	-55	-64		OX_3	69	-54	-44
ADE 5	OX_0	109	-	-	ADE 10	OX_0	95	-	-
	OX_1	95	-13	-12		OX_1	90	-5.0	-5.2
	OX_2	90	-19	-17		OX_2	43	-52	-54
	OX_3	81	-27	-25		OX_3	27	-68	-71

1102 Table 5. Pearson correlation between fractions of soil organic carbon extracted with
1103 NaOH by Santos et al. (2018) and rheological variables of Archaeological Dark Earths
1104 (ADEs) 1, 2 3 and 4.

SOC fractions	γ_{LVR}	τ_{LVR}	γ_{YP}	G'_{YP}	τ_{max}	**Iz**
FA	0.30	0.88	0.24	-0.67	0.92 *	0.03
HA	-0.52	-0.17	0.38	-0.39	-0.12	0.43
HUM	0.15	-0.88	-0.53	0.48	-0.80	-0.40
HA/FA	-0.45	-0.77	-0.05	0.42	-0.80	0.15
(FA+HA)/HUM	-0.36	0.96 *	0.79	-0.95 *	0.96 *	0.64

1105 γ_{LVR}: Strain limit, τ_{LVR}: shear stress at the end of the linear viscoelastic range; γ_{YP}: strain at yield point;
1106 G'_{YP}: storage modulus value at the yield point: τ_{max}: maximum shear stress; Iz: integral z; FA: fulvic acid;
1107 HA: humic acid, HUM: humin fraction; HA/FA: ratio between carbon content in the form of humic acids
1108 and fulvic acids; AE/HUM: ratio of the alkaline extract carbon content (sum of FA and HA) and the humin
1109 fraction carbon content (HUM).

2.2 ESTUDO II - SPECIFIC SURFACE AREA EFFECT ON SOIL ELASTICITY AND MICROSTRUCTURE RESISTANCE EVALUATED BY RHEOMETRY

[3]Specific surface area effect on soil elasticity and microstructure resistance evaluated by rheometry

Alan Carlos Batistão[a,*], Dörthe Holthusen[a], José Miguel Reichert[a], Rodrigo Pivoto Mulazzani[a] and Paulo Ivonir Gubiani[a]

[a]Soil Department, Federal University of Santa Maria (UFSM), Brazil.

[*]Corresponding author at: Avenida Roraima 1000, prédio 42, Cidade Universitária, Camobi, Santa Maria, RS, CEP: 97105-900, Brazil. E-mail address: alanbatistao@gmail.com (A. Batistão).

Abstract - The specific surface area (SSA) plays a key role in several soil processes, influencing aggregate formation and stabilization, particularly at the particle-particle level. The objective of this study was to evaluate the influence of SSA on the resistance to deformation of soil microstructure under repeated stress. We collected unstructured samples from the surface horizon of thirteen soils with distinct granulometry and clay mineralogy, and thus large variation in SSA. The soils were air-dried, ground and sieved in 2 mm mesh. Soil SSA was determined by the ethylene glycol monoethyl ether method. Furthermore, we prepared twelve samples in metal rings of approximately 10 cm^3, compacting the soil to reach 75% of the maximum density estimated by the clay content. Six saturated samples and six drained samples at -6 kPa matric potential were

[3] Artigo formatado de acordo com as normas da revista Applied Clay Science

submitted to an amplitude sweep test in a compact modular rheometer, obtaining the following rheological variables: initial value of storage modulus (G'_i); strain (γ_{LVE}) and shear stress (τ_{LVE}) at the end of linear viscoelastic range; strain ($\gamma\tau_{máx}$) and stress (τ_{max}) at maximum shear stress point; strain (γ_{YP}) and storage modulus (G'_{YP}) in yield point; (τ_{max}); and integral Z (Iz). Then, we performed regression analysis, using soil SSA as predictor of rheological variables. Increasing SSA from 8.29 to about 100 $m^2\ g^{-1}$ increased the γ_{LVE}, $\gamma\tau_{máx}$, γ_{YP} and Iz in saturated samples, as well as the γ_{LVE} and $\gamma\tau_{máx}$ in drained samples. However, a reduction of these parameters occurred in soils with higher SSA in both moisture conditions, which is probably due to formation of pseudosand composite-particles and thus reduced surface accessibility. The SSA had no significant influence on the resistance variables of τ_{LVE}, τ_{max} and G'_{YP}, but these were increased by increasing compressive force, cations concentration, and silt and sand content.

Key-words: soil rheology, clay content, soil deformation,

1 INTRODUCTION

Many processes in soils are strongly affected by the specific surface area (SSA), as particle surfaces, both internal and external, are the location for chemical (exchange) reactions and physical interactions (Sparks, 2003; Sposito, 2008). Soils present a great variation in SSA, ranging from less than 0.1 $m^2\ g^{-1}$ (quartz) to more than 800 $m^2\ g^{-1}$ (montmorillonite), according to size and type of soil mineral particles (Brady and Weil, 2013; Pennell, 2016). In soils of similar particle size distribution, the SSA will be higher in the one with greater amount of expandable clay minerals (Lal and Shukla, 2004), due to exposure of inner surface areas.

Soil SSA is one of the main reason of the high impact of soil texture on soil chemical and physical properties, the texture being considered one of the most stable soil physical property. Soil texture influences e.g. the particle density (Brady and Weil, 2013), porosity and pore size distribution (Cavalli et al., 2020; Nimmo, 2005), air permeability (Mentges et al., 2016), water retention, flow and availability to plants (Carlesso and Santos, 1999; Reichert et al., 2009a), and compression, elasticity, and shear strength (Gubiani et al., 2018; Reichert et al., 2018a, 2018b; Suzuki et al., 2013, 2008). In addition, texture exerts great influence on formation and stabilization of soil aggregates (Bronick and Lal, 2005; Reichert et al., 2009b; Reichert and Norton, 1994a).

In soils with high SSA, there are in general more functional groups available on mineral surfaces, amplifying the particles' inherent electrostatic force and reactivity (Kämpf et al., 2012). This favors flocculation and thus the beginning of aggregate formation. The high reactivity can also increase the resistance of structure to deformation by formation of organo-metallic complexes with high binding energy (Sposito, 2008). Likewise, as SSA increases, the importance of electrical and capillary forces at contact points between particles also increases (Santamarina et al., 2002), providing greater stability to structure. Correlating the mechanical behavior with soil physical and chemical attributes, Silva and Carvalho (2007) observed higher cohesion in horizons with higher fine clay content, and attributed this result to higher SSA of these particles.

Although the clay particles contribute greatly to soil SSA due to their size, the particle shape also influences the specific soil surface (Hillel, 2004). Flat or elongated particles exhibit a larger surface area than particles with a cubic or spherical shape (Santamarina and Cho, 2004). Neglecting these aspects by only taking into account

74 the texture or single fractions, might give rise to misleading results. Physical processes
75 that govern soil behavior, change with small differences in SSA (Santamarina et al.
76 2002), where soils with the same clay content and just slightly different SSA might
77 present a very different deformation behavior. Therefore, using SSA as a parameter
78 could improve the evaluation of soil physical and mechanical behavior. For instance,
79 studying the potential of soil expansion and contraction with different mineralogical
80 compositions, Ross (1978) observed a higher relationship of soil linear extensibility
81 index with SSA than with clay content. Moreover, SSA affects soil aggregate stability
82 and surface sealing caused by raindrop impact (Reichert et al., 2009b, 1994; Reichert
83 and Norton, 2013, 1996, 1994b).

84 With respect to soil microstructure, there are contradictory results of the effect
85 of clay on shear strength. Some studies relate increased shear strength to greater clay
86 content (Pértile et al., 2016), while others observed higher resistance in sandier soils
87 (Stoppe and Horn, 2018). However, these studies compare soils with quite different
88 texture, not testing the effect of a gradual increase in clay content on properties of soil
89 microstructure, especially with regard to SSA.

90 Using SSA could improve our understanding of processes related to
91 aggregation of particles as related to soil microstructural resistance. Therefore, the
92 objective of this study was to evaluate the influence of SSA on elasticity and resistance
93 of soil microstructure to deformation by means of rheometry in an amplitude sweep
94 test that simulates repeated (oscillating) stresses.

95

2 MATERIAL AND METHODS

2.1 Description of study area

The study was carried out with samples from 13 soils from southern Brazil (Figure 1), formed under different pedogenetic conditions, to obtain samples with different granulometric composition and, consequently, with significant variation in specific surface area (SSA). Samples with altered structure were collected in the layer of 0-20 cm depth, in accordance with recommendations of Santos et al. (2013). For granulometric, chemical and rheological analyses, the samples were air-dried, ground and sieved in a 2-mm mesh.

2.2 Granulometric, chemical and mineralogical characterization

Soil texture was determined by the pipette method, using NaOH 0.25 M as a chemical dispersant, followed by horizontal shaking, together with two nylon balls, at 120 rpm during 4h (Suzuki et al., 2015). After shaking, the sand fraction was separated by sieving at a mesh opening of 0.053 mm, while the clay fraction was separated by sedimentation and silt was calculated as the difference between these two (EMBRAPA, 2017).

The determination of specific surface area was performed by the reference method based on retention of ethylene glycol monoethyl ether (EGME) to soil surface particles, as proposed Cihacek and Bremner (1979). Aluminum crucibles containing approximately 1 g of oven-dried soil at 105 ° C and 3 ml of EGME were placed in a desiccator containing two petri dishes, one with 40 ml EGME and the other with 200 g $CaCl_2$. The desiccator was closed and the system rested for 45 min. Then 0.250 mmHg vacuum was applied for 45 minutes, letting them stand for approximately 6 hours. After this time, the crucibles were weighed and immediately returned to the desiccator,

121 applying the vacuum for 45 minutes again. This last procedure was performed until a
122 constant weight was reached. SSA was calculated by dividing EGME mass retained in
123 the sample after reaching constant weight by $3.71x10^{-4}$ (amount of EGME required to
124 cover an area of 1 m^2), according Embrapa (2017).

125 The concentration of cations was evaluated considering the exchangeable
126 potassium (K^+), calcium (Ca^{2+}), magnesium (Mg^{2+}), sodium (Na^+) and aluminum (Al^{3+})
127 in soil, as well as the potential and effective cation exchange capacity (CEC). The Na^+
128 and K^+ were extracted by the double acid extraction method ($Mehlich^{-1}$) with acid
129 solution of HCl 0.05 mol L^{-1} and H_2SO_4 0.0125 mol L^{-1} and quantified by flame
130 photometry. The Ca^{2+}, Mg^{2+} e Al^{3+} were extracted with KCl 1.0 mol L^{-1}, where Ca^{2+} and
131 Mg^{2+} were determined by atomic absorption spectrometry, and Al^{3+} quantified by acid-
132 base titration with NaOH 0.0125 mol L^{-1} (EMBRAPA, 2017).

133 Based on the results of the chemical analyses, we calculated the sum of bases
134 (SB), cation exchange capacity (CEC), base saturation (V%), and aluminum saturation
135 (m). The determination of pH was performed in water, at a 1:2.5 ratio (10 mL of soil for
136 25 mL of distilled water) with subsequent reading in a potentiometer (EMBRAPA,
137 2017). Soil characterization is described in table 1.

138

139

Table 1 - Characterization of soils with different specific surface area.

SiBCS[1]	**PVd**	**LVdf**	**PVd**	**PBACal**	**SXe**	**LVaf**	**LVd**	**PVAd$_1$**	**CXe**	**RRe**	**PVAd$_2$**	**PVAd$_3$**	**PVAd$_4$**
Soil Taxonomy[2]	Ultisol	Oxisol	Ultisol	Ultisol	Alfisol	Oxisol	Oxisol	Ultisol	Inceptisols	Entisol	Ultisol	Ultisol	Ultisol
Textural class	SL	VC	SL	SL	SL	Clay	SCL	SCL	CL	SiL	Sand	SL	SL
physical properties													
SSA ($m^2\ g^{-1}$)	30.7	162	38.2	37.8	45.9	108	64.7	71.1	100	75.0	11.5	35.9	54.9
Sand ($g\ g^{-1}$)	0.62	0.05	0.72	0.61	0.67	0.24	0.63	0.60	0.27	0.15	0.94	0.70	0.63
Silt ($g\ g^{-1}$)	0.27	0.21	0.12	0.29	0.22	0.25	0.10	0.07	0.40	0.60	0.03	0.19	0.22
Clay ($g\ g^{-1}$)	0.11	0.74	0.15	0.10	0.11	0.51	0.27	0.33	0.32	0.24	0.03	0.10	0.15
ρ ($g\ cm^{-3}$)	1.43	0.99	1.40	1.44	1.43	1.15	1.32	1.28	1.28	1.34	1.48	1.43	1.40
chemical properties													
C ($g\ kg^{-1}$)	6.90	19.1	9.80	10.0	7.20	18.2	19.0	14.2	18.9	12.8	3.00	8.40	10.5
pH	4.70	5.40	5.30	5.20	5.50	5.20	6.30	5.20	5.20	6.50	5.20	5.20	5.00
P ($mg\ dm^{-3}$)	10.0	4.90	10.1	6.10	9.30	10.1	25.3	19.9	19.8	3.70	6.00	14.3	20.2
K ($cmolc\ dm^{-3}$)	0.15	0.11	0.18	0.62	0.08	0.07	0.17	0.55	0.43	0.07	0.06	0.05	0.11
Ca ($cmolc\ dm^{-3}$)	1.45	5.55	2.76	4.41	3.66	3.71	7.76	4.63	4.39	5.91	0.25	1.68	2.13
Mg ($cmolc\ dm^{-3}$)	0.63	1.93	1.15	1.46	1.40	1.39	2.09	1.29	1.08	2.78	0.10	0.80	1.11
Na ($cmolc\ dm^{-3}$)	0.02	0.02	0.02	0.03	0.05	0.02	0.02	0.03	0.10	0.03	0.02	0.02	0.05
Al ($cmolc\ dm^{-3}$)	1.10	0.20	0.20	0.50	0.00	0.40	0.00	0.40	0.50	0.00	0.20	0.20	0.60
H+Al ($cmolc\ dm^{-3}$)	8.70	3.10	3.50	2.80	3.50	6.20	3.50	3.90	4.90	2.50	1.40	2.80	4.40
BS ($cmolc\ dm^{-3}$)	2.25	7.61	4.10	6.53	5.20	5.19	10.0	6.50	6.00	8.79	0.43	2.55	3.40
CEC_e ($cmolc\ dm^{-3}$)	3.35	7.81	4.30	7.03	5.20	5.59	10.0	6.90	6.50	8.79	0.63	2.75	4.00
CEC_p ($cmolc\ dm^{-3}$)	10.9	10.7	7.60	9.33	8.70	11.4	13.5	10.4	10.9	11.3	1.83	5.35	7.80
V (%)	20.6	71.1	54.0	70.2	60.4	45.5	74.3	62.5	55.6	77.8	23.7	48.2	44.1
m (%)	33.3	2.60	4.70	7.10	0.00	7.10	0.00	5.80	7.80	0.00	33.3	7.40	15.4

[1] Classification according to the Brazilian Soil Classification System; [2]Classification according Soil Taxonomy; PVd: Argissolo Vermelho Distrófico arênico; LVdf: Latossolo Vermelho Distroférrico típico; PBACal: Argissolo Bruno- Acinzentado Alítico humbrico; SXe: Planossolo Háplico Eutrófico arênico; LVaf: Latossolo Vermelho Aluminoférrico húmico; LVd: Latossolo Vermelho Distrófico típico; PVAd$_1$: Argissolo Vermelho-Amarelo Distrófico típico; CXe: Cambissolo Háplico Eutrófico; RRe: Neossolo Regolítico Eutrófico fragmentário; PVAd$_2$: Argissolo Vermelho-Amarelo Distrófico arênico abrúptico; PVAd$_3$: P Argissolo Vermelho-Amarelo Distrófico úmbrico; PVAd$_4$: Argissolo Vermelho-Amarelo Distrófico típico. ρ: bulk density; CEC_e: effective cation exchange capacity, CEC_p potential cation exchange capacity; SSA: specific surface area; BS: bases sum, V: bases saturations, m: Al saturation. SL: sand loam; VC: very clay; SCL: sand clay loam; CL: clay loam; SiL: silt loam.

147 **2.3 Samples preparation**

148 The samples were moistened with distilled water, maintaining a variation of
149 gravimetric water content between 0.10 and 0.35 g g^{-1}, according to the textural class,
150 and left in air-tight sealed containers for approximately 24 hours. Afterwards, the moist
151 samples were compacted in metallic rings of 3.6 cm in diameter and 1.0 cm in height,
152 with 12 replicates for each soil type.

153 To maintain the samples in similar compaction condition and to avoid the effect
154 of soil density on rheological variables, the soil mass used to compact the samples
155 was calculated in order to reach the compaction degree of 75% of maximum soil bulk
156 density, according to equation 1. The maximum density was estimated based upon the
157 clay content (Marcolin and Klein, 2011) as observed in equation 2.

$$m = v * (0.75 * \rho_{max}) \quad (1)$$

$$\rho_{max} = -0.0092 * \text{Clay} + 2.0138 \quad (2)$$

158 where m is dry soil mass (g), v is the final sample volume (cm^3), ρ_{max} is the maximum
159 soil bulk density (g cm^{-3}), and clay is the clay content (%).

160 The samples were saturated with distilled water for approximately 24 h. Half of
161 the samples were analyzed in a saturated moisture condition, and the other half was
162 drained in sand columns at -6 kPa matric potential (Reinert and Reichert, 2006).

163 All samples were analyzed in a compact modular rheometer (Anton Paar MCR
164 102), with a parallel plate measuring device, a fixed roughened lower plate of 50 mm
165 in diameter and a roughened upper rotary plate of 25 mm in diameter (PP25 / P2
166 model) according to Markgraf et al. (2006). The samples were placed on the bottom
167 plate, liberated from the metal rings, cut in height of 4 mm and diameter 25 mm for
168 analysis in the apparatus (Pértile et al., 2018), and submitted to the oscillatory test with
169 amplitude sweep and controlled strain. The gravimetric soil moisture was measured

and the normal tension on each sample was noted at the beginning of the test, as described in table 2.

Table 2 – Mean (± standard error) of normal force (σ_n) and gravimetric moisture (θ_g) at the test begging of soils with different specific surface area submitted to the amplitude sweep test with controlled deformation at matric potential of 0 and -6 kPa. Rio Grande do Sul, Brazil.

Soil	SSA ($m^2\ g^{-1}$)	0 kPa		6 kPa	
		σ_n (N)	θ_g ($g\ g^{-1}$)	σ_n (N)	θ_g ($g\ g^{-1}$)
$PVAd_2$	11.5	5.52 (±1.50)	0.31 (±0.01)	8.86 (±0.80)	0.06 (±0.00)
$PVAd_3$	30.8	2.46 (±0.46)	0.32 (±0.01)	5.65 (±0.91)	0.15 (±0.00)
PBACal	35.9	4.76 (±1.41)	0.32 (±0.00)	7.61 (±0.82)	0.14 (±0.00)
SXe	37.8	1.16 (±0.31)	0.34 (±0.00)	7.39 (±1.06)	0.18 (±0.00)
PVd_1	38.2	0.67 (±0.11)	0.33 (±0.01)	4.61 (±0.64)	0.14 (±0.00)
$PVAd_4$	45.9	1.08 (±0.23)	0.31 (±0.00)	5.29 (±0.68)	0.15 (±0.00)
PVd_2	54.0	0.98 (±0.46)	0.35 (±0.02)	6.49 (±0.51)	0.16 (±0.00)
RRe	64.7	2.33 (±0.57)	0.42 (±0.00)	5.68 (±0.90)	0.20 (±0.00)
LVd	71.1	2.19 (±0.37)	0.40 (±0.01)	8.36 (±0.72)	0.20 (±0.00)
$PVAd_1$	75.0	0.13 (±0.04)	0.42 (±0.01)	5.14 (±0.66)	0.27 (±0.00)
CXe	100	3.31 (±0.64)	0.44 (±0.01)	9.03 (±0.73)	0.27 (±0.00)
LVaf	108	1.01 (±0.12)	0.53 (±0.00)	3.20 (±0.43)	0.27 (±0.00)
LVdf	162	0.79 (±0.06)	0.64 (±0.03)	3.81 (±0.35)	0.33 (±0.00)

PVd: Argissolo Vermelho Distrófico arênico; LVdf: Latossolo Vermelho Distroférrico típico; PBACal: Argissolo Bruno- Acinzentado Alítico humbrico; SXe: Planossolo Háplico Eutrófico arênico; LVaf: Latossolo Vermelho Aluminoférrico húmico; LVd: Latossolo Vermelho Distrófico típico; $PVAd_1$: Argissolo Vermelho-Amarelo Distrófico típico; CXe: Cambissolo Háplico Eutrófico; RRe: Neossolo Regolítico Eutrófico fragmentário; $PVAd_2$: Argissolo Vermelho-Amarelo Distrófico arênico abrúptico; $PVAd_3$: P Argissolo Vermelho-Amarelo Distrófico úmbrico; $PVAd_4$: Argissolo Vermelho-Amarelo Distrófico típico.

2.4 Amplitude sweep test

The rheometric analyses were controlled and executed automatically by the software Rheoplus/32 V3.62 Anton Paar under the following conditions: plate distance

187 (gap) = 4 mm; rest period before the start of the test = 30 s; strain amplitude =
188 continuous ramp from 0.0001 to 100%; angular frequency = 0.5 Hz; temperature = 20
189 °C; normal force = between 0 e 12 N; number of measurement points = 30; and test
190 duration = about 14 min.

191 In oscillatory amplitude sweep tests, the shear stress (τ, Pa) is a result of the
192 force required to generate shear strain (γ, %) along the shear surface (Holthusen et
193 al., 2010), being calculated from the torque (M, mN) measured at each γ level and the
194 corresponding upper plate radius (r, m), according to equation 3, while γ is determined
195 by the ratio of deflection distance (s, m) at the sample's outer edge and gap size (h,
196 m), as given by equation 4.

$$\tau = \frac{2M}{\pi r^3} \tag{3}$$

$$\gamma = \frac{s}{h} * 100 \tag{4}$$

197 From these parameters, we calculate the storage modulus (*G'*, Pa), the loss
198 modulus (*G"*, Pa) and the loss factor (tan δ, dimensionless) (Figure 2a) with equations
199 5, 6 and 7 respectively. This adjustment derives from the presence of viscoelastic
200 behavior under oscillatory shear and the thus complex shear modulus G*, which
201 accounts for both elastic *(G')* and plastic/viscous behavior (*G"*) (Holthusen et al., 2010;
202 Markgraf et al., 2006; Mezger, 2014; Pértile et al., 2018, 2016).

$$G' = \frac{\tau}{\gamma} cos\delta \tag{5}$$

$$G'' = \frac{\tau}{\gamma} sen\delta \tag{6}$$

$$\tan\delta = \frac{G''}{G'} \tag{7}$$

From the curves of τ, G', G" and tan δ as a function of the γ, the rheological variables were obtained according to figure 2 and their interpretation are summarized in table 3.

Table 3. Interpretation of rheological variables obtained from oscillation amplitude sweep test with controlled strain.

Rheological variable	**Abbreviation**	**Interpretation**
Initial value of storage modulus	G'_i	Soil resistance at the test beginning (Figure 2a).
Strain at the end of linear viscoelastic range	γ_{LVR}	Strain value that limits the fully elastic strain range (LVR). Strains greater than γ_{LVR} promote irreversible and cumulative modifications in the soil microstructure, though initially with predominance of the elastic behavior (Figure 2b).
Stress at the end of linear viscoelastic range	τ_{LVR}	Resistance that the soil sample offers to rupture at the end of linear viscoelastic range (Figure 2b).
Strain at the maximum shear stress point	$\gamma_{\tau max}$	Strain range applied to achieve the maximum shear stress (figure 2b)
Maximum shear stress	τ_{max}	Maximum internal resistance that the soil sample offers to resist the rupture of its microstructure
Strain at the yield point	γ_{YP}	Strain range prior to yield point (YP) or crossover. It delimits the transition range between elastic and viscous behavior. From γ_{YP}, the strains are totally irreversible, and the soil starts to show a viscous behavior (figure 2b).
Storage modulus value at the yield point	G'_{YP}	Soil resistance at the yield point (Figure 2a).
Integral z	Iz	Calculated by the area between the actual tan δ during the amplitude sweep test until the YP (where tan δ = 1) and a horizontal line of tan δ = 1. The higher its value, the greater the elastic behavior of the soil and the greater is its microstructural rigidity (Figure 2a).

2.5 Statistical analysis

The study was conducted in a factorial scheme, and SSA 2 13 with moisture conditions (0 and -6 kPa) with 6 replicates. We tested for normality (Shapiro and Wilk, 1965) and homoscedasticity (Levene, 1960). Afterwards, we performed analysis of variance by means of the F test, and, when significant, we compared the moisture condition by the Scott Knott test at 5% of significance and SSA by regression analysis. Furthermore, Pearson correlation analysis was performed to verify relationship between other soil properties and the rheological variables. All data were analyzed using the R statistical environment, version 3.5.0.(R Development Core Team, 2017).

3 RESULTS

Soil specific surface area having significant adjustment to the polynomial fit model, with R^2 explained more than 62% and 78% of the strain variance in the linear viscoelastic range (γ_{LVR}) for saturated samples (0 kPa) and for drained samples (-6 kPa) respectively (Figure 3a). The γ_{LVR} increased by 160% up to SSA of 95 $m^2\ g^{-1}$ for samples analyzed at 0 kPa matric potential (Ψ_m), and by 222% up to SSA of 117 $m^2\ g^{-1}$ for samples at of -6 kPa Ψ_m. However, from these SSA values, γ_{LVR} reduced about 38% in samples with 0 kPa and 12% in samples with -6 kPa up to SSA of 162 $m^2\ g^{-1}$. The γ_{LVR} was higher in saturated samples in soils with SSA of up to 30 $m^2\ g^{-1}$. There was no significant difference in γ_{LVR} between the Ψ_m for soils with SSA in the range from 30 to 100 $m^2\ g^{-1}$. However, γ_{LVR} was higher in samples drained at 6 kPa in soils with SSA above 100 $m^2\ g^{-1}$.

The deformation at the maximum shear stress point (γ-τ_{max}) also showed significant polynomial adjustment with SSA in both Ψ_m, with R^2 explaining 50% and 70% of the data variation in the Ψ_m of 0 and -6 kPa respectively (Figure 3b). The γ-τ_{max}

235 increased about 8-folds up to SSA of 97 m^2 g^{-1} in samples analyzed at 0 kPa and 4-
236 folds up to the SSA of 101 m^2 g^{-1} in samples analyzed at -6 kPa. This means that the
237 increase of 1 m^2 g^{-1} up to these surface area values increased by 0.03 and 0.01% (in
238 absolute values) the strain ranges up to the maximum shear stress for samples at 0
239 and -6 kPa respectively. However, there was a subsequent reduction about 2-folds up
240 to highest SSA for both Ψ_m. There were no differences in γ-τ_{max} between Ψ_m in soils
241 with low SSA. However, in soils over 90 m^2 g^{-1}, samples drained at -6 kPa showed
242 higher γ-τ_{max} than saturated samples.
243 For samples at 0 kPa, the increase of SSA provided almost linear increase of
244 2.4-folds in strain at the yield point (γ_{YP}) from lowest to highest SSA value, explaining
245 more than 75% of the variation of this rheological variable (Figure 3c). In absolute
246 values, the increase of 1 m^2 g^{-1} in superface area provided an increase of 0.28% in the
247 γ_{YP}, delaying the soil crossover. Draining at Ψ_m of -6 kPa delayed crossover. Only two
248 soils showed crossover within the strain range used in the analysis (0.0001 to 100%).
249 Thus, it was not possible to verify an evident effect of SSA on γ_{YP} in this Ψ_m.
250 In saturated samples, the integral z (Iz) increased by around 146% from the soil
251 of lowest SSA at the SSA of 139.11 m^2 g^{-1}, with a subsequent slight reduction by
252 approximately 2% until the highest SSA, following a polynomial fit model (Figure 3d).
253 The increase of each surface area unit (1 m^2 g^{-1} of soil) increased 0.1 unit of Iz. There
254 was no relationship between Iz and SSA for samples drained at -6 kPa, that ranged
255 from 13 to 78, with an average of 51. In relation to Ψ_m, the samples drained at -6 kPa
256 presented higher structural stability when compared to the saturated samples, and the
257 differences in Iz between the two Ψ_m also had no relation to the SSA.
258 Soil resistance evaluated by the storage module at the beginning of the test (G'_i)
259 was not related to SSA for samples analyzed under saturated conditions (Figure 4a).

In samples drained at -6 kPa, there was a decrease in G'_i with increase of SSA up to 114 $m^2 g^{-1}$ and a subsequent increase of 27% to the highest SSA. The reduction in Ψ_m increased G'_i in all soils, especially those with lower SSA.

The shear resistance at the end of viscoelastic linear range (τ_{LVR}), maximum shear stress (τ_{max}) and storage modulus at the yield point (G'_{YP}) were not related to SSA in any of the Ψ_m analyzed (figure 4b-d). The τ_{LVR} ranged from 5.7 to 97 Pa at 0 kPa and from 172 to 445 Pa at -6 kPa. On average, samples with Ψ_m of -6 kPa were 6-folds higher than samples with Ψ_m of 0 kPa (Figure 4b).

The τ_{max} also showed great variation, ranging from 59 to 925 Pa and from 2002 to 5537 Pa in the Ψ_m of 0 and -6 kPa respectively and the average difference of τ_{max} between Ψ_m was approximately 8-folds (Figure 4c). The G'_{YP} ranged from 31 to 157 Pa, with an average of 90 Pa in soils at 0 kPa. G'_{YP} was about 21-folds higher in the only two crossover points at -6 kPa compared with their respective values at 0 kPa (Figure 4d).

However, these variables of microstructural resistance correlated with other soil properties (Table 4). Except G'_i, resistance variables showed positive significant correlation with σ_n, and Ca/Mg ratio, as well as a negative correlation with Mg/K ratio when analyzed at 0 kPa. At matric potential of -6 kPa, besides the SSA, the G'_i correlated negatively with σ_n, clay content, C and Mg concentration, Ca/K and Mg/K ratio, as well as base saturation and cation exchange capacity, but correlated positively with sand content and Al concentration. τ_{LVR} and τ_{max} show significant and positive correlation with σ_n, K concentration and Ca/Mg ratio. In addition, τ_{max} also was positively influenced by Na concentration.

Table 4 – Pearson correlation coefficient of microstructural resistance variables storage modulus at the test begging (G'_i) shear stress at the end of the linear viscoelastic range (τ_{LVE}), maximum shear stress (τ_{max}), integral zone (Iz) with normal force (σ_n), physical and chemical properties of soils with different specific surface area (SSA) submitted to the amplitude sweep test with controlled deformation in the matric potential of 0 and -6 kPa. Rio Grande do Sul – Brazil.

Soil properties	**0 kPa**				**6 kPa**		
	G'_i	**τ_{LVR}**	**τ_{max}**	**G'_{YP}**	**G'_i**	**τ_{LVR}**	**τ_{max}**
σ_n	0.28	0.77**	0.69**	0.56*	0.75**	0.71**	0.57*
SSA	0.01	-0.08	0.03	-0.04	-0.60**	0.07	0.18
C	-0.05	0.02	0.23	0.15	-0.74**	0.13	0.41
Sand	-0.11	0.23	0.12	0.27	0.66**	0.00	-0.12
Silt	0.24	-0.32	-0.23	-0.51	-0.40	-0.01	0.09
Clay	-0.04	-0.06	0.01	0.03	-0.56*	0.01	0.10
pH	-0.16	-0.27	-0.17	0.04	-0.45	-0.22	-0.03
P	0.11	0.32	0.52	0.31	-0.14	0.32	0.55
K	-0.19	0.22	0.33	0.39	0.17	0.73**	0.68**
Ca	-0.20	-0.20	0.00	0.13	-0.62**	0.08	0.28
Mg	-0.08	-0.54	-0.40	-0.27	-0.68**	-0.19	-0.03
Na	0.00	0.27	0.43	0.06	-0.08	0.54	0.71**
Al	0.17	0.23	0.17	-0.14	0.29	0.28	0.12
Ca/Mg	-0.32	0.60*	0.75**	0.77**	-0.10	0.66**	0.79**
Ca/K	0.12	-0.55	-0.48	-0.46	-0.67**	-0.55	-0.37
Mg/K	0.22	-0.61*	-0.57*	-0.58*	-0.57*	-0.54	-0.40
H+Al	0.14	0.08	0.10	-0.25	-0.19	-0.04	0.02
SB	-0.18	-0.27	-0.07	0.06	-0.63*	0.07	0.26
CEC_e	-0.17	-0.25	-0.06	0.05	-0.62*	0.11	0.28
CEC_p	-0.08	-0.19	0.00	-0.10	-0.68**	0.04	0.24
V	-0.08	-0.42	-0.23	-0.02	-0.54	0.05	0.21
m	-0.02	0.51	0.27	0.15	0.72**	0.14	-0.15

SSA: specific surface area; C: carbon; CEC_e: effective cation exchange capacity, CEC_p: potential cation exchange capacity; V: saturation of bases; m: saturation of aluminum.

** and * indicate significant correlation at $p \leq 0.01$ and $p \leq 0.05$ respectively.

4 DISCUSSION

The increase in γ_{LE}, γ_{YP}, $\gamma_{\tau max}$ and Iz with increasing SSA is due to a lubricating effect of clay particles in soils. In soils made up of particles of different sizes, the smaller particles fill spaces formed between the larger ones, reducing the friction and facilitating the movement related to shearing of larger particles (Ghezzehei and Or, 2001; Reichert et al., 2010; Vallejo and Mawby, 2000). These results corroborate with those found by Markgraf and Horn (2007) who also found higher strain limits in soils with higher clay content when comparing the microstructural resistance of Oxisols occurring in southern Brazil.

Nevertheless, there was a reduction of γ_{LE}, γ_{YP} and Iz in soils with SSA higher than 100 m^2 g^{-1}. This reduction is probably associated with the presence of pseudosand. In soils with high clay content, the cementing action of Fe-(hydr)oxides and other inorganic compounds produces very stable microaggregates (Brady and Weil, 2013), which can reach the diameter of the silt fraction (pseudosilt) or even sand (pseudosand). Donagemma et al. (2003) observed the presence of pseudosand and pseudosilt in all Oxisols studied, and that more than 50% of silt fraction of these were constituted of pseudosilt. In LVaf (SSA of 108 m^2 g^{-1}) and LVdf (SSA of 162 m^2 g^{-1}), the presence of pseudosand was observed visually and also verified by sensation of roughness during tactile evaluation, according Santos et al. (2013).

Pseudosands, because of angular shape and rough surface (Markgraf and Horn, 2007), increase friction between particles, hindering their shear movement and reducing the soil microstructural elasticity, with a more pronounced effect on the linear viscoelastic deformation range. Pértile et al. (2018) found only a small difference between the γ_{LVE} of a Oxisol with high clay content (603 g kg^{-1}) and of a sandy loam Ultisol (57 g kg^{-1}) due to the presence of pseudosands. Markgraf and Horn (2007) also

observed a decrease in elasticity of microstructure due to the presence of pseudosands. The same authors, when removing organic matter and Fe-(hidr)oxides of soil, observed transitions of pseudosands complexes to uniform surfaces of disconnected particles, with reduced friction and increased microstructure elasticity.

The reduction of water content with range of Ψ_m from 0 kPa to -6 kPa increased the purely elastic strain (i.e. γ_{LVR}), the strain at the maximum shear stress, especially in soils with higher SSA (above 80 $m^2\ g^{-1}$), as well as increased the integral z, which is in agreement with those found by Holthusen et al. (2019) and Pértile et al. (2016). These authors found a tendency in soil elasticity to increase as the Ψ_m became more negative, with pronounced effect in clayey soils.

This occurs because the increase in SSA provides greater expression of adhesion and cohesion forces (Reichert et al., 2010), favoring contact and bonding between soil particles by capillary forces related to water menisci (Ghezzehei and Or, 2001, 2000). However, in same water content, the increase in clay-water attraction by van der Waals forces at higher SSA, provide the coating of particles by water molecules and decreases the contact angle of water menisci with clay particles to near zero (Lourenço et al., 2012). This causes particle lubrication and facilitates the mobility between them (Hillel, 2004; Osipov, 2015). In this way, the particles move without losing contact, favoring the elasticity of soil microstructure.

The greater contact between the particles by the reduction of water content was also expressed in all variables of microstructural resistance. Drainage increases soil water tension, which increases the curvature of water menisci, causing a contraction force and approaching the particles (Hillel, 2004). In addition, drainage eliminates the water, a friction-reducing component (Holthusen et al., 2012b). This approach can form stable bonds at rest (Osipov, 2015), increasing the microstructure stability.

Differently from what was expected, no relationship was observed between SSA and microstructural strength evaluated by shear stress at the end of linear viscoelastic range (τ_{LVE}), with maximum shear stress (τ_{max}) or with the storage module value at the yield point (G'_{YP}) in both matric potentials. We expected higher microstructural strength with increase of SSA, due to the greater expression of adhesion and cohesion forces, especially at Ψ_m of -6 kPa.

Increasing microstructural strength with increasing SSA is related to the mutual particle attraction due to adhesive and cohesive forces. Pértile et al. (2016), studying the influence of water content on soil rheological variables, verified higher τ_{max} in horizons with higher clay content when analyzed under saturation conditions. They also observed increase of τ_{max} with increased water drainage/more negative matric potential, with a more pronounced effect in clay soils.

However, these rheological variables had a significant correlation with other soil characteristics, such as normal force (σ_n) at the test beginning. The σ_n had a significant effect on G'_i, τ_{LVE}, and τ_{max}, providing greater microstructural strength as the force on the sample surface increases. Soils that started the amplitude sweep test with similar values of σ_n, despite different SSA, presented similar microstructural resistance. In addition, soils with little variation in SSA but with large differences in the initial σ_n presented very distinct microstructural resistance.

Holthusen et al., (2017) found that σ_n has a strong impact on most rheological parameters. These authors proposed a modification of amplitude sweep test (AST), using controlled σ_n in determination of soil microstructure resistance. They observed a nonlinear increase of Iz and τ_{max} with increase of compressive force in Oxisols. We found similar results, where we verified increase of microstructural resistance with increase of the compressive force on the samples. However, the σ_n variation observed

369 in this study was dependent on the procedure during the preparation of sample before
370 the analysis.

371 In the standard AST, the distance between parallel plates is fixed, usually at 4
372 mm (Holthusen et al., 2010; Markgraf et al., 2006). The samples are prepared in metal
373 rings with an approximate volume of 10 cm^3, need to be cut to a height of approximately
374 4.5 mm for analysis on rheometer (Pértile et al., 2018). This difference in height
375 between the sample and the gap causes variation in σ_n, that, besides sample handling,
376 also depends on water content, sample density and grain size distribution.

377 Regardless of Ψ_m, higher σ_n provides a greater approximation between
378 particles, and can have different effects on shear strength of microstructure, depending
379 on the size and shape of the particles. In soils with predominance of large and rounded
380 particles, like those of sand and silt (lower SSA), the compressive force provides
381 rearrangement of particles, increasing the packing density (Cho et al., 2006;
382 Santamarina and Cho, 2004). This densification causes increase of contact area and
383 number between individual particles (Osipov, 2015), reducing their ability to move.
384 Hence, for the particles to move, they need to roll over each other, provoking the
385 phenomenon of dilatation (Holthusen et al., 2019). This process demands a high force
386 and leads to a turbulent shear (Markgraf et al., 2006) and also could explain the
387 relationship between increase of sand content with higher G'_i for samples at -6 kPa.

388 Furthermore, angular and rough particles provide greater shear strength
389 (Santamarina and Cho, 2004). This can be associated with higher shear stress
390 observed in soils with high σ_n and large amount of silt, since the decrease in mean
391 particle diameter tends to reduce its sphericity, that is, they become angular as the
392 surfaces become rougher (Vepraskas and Cassell, 1987). In addition, soils with
393 particles predominantly of platy format (high SSA), the compression force can cause

394 particle alignment, mainly with greater thickness of the water films in the contact points
395 between particles (Osipov, 2015; Santamarina and Cho, 2004), as in soils in saturated
396 condition. This alignment decreases the particles resistance to movement, leading to
397 a sliding shear (Holthusen et al., 2017; Markgraf et al., 2006; Reichert et al., 2010;
398 Santamarina and Cho, 2004), as observed in the inverse relationship between SSA
399 and G'_i.

400 The positive relationship between the microstructure strength evaluated by τ_{LVE}
401 and τ_{max} on the -6 kPa matrix potential may be due to the cementing effect of salts at
402 the points of contact between the soil particles. Na and K, compared to Ca and Mg,
403 have low hydration energy and they can be more easily dehydrated (Essington, 2004;
404 Sposito, 2008). With the reduction of soil water content, these ions can precipitate at
405 the contact areas between particles. When crystallizing at the particle-water–air
406 surface, salts build up a much stronger linkage than cohesive bridges between
407 particles and can result in a strength increase (Holthusen et al., 2012a). The cementing
408 effect of cations was reported by Holthusen et al. (2012a), which verified increase in
409 the τ_{max} of the microstructure with an increase of K concentration in different matric
410 potentials for some soils in Germany. Soulié et al. (2007) verified an increase in
411 compressive strength in natural sandy material with increasing of crystallization index
412 of NaCl.

413 For τ_{LVE} G'_{YP} and τ_{max}, there was effect of concentration and type of cation,
414 where the increase in Ca/Mg ratio increased the microstructure strength. Reason for
415 this is that molecular forces at the solid-liquid interface can act on the repulsion or
416 attraction of particles, mostly controlled and taking place in the diffuse double layer
417 (DDL). According to DDL theory, the increase of concentration and valency of cations
418 that compose the electrolytic soil solution, reduces the repulsive forces between the

particles with negative electrical charges, favoring the flocculation process (Hillel, 2004). In this way, the cations with higher valency (Ca^{+2}, Mg^{+2} and Al^{+3}) increase the soil microstructure resistance.

However, the effect on DDL can be different according to the physico-chemical characteristics of ions and type of interaction with particles (Anderson and Sposito, 1992; Chorover and Sposito, 1995). The ability of the cation to approach the particles will depend, besides their electric charge, of its size expressed by the hydrated ray. The Ca^{+2}, compared to Mg^{+2}, has a lower hydrated radius and greater binding energy, being able to be closer to particle surface and be maintained with a greater for (Sparks, 2003; Sposito, 2008), presenting greater aggregation power. This could explain the higher shear strength in soils with higher Ca/Mg ratio.

As mentioned above, the rheological variables of resistance (τ_{LVE}, τ_{MAX} and G'_{YP}), mainly in unsaturated soil conditions are quite dependent on particle characteristics, such as size, shape and roughness, and the phenomena that keep them close, such as the compressive force (σ_n) and molecular force (DDL). Any modification in these factors, even if small, can reduce the soil microstructural resistance. Therefore, it is essential to improve the understanding of these effects on the interaction between particles, and consequently on the microstructural strength.

Therefore, we suggest in future work, to evaluate the impact of σ_n on the elasticity and shear strength of the microstructure in soil samples with particles of similar size, but with different shape and roughness. Another proposal would be to work with samples of the same particle shape, evaluating the effect of different classes of diameters on the microstructure elasticity and resistance. This would help to understand how the size and shape of particles act on the shear resistance of the microstructure.

5 CONCLUSIONS

We conducted rheological analysis by means of an amplitude sweep test on thirteen Brazilian soils of varying specific surface area (SSA) due to different textures and clay minerals and we verified that.

The increase in SSA provides increased the soil elasticity as was proven by increased deformation at the end of the linear viscoelastic range, the strain at maximum shear stress point, and at the yield point and integral Z. However, the formation of pseudosands reduced the elasticity of microstructure again, despite a higher SSA.

The microstructural strength evaluated by the stress at the end of the linear viscoelastic interval, maximum shear stress and yield point storage modulus were not related to SSA. These variables were more dependent on the normal force applied on the sample during the amplitude sweep test. Thus, to compare microstructure strength between soils, it is necessary to modify the test and apply a controlled normal force on the samples.

Acknowledgements

This study was supported by the Federal University of Santa Maria (UFSM) and the Coordination for the Improvement of Higher Education Personnel (Capes) in the form of a doctoral scholarship to the first author.

6 REFERENCES

Anderson, S.J., Sposito, G., 1992. Proton surface-charge density in soils with structural and ph-dependent charge. Soil Science Society of America Journal 56, 1437. https://doi.org/10.2136/sssaj1992.03615995005600050017x

Brady, N.C., Weil, R.R., 2013. Elements of Nature and Soil Properties, 3rd ed. Bookman, Porto Alegre.

Bronick, C.J., Lal, R., 2005. Soil structure and management: a review. Geoderma 124, 3–22. https://doi.org/10.1016/j.geoderma.2004.03.005

Carlesso, R., Santos, R.F., 1999. Disponibilidade de água às plantas de milho em solos de diferentes texturas. Revista Brasileira de Ciência do Solo 23, 17–25. https://doi.org/10.1590/S0100-06831999000100003

Cavalli, J.P., Reichert, J.M., Rodrigues, M.F., de Araújo, E.F., 2020. Composition and functional soil properties of arenosols and acrisols: Effects on eucalyptus growth and productivity. Soil and Tillage Research 196, 104439. https://doi.org/10.1016/j.still.2019.104439

Cho, G.-C., Dodds, J., Santamarina, J.C., 2006. Particle shape effects on packing density, stiffness, and strength: natural and crushed sands. Journal of Geotechnical and Geoenvironmental Engineering 132, 591–602. https://doi.org/10.1061/(ASCE)1090-0241(2006)132:5(591)

Chorover, J., Sposito, G., 1995. Surface charge characteristics of kaolinitic tropical soils. Geochimica et Cosmochimica Acta 59, 875–884. https://doi.org/10.1016/0016-7037(94)00357-2

Cihacek, L.J., Bremner, J.M., 1979. A simplified ethylene glycol monoethyl ether procedure for assessment of soil surface area. Soil Science Society of America

489 Journal 43, 821–822.
490 https://doi.org/10.2136/sssaj1979.03615995004300040045x
491 Donagemma, G.K., Ruiz, H.A., Fontes, M.P.F., Ker, J.C., Schaffer, C.E.G.R., 2003.
492 Dispersão de Latossolos em resposta à utilização de pré-tratamentos na
493 análise textural. Revista Brasileira de Ciência do Solo 27, 765–772.
494 https://doi.org/10.1590/S0100-06832003000400021
495 EMBRAPA, 2017. Manual de Métodos de Análise de Solo, 3rd ed. Embrapa, Brasília.
496 Essington, M.E., 2004. Soil and water chemistry: an integrative approach. CRC Press,
497 Boca Raton, Fla.
498 Ghezzehei, T. a., Or, D., 2001. Rheological properties of wet soils and clays under
499 steady and oscillatory stresses. Soil Science Society of America Journal 65,
500 624–624. https://doi.org/10.2136/sssaj2001.653624x
501 Ghezzehei, T. a, Or, D., 2000. Dynamics of soil aggregate coalescence and theological
502 processes. Water Resources Research 36, 367–379.
503 Gubiani, P.I., Pértile, P., Reichert, J.M., 2018. Relationship of precompression stress
504 with elasticity and plasticity indexes from uniaxial cyclic loading test. Soil and
505 Tillage Research 180, 29–37. https://doi.org/10.1016/j.still.2018.02.004
506 Hillel, D., 2004. Introdution to environmental soil physics. Academic Press, San Diego.
507 Holthusen, D., Pértile, P., Reichert, J.M., Horn, R., 2019. Viscoelasticity and shear
508 resistance at the microscale of naturally structured and homogenized
509 subtropical soils under undefined and defined normal stress conditions. Soil and
510 Tillage Research 191, 282–293. https://doi.org/10.1016/j.still.2019.04.014
511 Holthusen, D., Pértile, P., Reichert, J.M., Horn, R., 2017. Controlled vertical stress in
512 a modified amplitude sweep test (rheometry) for the determination of soil

513 microstructure stability under transient stresses. Geoderma 295, 129–141.
514 https://doi.org/10.1016/j.geoderma.2017.01.034
515 Holthusen, D., Peth, S., Horn, R., 2010. Impact of potassium concentration and matric
516 potential on soil stability derived from rheological parameters. Soil and Tillage
517 Research 111, 75–85. https://doi.org/10.1016/j.still.2010.08.002
518 Holthusen, D., Peth, S., Horn, R., Kühn, T., 2012a. Flow and deformation behavior at
519 the microscale of soils from several long-term potassium fertilization trials in
520 Germany. Journal of Plant Nutrition and Soil Science 175, 535–547.
521 https://doi.org/10.1002/jpln.201100073
522 Holthusen, D., Reeb, D., Horn, R., 2012b. Influence of potassium fertilization, water
523 and salt stress, and their interference on rheological soil parameters in planted
524 containers. Soil and Tillage Research 125, 72–79.
525 https://doi.org/10.1016/j.still.2012.05.003
526 Kämpf, N., Marques, J.J., Curi, N., 2012. Mineralogia de solos brasileiros, in:
527 Pedologia: Fundamentos. Sociedade Brasileira de Ciência do Solo, Viçosa.
528 Lal, R., Shukla, M., 2004. Principles of soil physics, Books in soils, plants and the
529 environment. Marcel Dekker, New York, NY.
530 Levene, H., 1960. Robust tests for equality of variances, in: Olkin, I., Ghurye, S.G.,
531 Hoeffding, W., Madow, W.G., Mann, H.B. (Eds.), Contributions to Probability
532 and Statistics: Essays in Honor of Harold Hotelling (Ingram Olkin, Sudhist G.
533 Ghurye, Wassily Hoeffding, William G. Madow, and Henry B. Mann, Eds.).
534 Stanford University Press, Menlo Park, pp. 278–292.
535 https://doi.org/10.1137/1003016

Lourenço, S.D.N., Gallipoli, D., Augarde, C.E., Toll, D.G., Fisher, P.C., Congreve, A., 2012. Formation and evolution of water menisci in unsaturated granular media. Géotechnique 62, 193–199. https://doi.org/10.1680/geot.11.P.034

Marcolin, C.D., Klein, V.A., 2011. Determinação da densidade relativa do solo por uma função de pedotransferência para a densidade do solo máxima. Acta Scientiarum. Agronomy 33. https://doi.org/10.4025/actasciagron.v33i2.6120

Markgraf, W., Horn, R., 2007. Scanning electron microscopy–energy dispersive scan analyses and rheological investigations of South-Brazilian soils. Soil Science Society of America Journal 71, 851–851. https://doi.org/10.2136/sssaj2006.0231

Markgraf, W., Horn, R., Peth, S., 2006. An approach to rheometry in soil mechanics—Structural changes in bentonite, clayey and silty soils. Soil and Tillage Research 91, 1–14. https://doi.org/10.1016/j.still.2006.01.007

Mentges, M.I., Reichert, J.M., Rodrigues, M.F., Awe, G.O., Mentges, L.R., 2016. Capacity and intensity soil aeration properties affected by granulometry, moisture, and structure in no-tillage soils. Geoderma 263, 47–59. https://doi.org/10.1016/j.geoderma.2015.08.042

Mezger, T.G., 2014. The Rheology Handbook, 4th ed. Vincentz Network, Hanover.

Nimmo, J.R., 2005. Porosity and pore-size distribution, in: Encyclopedia of Soils in the Environment. Elsevier, pp. 295–303. https://doi.org/10.1016/B0-12-348530-4/00404-5

Osipov, V.I., 2015. Physicochemical theory of effective stress in soils, SpringerBriefs in Earth Sciences. Springer International Publishing, Cham. https://doi.org/10.1007/978-3-319-20639-4

560 Pennell, K.D., 2016. Specific Surface Area, in: Reference Module in Earth Systems
561 and Environmental Sciences. Elsevier. https://doi.org/10.1016/B978-0-12-
562 409548-9.09583-X
563 Pértile, P., Holthusen, D., Gubiani, P.I., Reichert, J.M., 2018. Microstructural strength
564 of four subtropical soils evaluated by rheometry: properties, difficulties and
565 opportunities. Scientia Agricola 75, 154–162. https://doi.org/10.1590/1678-
566 992x-2016-0267
567 Pértile, P., Reichert, J.M., Gubiani, P.I., Holthusen, D., Costa, A. da, 2016. Rheological
568 parameters as affected by water tension in subtropical soils. Revista Brasileira
569 de Ciência do Solo 40, 1–14. https://doi.org/10.1590/18069657rbcs20150286
570 R Development Core Team, 2017. R: A language and environment for statistical
571 computing. R Foundation for Statistical Computing, Vienna.
572 Reichert, J.M., Albuquerque, J.A., Kaiser, D.R., Reinert, D.J., Urach, F.L., Carlesso,
573 R., 2009a. Estimation of water retention and availability in soils of Rio Grande
574 do Sul. Revista Brasileira de Ciência do Solo 33, 1547–1560.
575 https://doi.org/10.1590/S0100-06832009000600004
576 Reichert, J.M., Cechin, N.F., Reinert, D.J., Rodrigues, M.F., Suzuki, L.E.A.S., 2018a.
577 Ground-based harvesting operations of Pinus taeda affects structure and pore
578 functioning of clay and sandy clay soils. Geoderma 331, 38–49.
579 https://doi.org/10.1016/j.geoderma.2018.06.012
580 Reichert, J.M., Mentges, M.I., Rodrigues, M.F., Cavalli, J.P., Awe, G.O., Mentges, L.R.,
581 2018b. Compressibility and elasticity of subtropical no-till soils varying in
582 granulometry organic matter, bulk density and moisture. CATENA 165, 345–
583 357. https://doi.org/10.1016/j.catena.2018.02.014

584 Reichert, J.M., Norton, L.D., 2013. Rill and interrill erodibility and sediment
585 characteristics of clayey Australian Vertosols and a Ferrosol. Soil Research 51,
586 1. https://doi.org/10.1071/SR12243
587 Reichert, J.M., Norton, L.D., 1996. Fluidized Bed Combustion Bottom-Ash Effects on
588 Infiltration and Erosion of Variable-Charge Soils. Soil Science Society of
589 America Journal 60, 275.
590 https://doi.org/10.2136/sssaj1996.03615995006000010042x
591 Reichert, J.M., Norton, L.D., 1994a. Aggregate stability and rain-impacted sheet
592 erosion of air-dried and prewetted clayey surface soils under intense rain. Soil
593 Science 158, 159–169. https://doi.org/10.1097/00010694-199409000-00001
594 Reichert, J.M., Norton, L.D., 1994b. Fluidized Bed Bottom-Ash Effects on Infiltration
595 and Erosion of Swelling Soils. Soil Science Society of America Journal 58, 1483.
596 https://doi.org/10.2136/sssaj1994.03615995005800050030x
597 Reichert, J.M., Norton, L.D., Favaretto, N., Huang, C., Blume, E., 2009b. Settling
598 velocity, aggregate stability, and interrill erodibility of soils varying in clay
599 mineralogy. Soil Science Society of America Journal 73, 1369.
600 https://doi.org/10.2136/sssaj2007.0067
601 Reichert, J.M., Norton, L.D., Huang, C., 1994. Sealing, amendment, and rain intensity
602 effects on erosion of high-clay soils. Soil Science Society of America Journal
603 58, 1199. https://doi.org/10.2136/sssaj1994.03615995005800040028x
604 Reichert, J.M., Reinert, D.J., Suzuki, L.E.A.S., Horn, R., 2010. Mecânica do solo, in:
605 Física Do Solo. Sociedade Brasileira de Ciência do solo, p. 298.
606 Reinert, D.J., Reichert, J.M., 2006. Coluna de areia para medir a retenção de água no
607 solo: protótipos e teste. Ciência Rural 36, 1931–1935.
608 https://doi.org/10.1590/S0103-84782006000600044

609 Ross, G.J., 1978. Relationships of specific surface area and clay content to shrink-
610 swell potential of soils having different clay mineralogical compositions.
611 Canadian Journal of Soil Science 58, 159–166. https://doi.org/10.4141/cjss78-
612 020
613 Santamarina, J.C., Cho, G.C., 2004. Soil behaviour: The role of particle shape, in:
614 Advances in Geotechnical Engineering: The Skempton Conference. Thomas
615 Telford, Londres, pp. 604–617. https://doi.org/10.1680/aigev1.32644.0035
616 Santamarina, J.C., Klein, K.A., Wang, Y.H., Prencke, E., 2002. Specific surface:
617 determination and relevance. Canadian Geotechnical Journal 39, 233–241.
618 https://doi.org/10.1139/t01-077
619 Santos, R.D. dos, Lemos, R.C. de, Santos, H.G. dos, Ker, J.C., Anjos, L.H.C. dos,
620 Shimizu, S.H., 2013. Manual de descrição e coletas de solo no campo, 6th ed.
621 Sociedade Brasileira de Ciência do Solo, Viçosa.
622 Shapiro, S.S., Wilk, M.B., 1965. An analysis of variance test for normality (Complete
623 Samples). Biometrika 52, 591. https://doi.org/10.2307/2333709
624 Silva, A.J.N. da, Carvalho, F.G. de, 2007. Coesão e resistência ao cisalhamento
625 relacionadas a atributos físicos e químicos de um Latossolo Amarelo de
626 tabuleiro costeiro. Revista Brasileira de Ciência do Solo 31, 853–862.
627 https://doi.org/10.1590/S0100-06832007000500003
628 Soulié, F., El Youssoufi, M.S., Delenne, J.-Y., Voivret, C., Saix, C., 2007. Effect of the
629 crystallization of a solute on the cohesion in granular materials. Powder
630 Technology 175, 43–47. https://doi.org/10.1016/j.powtec.2007.01.025
631 Sparks, D.L., 2003. Environmental soil chemistry, 2nd ed. Academic Press, California.
632 Sposito, G., 2008. The chemistry of soils, 2nd ed. Oxford University Press, NewYork.

633 Stoppe, N., Horn, R., 2018. Microstructural strength of tidal soils – a rheometric
634 approach to develop pedotransfer functions. Journal of Hydrology and
635 Hydromechanics 66, 87–96. https://doi.org/10.1515/johh-2017-0031
636 Suzuki, L.E.A.S., Reichert, J.M., Albuquerque, J.A., Reinert, D.J., Kaiser, D.R., 2015.
637 Dispersion and flocculation of Vertisols, Alfisols and Oxisols in Southern Brazil.
638 Geoderma Regional 5, 64–70. https://doi.org/10.1016/j.geodrs.2015.03.005
639 Suzuki, L.E.A.S., Reichert, J.M., Reinert, D.J., 2013. Degree of compactness, soil
640 physical properties and yield of soybean in six soils under no-tillage. Soil
641 Research 51, 311. https://doi.org/10.1071/SR12306
642 Suzuki, L.E.A.S., Reinert, D.J., Reichert, J.M., Lima, C.L.R. de, 2008. Estimativa da
643 susceptibilidade à compactação e do suporte de carga do solo com base em
644 propriedades físicas de solos do Rio Grande do Sul. Revista Brasileira de
645 Ciência do Solo 32, 963–973. https://doi.org/10.1590/S0100-
646 06832008000300006
647 Vallejo, L.E., Mawby, R., 2000. Porosity influence on the shear strength of granular
648 material–clay mixtures. Engineering Geology 58, 125–136.
649 https://doi.org/10.1016/S0013-7952(00)00051-X
650 Vepraskas, M.J., Cassell, D.K., 1987. Sphericity and roundness of sand in Coastal
651 Plain soils and elationships with soil physical properties. Soil Science Society of
652 America Journal 51, 1108–1112.
653
654

FIGURES

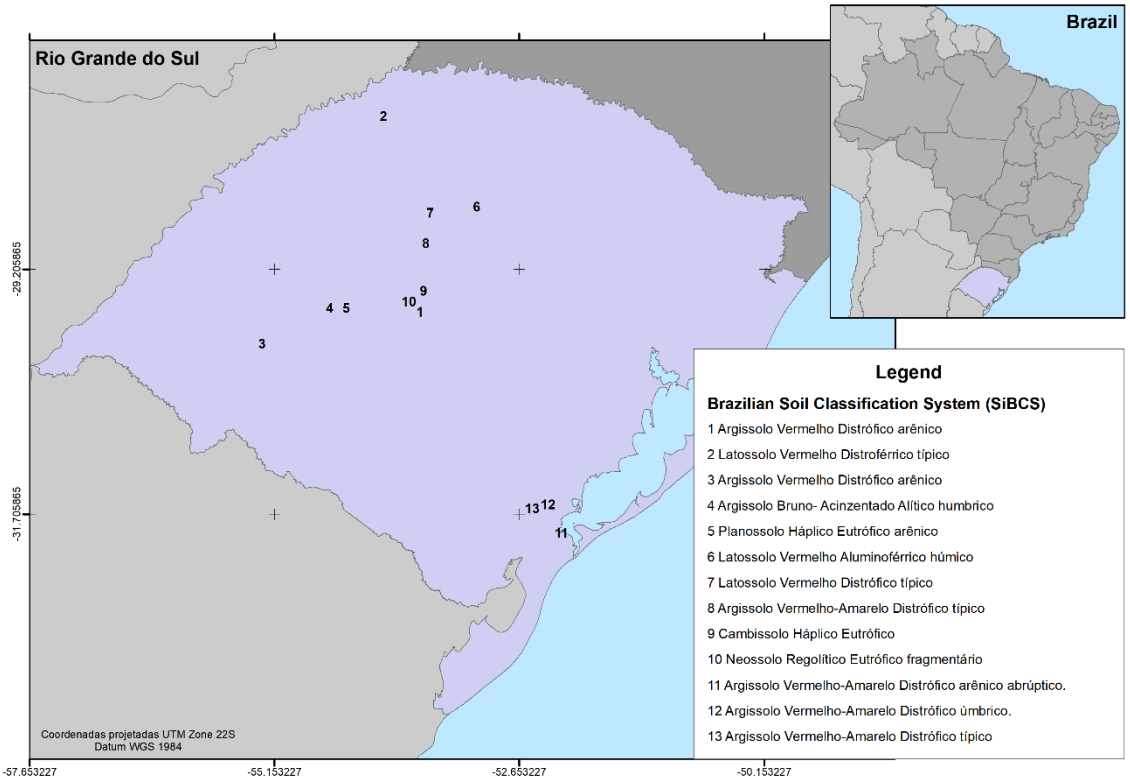

Figure 1. Location of soil sampling sites

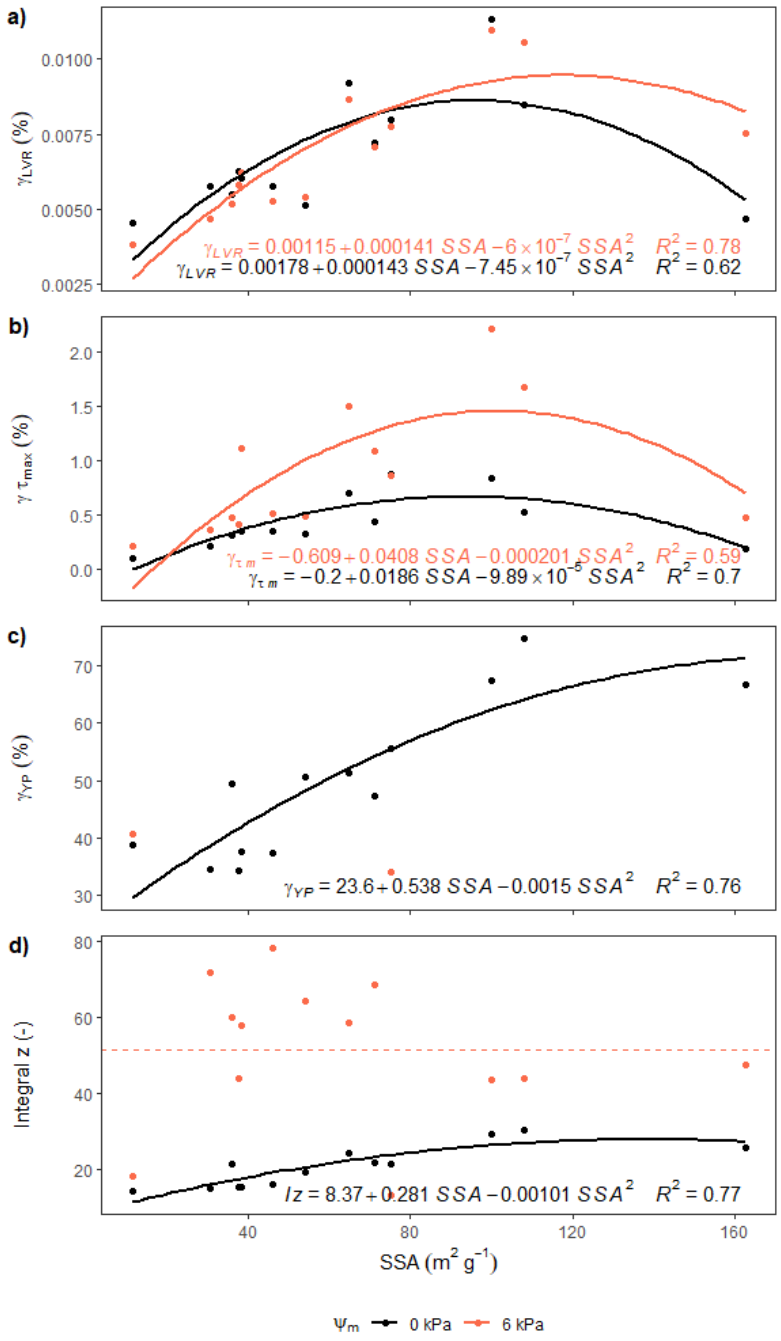

659

660 Figure 2. Microstructural elasticity evaluated by strain at the end of the linear
661 viscoelastic range (γ_{LVE}, b), strain at the maximum shear stress point ($\gamma_{\tau max}$, b), strain
662 (γ_{YP}, c) and storage modulus values (G'_{YP}, d) at the yield point as function of specific
663 surface area (SSA) at matric potential of 0 and -6 kPa.

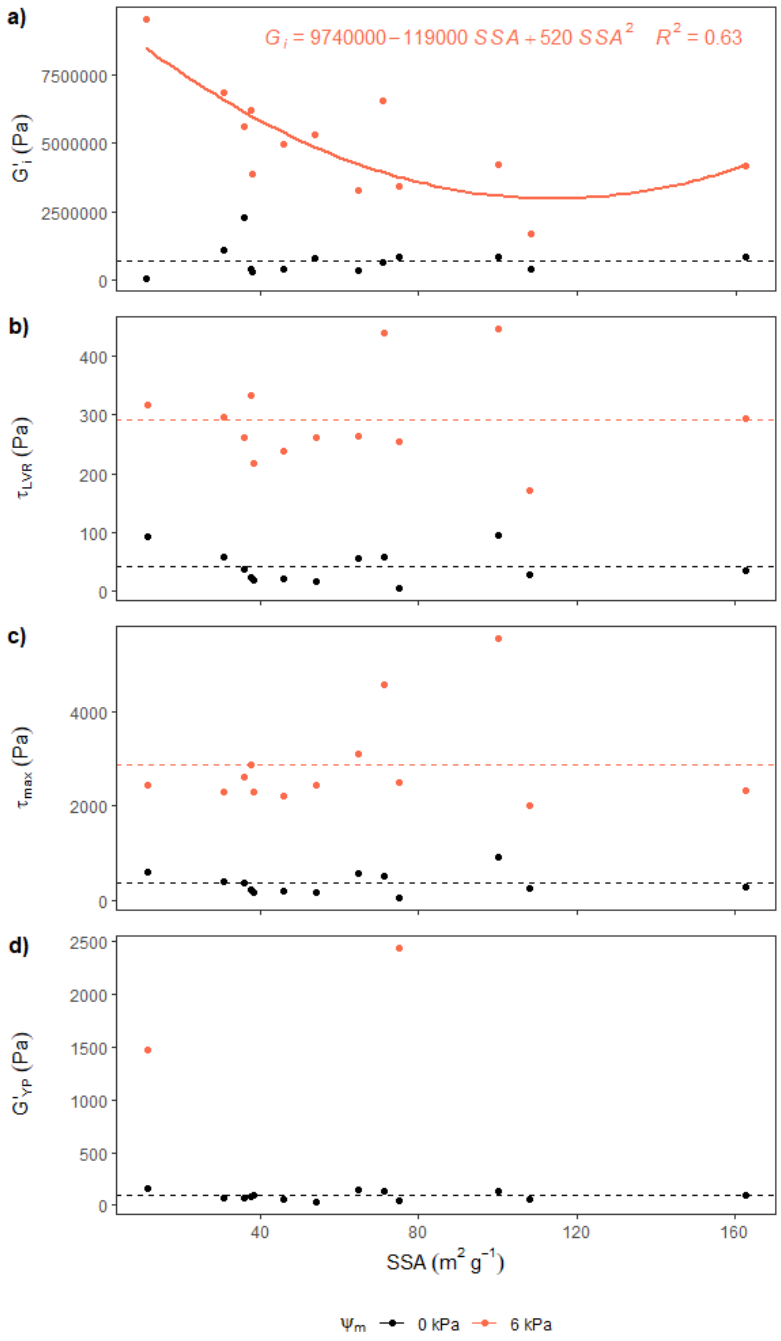

664

665

666 Figure 3 – Microstructural resistance evaluated by storage modulus at the test begging
667 (G'_{YP}, d), shear stress at the end of the linear viscoelastic range (τ_{LVE}, b), maximum
668 shear stress (τ_{max}, c), storage modulus values at the yield point (G'_{YP}, d) as function of
669 specific surface area (SSA) at matric potential of 0 and -6 kPa.

2.2 ESTUDO III - SOIL SOLUTION COMPOSITION AFFECTS MICROSTRUCTURE OF TROPICAL SALINE ALLUVIAL SOILS IN A SEMI-ARID ENVIRONMENT

[4] Soil solution composition affects microstructure of tropical saline alluvial soils in a semi-arid environment

Alan Carlos Batistão[a,*], Dörthe Holthusen[a], José Miguel Reichert[a], Jeane Cruz Portela[b]

[a] Soil Department, Federal University of Santa Maria (UFSM), Brazil.

[b] Agronomic and Forest Sciences Department, Federal Rural University of the Semi-Árido (UFERSA), Brazil.

[*]Corresponding author address: Avenida Roraima 1000, prédio 42, Cidade Universitária, Camobi, Santa Maria, RS, CEP: 97105-900, Brazil. E-mail address: alanbatistao@gmail.com (A. Batistão).

Abstract - The remediation of soils stressed by salinity improves soil quality for food production. However, information on how remediation techniques affect microstructural stability/elasticity and resistance is lacking. Hence, the objective of this study was to characterize the microstructure of saline alluvial soils from a semi-arid environment, and to evaluate how the techniques of leaching soil and Na^+ substitution by other cations affect the microstructure strength and elasticity evaluated by rheological techniques. Homogenized soil of sixteen horizons of four salinized soil profiles (an Abruptic Solonetz, a Eutric Gleysol, and two Hypereutric Planosols) were

[4] Artigo submetido à revista Soil & Tillage Research

collected in Northeast Brazil. Each horizon was analyzed separately in a completely randomized design, with three replications. The treatments corresponded to soils saturated with 0.1 mol L^1 of KCl (+K), $CaCl_2$ (+Ca) and $MgCl_2$ (+Mg), leaching of salts by successive leaching with alcohol 60%, and untreated soil (control). The soils were submitted to an amplitude sweep test with controlled deformation in a compact modular rheometer. The obtained variables were strain (γ_{LVR}) and stress (τ_{LVR}) at the end of the linear viscoelastic interval (γ_{LVR}), strain (γ_{YP}) and stress (G'_{YP}) at the yield point, shear stress (τ_{max}), and integral Z (Iz). The rheological properties varied greatly between the horizons of the same soil profile. Leaching of salts increased γ_{LVR} compared to control, while the saturation with cations caused reduction in γ_{LVR}, especially in soils of higher clay content. The saturation with saline solution increased γ_{YP} and Iz, with greater effect in soil treated with +K. Both leaching of salts and cation saturation increased soil shear strength at linear viscoelastic range and at yield point. Leaching of salts caused destabilization of soil microstructure which is an important finding that needs to be addressed by measures accompanying remediation of salinized soils to maintain soil physical quality.

Key words: rheology, stress-strain relationships, salinization, salt leaching, soil degradation.

1 INTRODUTION

Salinization is a worldwide problem. The area affected by salt accumulation is estimated to exceed 1.1 billion ha in the world, reaching over 100 countries, being widely distributed in Australia, Asia, South America and Africa (ITPS, 2015; Wicke et al., 2011). In Brazil, salinization occurs in Rio Grande do Sul, in the Pantanal of Mato

Grosso, in the mangrove areas of the Brazilian coast, and predominantly in the semiarid region of the Northeast (Ribeiro et al., 2003). In northeastern Brazil, the area affected by salts is approximately 85,931 km^2, distributed in seven northeastern states. In the state of Rio Grande do Norte, the salinized area occupies more than 16 % of the state's territory (Cordeiro, 1988).

Salinization is defined as the process of accumulation of soluble salts in the soil. It occurs naturally in arid and semi-arid regions due to the long period of water deficit and inefficient leaching in soils developed under imperfect drainage conditions, in which the upward water fluxes and high evaporation rates cause the accumulation at the surfaces (Pedrotti et al., 2015). Salinization causes degradation of soil structure as high sodium (Na^+) levels increase the dispersion of especially clay particles. Combined with the expansion and contraction of the soil by wetting and drying cycles, compacted layers are formed, impeding air and water transport into and within the soil (Dias and Blanco, 2010). Furthermore, saline soils show low water infiltration rate (Vasconcelos et al., 2013) and low saturated hydraulic conductivity (Freire et al., 2003). Soil consistency is generally hard in dry conditions, and dispersed and sticky in wet conditions (Dias and Blanco, 2010).

The mechanical processes that govern these macroscopic soil properties are determined by flocculation and dispersion processes that depend on molecular interactions on the particle level (Ghezzehei and Or, 2001; Vyalov, 1986). Salinization affects the dispersion by change of the nature and magnitude of particle bonds (Rengasamy and Olsson, 1991), and understanding the factors involved in the dispersion of soil particles is essential to understand its physical properties.

Interactions between soil particles can be assessed through rheology as the science that studies the behavior of a body subjected to external stresses (Mezger,

2014; Schramm, 2006). In recent years, rheology has been used to characterize soil microstructure. (Baumgarten et al., 2013, 2012; Khitrov and Khaydapova, 2019; Pértile et al., 2016; Stoppe and Horn, 2018; Zhukova et al., 2015), being also sensitive to detect the influence of salt concentration on microstructural strength and elasticity (Holthusen et al., 2010). In addition, the rheology can provide information on the impacts of Na^+ removal and substitution by other cations of the exchange complexes on the elasticity and microstructure strength of salinized tropical soils.

The impact of salinity only was addressed in very few studies on European soils, and there either by laboratory experiments, where salinity was artificially induced or in Marshland soils of the riparian zone (under sea salt influence). Hence, little is known about the microstructural mechanics of salinized tropical soils, although these occupy a large area and might serve for agricultural purposes, once remediated.

Different soil recovery strategies have been used to reduce the concentration of Na^+ and other soluble salts in the soil profile to decrease their detrimental effect on crop production and soil structure. These strategies have a great effect on dispersion and flocculation processes, comprising solubilization and consequent removal of salts by percolating water, and further replacement of Na^+ by other cations in the sort complexes (Barros et al., 2004).

Two fundamental techniques for soil recovery are used: 1) removal of salts by leaching and 2) replacement of dispersive salts by chemical remediation, i.e. use of soil amendment or mineral fertilization. Leaching consists in passing a sufficient amount of water through the soil profile to dissolve and transport excess salt to deeper soil layers, below the crop rooting area so they do not affect the plants anymore. Mineral fertilizers are incorporated to dissolve divalent cations (Ca^{+2} e Mg^{+2}) or aggregate them in soluble form, replacing Na^+ in cation exchange complexes

(Cordeiro, 1988). Both practices should occur in conjunction with proper drainage practices (Oliveira, 2011; Ribeiro et al., 2003).

Several chemical correctives can be used to replace exchangeable Na^+ in soils such as lime (calcium (hydr)oxide) and agricultural plaster (gypsum, calcium sulphate), aluminum sulfate, calcium chloride, sulfur, and sulfuric acid (Cordeiro, 1988). Because of low price and easy access, lime and gypsum are the most used products for this purpose (Melo et al., 2008), being the most used gypsum because of its higher solubility in relation to lime (Moreira et al., 2014).

These remediation practices provide improved chemical and physical properties of salinized soils, like decrease of electrical conductivity and sodium adsorption ratio (Barros et al., 2005, 2004; Melo et al., 2008), increase of water infiltration rate, aggregate stability and decrease of dispersed clay (Freire et al., 2003; Vasconcelos et al., 2013). Studies on the impact of monovalent salts showed that the effect of salinity on the microstructure can be divergent. Markgraf and Horn (2006) observed increased microstructural stability with increasing NaCl concentration in soils saturated with saline solution. On the other hand, Stoppe and Horn (2018) attributed an observed weakening of the microstructure to the presence of soluble Na^+ in the soil solution. While already salinity did not result in homogeneous effects on soil microstructural mechanics, even more complex processes are expected in remediated soil. In this regard, Holthusen et al. (2012b) concluded that salinity created a dense, though not persistent structure, and the addition of potassium (K^+), rather than compensating for the dispersive effect of Na^+, tended to amplify it.

The impact of remediation on microstructure of saline alluvial soils has not yet been studied, and can not be deduced from existing studies. Consequently, the objective of this study was to characterize the microstructure of saline alluvial soils

from a semi-arid environment, and to evaluate how the techniques of leaching of soluble salts and Na^+ substitution by other cations affect the microstructure strength and elasticity evaluated by rheological techniques.

2 MATERIAL AND METHODS

2.1 Description of the study area

The soils under research are located in the municipalities of Mossoró and Pau dos Ferros, in the state of Rio Grande do Norte, Brazil. The climate is Bsh type according to the Köppen classification, characterized as warm semi-arid, with annual average temperature of 26.7 °C and two well-defined dry and rainy seasons. The rainy season comprises the months February to April, with average annual rainfall of 830 mm (Brasil, 1971; Pfaltzgraff and Torres, 2010).

The physiography of the region is characterized by the Chapada-do-Apodi and the Serrana zone. The geology of the Chapada-do-Apodi zone originates from the Cretaceous Period and is formed by the Jandaíra Limestone, of gray to yellow coloration and fine to medium-grained rocks and generally coarser-grained gray or yellow dolomitic limestone (Brasil, 1971). This geological strata is found on top of Açu Sandstone, which consists of limestone sandstone, with subordinate shales and interspersed limestone layers on top, shale, siltstone and variegated sandstone of gray and purplish red color in the middle or in the lower part or by conglomerated sandstone (Kegel, 1965).

The geology of the Serrana zone, on the other hand, originates from the pre-Cambrian period, consisting mainly of gneisses and migmatites, with inclusions of basic eruptive rocks and acid plutonic rocks, with frequent pegmatite dikes and veins of quartz. The saprolite of these rocks, under the influence of pseudo-autochthonous

material, is the source material of most of the soils formed in the state of Rio Grande do Norte (Brasil, 1971).

The relief of the region is predominantly flat, with a slope below 5% and an altitude varying from 10 to 200 m. In some parts, smooth undulating relief occurs, formed by sets of hills with long slopes, with gentle slopes, open valleys and flat or slightly rounded tops (Brasil, 1971).

Vegetation varies between halophilic and hyperxerophilic Caatinga associations. Halophilic vegetation occurs in areas of northern coast on halomorphic soils, where there is great salinity due to the infiltration of seawater in the lower parts on the landscape. There is a predominance of species adapted to the high salt content like *Iresine portulacoides*, *Batis maritima,* and *Sesuvium portulacastrum*, *Copernicia cerifera* isolated species or in colonies, as well as areas without vegetation. The hyperxerophilous Caatinga vegetation is composed of woody species, ranging in size from shrub to arboreal, with dense to open vegetation and undergrowth composed of grasses, with predominance of *Combretum leprosum, Aspidosperma pyrifolium,* and *Jatropha pohliana* (Brasil, 1971).

2.2 Soil sampling

Four soil profiles of saline soils were sampled and georeferenced, whose classification and location can be observed in Figure 1. The soils were an Abruptic Solonetz (Epiarenic, Differentic, Ochric, Hypernatric) – (SN), an Eutric Gleysol (Abruptic, Clayic, Ochric, Protosodic) (GL), an Hypereutric Planosols (Ochric) – (PL1), and an Hypereutric Planosols (Ochric, Hypermagnesic) – (PL2) according to the World Reference Base for Soils (FAO, 2014).

All soils are located in a flat relief. The soils parent material is unconsolidated sediments texture sandy clay loam for SN, silty clay and sandy to GL, and alluvial sandy clay for PL1. The parent material of PL2 is gneiss saprolith. The vegetation cover consisted of halophyte plants in the GL, open shrubby hyperxerophilous Caatinga vegetation, and grasses on the SN and PL2, as well as spontaneous, legume and mangrove grasses in the PL1.

Trenches were opened at the selected points, and soil samples with altered structure were collected in the central portion of all diagnostic horizons. (Santos et al., 2013). The samples were air-dried; large aggregates were disrupted manually and sieved in 2 mm mesh, resulting in air-dried fine earth (ADE), used for particle size distribution, chemical, and rheological analysis.

2.3 Particle size distribution and chemical analysis

Particle size distribution was determined by the pipette method, using sodium hexametaphosphate as chemical dispersant, with shaking on a horizontal shaking table at 120 rpm for 4 hours (Suzuki et al., 2015). Sand fraction was separated by wet-sieving on a 0.053 mm mesh, while clay was separated by sedimentation, and silt calculated as the difference of the two to total soil mass (EMBRAPA, 2017).

Cation concentration was evaluated by means of the contents of exchangeable potassium (K^+), calcium (Ca^{2+}), magnesium (Mg^{2+}), sodium (Na^+), and aluminum (Al^{3+}) in the soil cation exchange complex. Exchangeable Na^+ and K^+ were extracted by double acid extractor method (Mehlich^{-1}) with acidic solution of HCl 0.05 mol L^{-1} and H_2SO_4 0.0125 mol L^{-1} and quantified by flame photometry. Ca^{2+}, Mg^{2+}, and Al^{3+} were extracted with KCl 1.0 mol L^{-1}, being Ca^{2+} and Mg^{2+} determined by atomic absorption

spectrometry and Al^{3+} quantified by acid-base titration with NaOH 0.0125 mol L^{-1} (EMBRAPA, 2017).

Based on the results of the chemical analyses, we calculated the sum of bases (SB), cation exchange capacity (CTC), base (V%) and aluminum saturation (m), and percentage of exchangeable sodium (PES). Soil pH was determined in 1:2.5 suspensions (10 mL of soil to 25 mL distilled water), with the help of a potentiometer (EMBRAPA, 2017). The results of the chemical characterization of the soil can be visualized in table 1.

206 Table 1 – Chemical and particle size characterization of saline alluvial soils analyzed.

HZ	Prof	Sand	Silt	Clay	ρ	pH	OM	P	K	Ca	Mg	Na	Al	H+Al	Sb	CEC_e	CEC_p	V%	m	PES
	cm	--------- g kg^{-1} ---------			g cm^{-3}		%	mg dm^{-3}	---------- cmolc dm^{-3} ----------									%	%	%
[1]Abruptic Solonetz (Epiarenic, Differentic, Ochric, Hypernatric) - SN / [2]Planossolo Nátrico Órtico típico																				
Ap	0-10	798	135	67	1.46	5.2	0.6	157	0.07	2.39	0.78	0.07	0	2	3.31	3.31	5.31	93.4	0	1.31
E	10-26	776	150	74	1.46	6.1	0.7	122	0.11	4.23	1.16	0.12	0.2	2.2	5.62	5.82	7.82	74.1	3.44	1.56
BA	26-40	664	159	177	1.39	7.7	0.4	24.8	0.33	4.08	1.26	2.26	0.1	1	7.92	8.02	8.92	62.8	1.25	25.3
Bt1	40-70	577	151	272	1.32	8.4	0.1	9.1	0.15	2.96	1.43	10.3	0.3	0.6	14.9	15.2	15.5	62.9	1.98	66.8
Bt2	70-160	518	145	337	1.28	8.7	0.1	3.9	0.09	3.47	2.17	14.9	0	0.5	20.7	20.7	21.2	71.8	0	70.5
BC	160-180+	639	115	246	1.34	8.5	0.1	3.4	0.07	2.18	2.22	14.2	0	0.5	18.6	18.6	19.1	88.5	0	74
Eutric Gleysol (Abruptc, Clayic, Ochric, Protosodic) GL / Gleissolo Háplico Sódico típico																				
A	0-3	100	806	95	1.45	7.5	1.3	36.6	0.71	18.5	17.3	64.7	0	0.6	101	101	102	99.4	0	63.6
Cg1	3-44	104	378	518	1.15	7.8	0.6	50.3	0.97	10.3	12.2	36.1	0	0.6	59.5	59.5	60.1	99	0	60.1
Cg2	44-80	389	280	331	1.28	7.7	0.4	87.6	1.02	5.6	10.1	32.9	0	0.5	49.6	49.6	50.1	99	0	65.6
Cg3	80-100	524	172	304	1.3	7.5	0.3	83.8	0.93	5.58	9.8	32.9	0	0.6	49.2	49.2	49.8	98.8	0	66.1
Hypereutric Planosols (Ochric) – PL1 / Planossolo Nátrico Órtico típico																				
A	0-3	434	465	102	1.44	7	0.3	4.2	0.08	5.4	4.96	0.82	0	0.8	11.3	11.3	12.1	96.1	0	6.78
AB	3-20	495	376	128	1.42	4.8	0.7	8.9	0.12	3.64	1.71	0.26	0	2	5.73	5.73	7.73	97.6	0	3.37
Bt	20-90	452	274	274	1.32	5.3	0.2	27.1	0.12	3.28	1.41	0.21	0	3.1	5.02	5.02	8.12	97.4	0	2.57
Hypereutric Planosols (Ochric, Hypermagnesic) – PL2 / Planossolo Nátrico Órtico típico																				
Ap	0-10	644	297	59	1.48	5	1.4	5.6	0.25	1.64	0.69	0.03	0.1	3.5	2.6	2.7	6.1	42.6	3.7	0.43
Bt	10-40	605	53	342	1.27	5	0.7	3.3	0.1	3.02	3.49	0.58	0.1	1.6	7.2	7.3	8.8	81.8	1.37	6.62
B	40-80	693	200	108	1.44	7.7	0.3	21.6	0.1	1.64	1.83	0.85	0	0.6	4.42	4.42	5.02	88.1	0	17

207 ρ: field density: OM: organic matter; CEC_e: effective cation exchange capacity; CEC_p: potential cation exchange capacity; SB: sum of bases; V: base saturation,
208 m: Al^{+3} saturation; PSS: percentage of sodium saturation. [1]according World Reference Base for soil resources (FAO, 2014); [2]according to Brazilian soil system
209 classification.

2.4 Experimental design

The horizons of each soil profile were analyzed separately in a completely randomized design, with three replications per treatment. The treatments were untreated soil (control), leached soil (LS), soil saturated with saline solution of Ca^{+2} (+Ca), Mg^{+2} (+Mg) and K^{+} (+K).

For leaching of soluble salts, approximately 100 g of TFSA was placed in a glass funnel containing two sheets of filter paper with a specific weight of 80 g m^{-2}. Then, the soil was washed with ethanol 60%, adding the next amount of ethanol only after the previous one had completely percolated. This procedure was performed until the filtrate did not show effervescence reaction anymore upon the addition of 0.05 M L^{-1} silver nitrate (EMBRAPA, 2017). Ethanol was used to simulate soil leaching due to its low surface tension, enabling the removal of soluble salts in intra-aggregate pores. After washing, the soil was air dried, sieved in 2 mm mesh, and prepared for rheological analysis.

2.5 Sample preparation for rheometry

The soil samples were moistened with distilled water to a gravimetric water content ranging from 0.08 to 0.25 g g^{-1}, according to the texture of each soil horizon (sandy to clayey soil texture) and left in airtight sealed containers for approximately 24 hours. Then, the moistened soil was compacted in metallic rings of approximately 3.6 cm in diameter and 1.0 cm in height to its corresponding field density (Table 1).

Control and leached soil samples were saturated with deionized water for approximately 48 h, while the remaining samples were subjected to saturation with 0.1 M solutions of $CaCl_2$, $MgCl_2$ and KCl in the treatments +Ca, +Mg and +K, respectively.

2.6 Rheometry

Rheological analyses were performed with a compact modular rheometer (Anton Paar MCR 102 - Figure 2a), with a parallel plate measuring device, a fixed roughened lower plate of 50 mm in diameter and a roughened upper rotary plate of 25 mm in diameter (PP25 / P2 model - Figure 2b). Directly after saturation, the soil samples were placed on the lower plate of the device and prepared for rheological analysis according to Pértile et al. (2018).

An amplitude sweep test was performed, being controlled and executed automatically by the software Rheoplus/32 V3.62 Anton Paar under the following conditions: plate distance = 4 mm (Figure 2c); rest period before the start of the test = 30 s; angular frequency = 0.5 Hz; temperature = 20 °C; normal force = between 0 e 12 N; number of measurement points = 30; test duration = about 14 min. In this test, an initial strain of 0.0001% was applied and progressively increased to 100%. Strain during the test (γ, %) as determined by the relationship between the deflection (s, m) at the upper edge of the sample and the distance between the plates (h, m - Figure 2c), i.e. by the sample height or size gap, being calculated by equation 1.

$$\gamma = \frac{s}{h} * 100 \quad (1)$$

The shear stress is the result of the force required to apply the strain along the shear surface (Holthusen et al., 2010), being calculated by the quotient between torque (M, Nm) measured at each applied strain and the radius of the upper plate (r, m), according to the equation 2.

$$\tau = \frac{2M}{\pi r^3} \quad (2)$$

255 With the soil presenting viscoelastic behavior, the storage (G ', Pa) and loss (G',
256 Pa) modules were calculated using equations 3 and 4, respectively, from strain and
257 shear stress.

$$G' = \frac{\tau}{\gamma} cos\delta \quad (3)$$

$$G'' = \frac{\tau}{\gamma} sen\delta \quad (4)$$

258 The G' represents the share of the elastic deformation, where the input energy
259 (by means of an external stress, e.g. strain) is stored and released once the external
260 stress does not act anymore. G" represents the viscous component, where the
261 imaginary part of the elasticity is lost, with the energy being transformed and then lost
262 in the form of shear heat to start flow, i.e. irreversible structural deformation
263 (SCHRAMM, 2006). Storage and loss modules make up the typical amplitude sweep
264 test curves, and are directly dependent on shear stress, strain and phase loss angle
265 (Holthusen et al., 2010).
266 The ratio of G" and G' results in the loss factor (tan δ) (equation 5), which can
267 be used to classify soil deformation and flow behavior.

$$\tan\delta = \frac{G''}{G'} \quad (5)$$

268 When G' is greater than G" (tan δ > 1), elastic strain predominates, but when G"
269 is greater than G', i.e. after their intersection at the yield point (YP) (Figure 2a), the
270 strains are predominantly plastic, and viscous flow occurs (Figure 2d) (Baumgarten et
271 al., 2013; Holthusen et al., 2010; Markgraf et al., 2006; Schramm, 2006).
272 From the curves of G' and G", we can define the linear viscoelastic range (LVR),
273 an interval of fully reversible strain, starting with the lowest strain and being limited by
274 G' deviating more than 5 % from a linear curve (Baumgarten et al., 2013; Holthusen et

al., 2010; Markgraf et al., 2006; Mezger, 2014). Strains beyond the LVR promote irreversible and cumulative changes in the material, representing a transition phase between elastic and viscous behavior, but still with a predominance of elastic behavior. The transition between elastic and viscous behavior ends at the yield point (YP), which occurs when the values of G' and G’ are equal, i.e. when tan δ = 1 (Figure 2d).

At the YP, the respective values of strain (γ_{YP}) and storage module (G'_{YP}) are obtained. The γ_{YP} is the critical level of strain, since from this point onwards there is a predominance of viscous behavior with irreversible soil strain (Baumgarten et al., 2013; Holthusen et al., 2010; Markgraf et al., 2012, 2006).

Another important rheological property is the integral z (I_z), which can be used to characterize the elasticity of the soil microstructure. I_z is calculated as the area between the actual tan δ during the amplitude sweep test until the YP (where tan δ = 1) and a horizontal line of tan δ = 1 (Equation 6, Figure 2d). The higher its value, the greater the elastic behavior of the soil and the greater its microstructural rigidity (Baumgarten et al., 2013; Stoppe and Horn, 2018).

$$Iz = \int_{0.0001}^{YP} \left(1 - \tan\delta\right) dx \tag{6}$$

where Iz is the integral z (dimensionless), δ is the phase shift angle, and x is the strain value.

To quantify soil microstructural shear strength, the rheological variables τ_{LVR}, τ_{max} and G'_{YP} were used. The shear stress at the end of the LVR, τ_{LVR} represents the shear strength that the sample offers when deformation reaches the end of the viscoelastic range. The parameter τ_{max} characterizes the maximum internal resistance of the material to resist the breakage of particle bonds. Finally, the storage modulus at the YP, G'_{YP}, corresponds to the soil resistance at the yield point.

298

299 **2.7 Statistical analysis**

300 The rheological variables were analyzed in the statistical environment R, version
301 3.5.0 (R Development Core Team, 2017). To compare the effect of treatments, tests
302 on normality (Shapiro and Wilk, 1965) and homoscedasticity (Levene, 1960) were
303 performed, transforming the rheological variables to $\sqrt{x+1}$, if necessary. Eventually,
304 an analysis of variance by the F-test was performed, and, when significant, the means
305 were compared by the Scott-Knott test at 5% of significance using the *ExpDes.pt*
306 package (Ferreira et al., 2018).

307

308 **3 RESULTS**

309 **3.1 Microstructure of the saline alluvial soils**

310 Strain at the end of the linear viscoelastic range (γ_{LVR}) ranged from 0.003% to
311 0.055%, with an average of 0.022%. The lowest value occurred on the A horizon of SN
312 and the highest value on the Cg_2 horizon of GL (Figure. 3). In the SN, γ_{LVR} increased
313 more than 13 times from A to Bt_1 horizon, followed by a reduction to approximately one
314 fourth in the BC horizon. In the GL, γ_{LVR} increased fourfold in the subsurface horizons
315 relative to the A horizon, while in PL1 the increase occurred gradually in depth, in
316 magnitudes of approximately 15% per horizon. In PL2, a slight decrease of about 9%
317 in γ_{LVR} from A horizon to Bt_1, increasing 85% from horizon Bt_1 to B.

318 <<Figure 3>>

319 Strain at the yield point (γ_{YP}) ranged from 15 to 42%, with an average of 30%.
320 The integral z (Iz) ranged from 4.9 to 15, with an average of 11.1 These variables
321 showed very similar patterns for the different soils and horizons. For both variables,
322 the lowest value occurred on the BA horizon of SN, and the highest value on the

surface horizon of the GL. There was also a reduction in γ_{YP} and Iz of the SN from soil surface to the transitional horizon BA in the magnitude of 47 and 54% respectively, with consecutive increase of approximately 1.5 and 2 times to BC. In soil PL1 a reduction of 26% occurred in γ_{YP} and of the 40% in Iz from A horizon to AB, followed by an increase of 22 and 60%, respectively in γ_{YP} and Iz, in the Bt horizon compared to the AB horizon. In the PL2, γ_{YP} and Iz increased by 23 and 17% in in the Bt_1 horizon, followed by reduction of 22 and 36% in subsequent horizon.

Stress at the end of the linear viscoelastic range (τ_{LVR}) and the maximum shear stress (τ_{max}) reached on average 30.5 and 181 Pa, respectively. Both variables showed a wide data range with regard to different soils and horizons. τ_{LVR} ranged from 0.4 Pa in the BA horizon of SN to 110 Pa in Cg_3 of GL, while the range of τ_{max} was from 3.4 Pa in AB horizon of PL1 to 598 Pa in Cg_3 do GL. With depth, these rheological parameters were modified differently in each soil. In the SN and PL2, the surface horizons showed the highest τ_{LVR} and τ_{max}, though accompanied by a great reduction of these variables in depth. Linear increase occurred with increasing profile depth for GL, in which the τ_{LVR} and τ_{max} were 11 and 7 times greater in the Cg_3 horizon than in the surface horizon, and only the subsurface horizons presented values above the average. In the PL1, the lowest value was found in the transitional AB horizon, and all horizons presented microstructural resistance below the overall mean.

Storage modulus at the yield point (G'_{YP}) was the rheological variable that presented the greatest variation between the horizons of the soil profiles analyzed, ranging from 13 Pa in the AB horizon of PL1 to 945 Pa in Cg_3 horizon of GL, with an average of 172 Pa. Only GL subsurface horizons showed G'_{YP} above average. In addition, the behavior of this variable followed similar trends to τ_{LVR} and τ_{max}, but with

values less discrepant between the surface and subsurface horizons for the SN and PL2.

3.2 Effect of remediation treatment on exchangeable cations and rheology

Different remediation treatments/techniques resulted in quite pronounced alteration of the soil's chemical composition, as revealed by exchangeable cations contents, expressed as cation saturation (Figure. 4).

As had been expected, the untreated soil (control) of the SN and GL soil exhibited a high Na^{+} saturation on the cation exchange complex with unaltered (GL) or decreasing Na^{+} saturation in deeper horizons (SN). However, the PL soils had comparatively low sodium contents, that furthermore increased with depth. Potassium (K^{+}) saturation contrasted the Na^{+} saturation, as it showed in general inverted behavior. Calcium (Ca^{+2}) and magnesium (Mg^{+2}) saturation increased with depth in SN. These cations were predominant in the exchange complexes of horizons with low Na^{+} saturation, mainly in PL1 and PL2.

Leaching was not only ineffective for the PL soils, but even increased the share of monovalent cations, at the expense of divalent cations Ca^{+2} and Mg^{+2}. In the SN, on the other hand, leaching at least in the Ap, A and BA horizon had little effect, though it also slightly reduced the Ca^{+2} share. In the deeper horizons the effect was very heterogeneous, as in the Bt_1 leaching was very effective, but in the next horizon already resulted in strongly increased Na^{+} saturation at the expense of Ca^{+2}. Only in the last horizon, leaching resulted in the desired effect.

Saturation of the samples with saline solutions of $CaCl_2$, KCl and $MgCl_2$ obviously increased the concentrations of Ca^{+2}, K^{+} Mg^{+2} at the exchange sites. Ca^{+2} saturation was always greater than 60% in +Ca treatment, with some horizons showing

372 Ca^{+2} saturation above 90%. With regard to the control, this treatment very effectively
373 replaced all other cations from the exchange complex, the most efficient in the SN and
374 PL1 soil, while it was less successful in the PL2 and GL soils.

375 Regardless of soil class or horizon, samples saturated with KCl had a K^+
376 saturation greater than 70%, with more than half of the horizons showing K^+ saturation
377 above 90%. In the GL soil, KCl could even exchange more cations than $CaCl_2$. Except
378 for the A horizon of GL, soil samples saturated with $MgCl_2$ also had Mg^{+2} saturation
379 above 70%, being over 95% in some horizons. Its effectiveness in replacing Na^+ was
380 comparable to KCl, however, in the GL soil it was inferior to both solutions of $CaCl_2$
381 and KCl.

382 << Figure 4>>

383 These changes in cations saturation in the exchange complexes caused
384 changes in the microstructural elasticity and strength of saline alluvial soils (Figures 5
385 to 10). Removal of soluble salts by leaching (LS) increased the deformation in the linear
386 viscoelastic range (γ_{LVR}) compared to untreated soil (control). This increase was more
387 pronounced in the subsurface horizons of the analyzed soil profiles, mainly in Cg_2 do
388 GL and Bt of PL1 horizons, where LS increased γ_{LVR} around 4 times (Figure 5).

389 Saturation with saline in treatments +Ca, +Mg and +K reduced the γ_{LVR}. The
390 largest reductions occurred in the Bt_1 e Bt_2 do SN horizons, with reduction of 89 and
391 84% respectively. For the Cg_3 of GL and AB of PL1, there was a reduction in γ_{LVR} only
392 for +K and +Ca, while in Cg_2 only +K reduced this rheological variable when compared
393 to control.

394 << Figure 5>>

395 The results of strain at the yield point (γ_{YP}) and integral z (Iz) had a very similar
396 behavior (Fig. 6 and 7). The LS advanced the soil yielding, i.e. decreased γ_{YP}, and

consequently Iz, in horizons Cg_2 of GL, Bt of PL1, Bt_1, Bt_2 and BC of SN and Bt of PL2 horizons, when compared to control. Similar to that found for γ_{LVR}, the effect of LS on γ_{YP} and Iz was greater with increasing of soil depth.

<< Figure 6>>

Regardless of cation type, the saturation with saline solution retarded the yield point, increasing the γ_{YP} and Iz, as seen in the Bt of PL1, BA, Bt_1 and BC of SN and in the B of PL2. In relation to cation types, there was a greater flow retardation in the horizons treated with +K, as verified in the Bt_1 of SN and in the B of PL2. In addition, the horizons AB of PL1 and BC do SN, only +K caused a significant increase in γ_{YP} and Iz compared to control.

<< Figure 7>>

As observed for γ_{YP} and Iz, the stress at the end of the linear viscoelastic range (τ_{LVR}) and the maximum shear stress (τ_{max}) also exhibited very similar behavior (Figures 8 and 9). Comparing the effect of treatments with control, both LS and saline saturation increased the microstructural strength evaluated by τ_{LVR} and τ_{max}, as seem in the Bt of PL1, BA, Bt_1, Bt_2 and BC horizons of SN, B of SN.

<< Figure 8>>

Moreover, +K provided a large increase of τ_{LVR} and τ_{max} compared to +Ca e +Mg, mainly in the subsurface horizons. In the horizons Cg_1 and Cg_2 of GL, and in Bt_1 of PL1, the +K was the only treatment that caused a significant increase of these rheological variables in relation to the control.

<< Figure 9>>

The LS caused a large increase in the microstructure strength evaluated by the value of the storage module at the yield point (G'_{YP}), as observed in the horizons Cg_2 of GL, Bt of PL1, and BA, Bt_1, Bt_2, BC of SN, as well as on the B horizon of PL2 (Figure

10). In five of these horizons, LS was the only treatment that caused a significant increase in $G'_{YP,}$ and only in the Cg_2 horizons of GL and AB of PL1 LS reduced the microstructural strength evaluated by this rheological variable.

Regarding saturation with saline solution, +K treatment was more effective in increasing G'_{YP} then +Ca or +Mg, as observed mainly in the A horizons of GL, AB and Bt of PL1 and A of SN. +K and +Mg treatment did not reduce G'_{YP} in no horizon when compared to control, unlike the +Ca, that reduced the G'_{YP} in Cg_3 of GL.

<<Figure 10>>

A summary of treatment effect on rheological variables can be seen in figure 11. Overall, LS increased γ_{LVR} and decreased γ_{YP} and Iz. However, LS did not significantly alter γ_{YP}, Iz, τ_{LVR} and τ_{max} for most horizons. In contrast, regardless of cation type, the saturation with saline solution reduced the γ_{LVR} and increased γ_{YP} and Iz. The LS, +Ca, +Mg and +K had a greater effect on the increase than on the decrease of microstructural resistance evaluated by the rheological variables τ_{LVR}, τ_{max} and G'_{YP}.

The +Mg treatment did not change significantly the rheological variables for most horizons. The +K treatment provided significant effect on $\gamma_{LVR,}$ γ_{YP}, Iz, τ_{LVR} and τ_{max} in most of analyzed horizons. Except for G'_{YP}, the number of times that +Ca caused any effect (either in the increase or decrease) in rheological variables was close to the number of times this treatment did not significantly affect them. Thus, considering the influence of cations on soil microstructure, we observed a greater effect of K^+, followed by Ca^{+2} and finally Mg^{+2} ($K^+ > Ca^{+2} > Mg^{+2}$).

<<Figure 11>>

4 DISCUSSION

Saline alluvial soils showed great variation in the elasticity and resistance of the microstructure. Moreover, the simulation of salinity remediation techniques affected rheological properties in different ways. In the following, we first stress on the rheology of saline alluvial soils, and then how soil microstructure is affected by salinity remediation techniques.

4.1 Rheology of saline alluvial soils

The increased strain at the end of the linear viscoelastic range (γ_{LVR}) subsurface horizons is related to increased clay content in depth ($r_{(\gamma_{LVR*Clay})}$ = 0.73, p-value = 0.001) and increased salinity ($r_{(\gamma_{LVR*PSS})}$ = 0.81, p-value = 0.001). A positive relationship between clay content and γ_{LVR} was also reported by Markgraf and Horn (2007) and Pértile et al. (2018). Clay particles act as lubricating agents, decreasing friction between larger particles and facilitating sliding motion between them (Ghezzehei and Or, 2001; Reichert et al., 2010; Vallejo and Mawby, 2000), increasing soil elasticity mainly in high soil moisture condition.

Furthermore, the significant increase in γ_{LVR} in the gley horizons of GL and in Bt_1 and Bt_2 horizons of SN denotes the presence of 2:1 clay minerals. Although the clay mineralogy of these soil classes is predominantly composed of kaolinite, the presence of micas, smectites, and illites in Brazilian semiarid soils has been reported by Barbosa et al. (2015), Ferreira et al. (2016), Galindo et al. (2008) and Oliveira et al. (2004), on very similar or even the same soils, higher content of these minerals in the subsurface horizons (Oliveira et al., 2004).

The presence of these minerals can be justified by the pedogenetic condition of semi-arid soils, with scarce and poorly distributed rainfall, combined with high

temperature, long dry period and imperfect drainage conditions. These conditions favor the process of Al, Si and bases dissolution derived from weathering of primary minerals in the soil under low to moderate silica leaching, followed by precipitation of 2:1 clay minerals (Kämpf et al., 2009; Melo and Wypych, 2009).

Expansive 2:1 clay minerals are known to increase the linear viscoelastic range (LVR) (Holthusen et al., 2019, 2017; Khaydapova et al., 2015; Khitrov and Khaydapova, 2019; Pértile et al., 2018, 2016; Zhukova et al., 2015). The reason is their high electrochemical activity (Fontes et al., 2001), favoring the absorption of water and cations on the surface and the interlayer of minerals (Kämpf et al., 2012) and increasing the electrostatic, molecular and capillary forces (Mitchell and Soga, 2005). These factors contribute to greater soil elasticity (Markgraf et al., 2006; Mitchell and Soga, 2005) at low strain intensity (i.e. earlier to γ_{LVR}).

The highest LVR in the horizons with 2:1 clay mineral probably was caused by the presence of soluble salts, mainly of Na^+ in subsurface horizons of SN and GL. The proportion of Na^+ in the cation exchange complex causes different effects on soil physical properties (Freire et al., 2003), depending of mineralogy, degree of weathering and soil clay content (Matos et al., 2014). Sodium and other soluble salts can penetrate in the interlayer of 2:1 clay minerals and increase their expansion (Rengasamy and Olsson, 1991). This also favors soil elasticity at low deformation.

However, the increase in elasticity in the gley horizons of the GL and in Bt_1 and Bt_2 horizons of SN at low strains did not result in increased elasticity at high strains, that is, the deformation required to achieve flow as denoted by strain at the yield point (γ_{YP}). This result corroborates those found by Holthusen et al. (2019, 2017), Khaydapova et al. (2015), Pértile et al. (2018) and Zhukova et al. (2015) who studied the rheological behavior of soils with different mineralogical compositions, and found

495 greater γ_{LVR} and smaller γ_{YP} and Iz in soils with 2:1 clay minerals when compared to
496 kaolinitic or oxide soils.

497 The expansion phenomena of 2:1 clay mineral by presence of soluble salts in
498 these soils with high moisture condition cause particle alignment, associated with weak
499 interparticle bonds due salts in soil solution, allow the sliding movement between soil
500 particles. These processes favor plastic behavior by anticipating soil flow, i.e. smaller
501 γ_{YP} (Zhukova et al., 2015).

502 The smallest γ_{YP}, and consequently Iz, verified in the transitional horizons,
503 mainly on the AB horizon of PL1, is correlated to increased sand content ($r_{(\gamma YP*Sand)}$ =
504 -0.54, p-value = 0.032). These results corroborate with those found by Stoppe e Horn
505 (2018), which showed decreased elasticity in sandy and loamy soils. Soils with higher
506 proportion of large particles have lower elasticity due to the low attraction force that
507 holds the particles together (Holthusen et al., 2019; Markgraf et al., 2006; Pértile et al.,
508 2018, 2016). Also particles of larger diameter usually have spherical shape (Cho et al.,
509 2006; Santamarina and Cho, 2004; Vepraskas and Cassell, 1987), which impedes
510 sliding and thus disfavors the elastic behavior of the soil.

511 Particle size distribution also affected the microstructure resistance evaluated
512 by the stress at the end of the linear viscoelastic range (τ_{LVR}) and by the maximum
513 shear stress (τ_{max}). The surface horizons of SN and PL2, with high sand (>640 g kg^{-1})
514 and low clay contents (<80 g kg^{-1}), showed high shear resistance. This is due to the
515 friction between large and rough particles and to the reorganization of the stacking of
516 this particles during oscillatory shear tests (Cho et al., 2006), enabling a compact and
517 more stable arrangement of low energy level (Stoppe and Horn, 2018).

518 On horizons with similar sand content, but with higher clay content, as the BA
519 horizon of SN and Bt horizon of PL2, reduction of microstructural strength was verified.

In larger amounts in the soil, clay particles can attach to the silt and sand particles, reducing friction and facilitating sliding between them (Vallejo and Mawby, 2000), resulting in lower shear strength.

4.2 Exchangeable cations composition due to salinity remediation and microstructure of saline alluvial soils.

The type of cation at the exchange sites had a low impact on rheological parameters in the surface horizons. The effect of cation type on microstructure elasticity was more pronounced with increasing soil depth due to particle size distribution and clay type. In the subsurface horizons, there is an increase in clay content allowing for greater contact between the soil particles (Santamarina, 2003). Contact between particles may be due to their own weight, electrical forces and molecular interactions, and capillary forces. These forces act with different intensity according to the characteristics of the particles, changing the form of accommodation between them (Molina Junior, 2017).

In soils with a predominance of larger diameter particles (sand and silt), as observed in the surface horizons of the studied soils, the action of electrical forces on particle contact is small. Moreover, as the soil was analyzed under a saturated condition, the capillary forces associated with the menisci are almost non-existent. Thus, the contact between the larger particles would depend only on the gravitational force due to the weight of the particles. This force is hardly altered by changing the electrolyte concentration of the soil solution. (Santamarina, 2003). This could explain the low effect of type cation on soil solution of surface horizons.

However, as particle diameter decreases, as is in the case in deeper horizons by means of increasing (silt and) clay content, the importance of weight is reduced,

545 and the influence of electrical forces on particle contact increases (Santamarina et al.,
546 2002). Also, ion adsorption phenomena modify the electric field on the surface of soil
547 colloids (Essington, 2004; Sposito, 2008). Thus, in soils with higher clay content,
548 modification of the exchangeable cation concentration and type, as well of the
549 electrolyte solution would have greater influence on the contact between soil particles,
550 mainly in soils with higher particle reactivity, with presence of expandable clay
551 minerals.

552 Leaching of soluble salts increased purely elastic strain (previous to γ_{LVR}), but
553 this increase in elasticity was not accompanied by greater resistance at the end of
554 LVR. This indicates that, at low deformations, the bonds between particles are due to
555 surface electrostatic forces. The leaching of salts from the soil solution, mainly of Na^+,
556 allowed particles to approximate more closely, limited by the particle surface
557 electrostatic potential (Rengasamy and Olsson, 1991). By applying a slight
558 deformation to the soil, the particles tend to get closer, providing overlapping of
559 electrical potentials, where a repulsive energy is stored. When strain ceased, repulsive
560 energy is released, causing the particles to return to a position where there is no
561 overlap of electrical potentials.

562 However, the leaching of soluble salts (LS) caused a reduction in microstructural
563 elasticity in high strains. This reduction was accompanied by increased yield strength
564 (G'_{YP}), suggesting the formation of metallic-mineral complexes. As the deformation
565 increases, the particles are forced to get even closer. If the distance between the
566 particles is small, polyvalent cations can join the surface of the particles forming
567 polycationic bridges. These bonds have a rather stiff instead of elastic character
568 (Holthusen et al., 2010), which decreases the soil elasticity. They are also quite strong
569 compared to other intermolecular forces, being more resistant to breakage (Bronick

570 and Lal, 2005; Chorover and Sposito, 1995; Fontes et al., 2001), which explains the
571 increase in microstructural shear strength.

572 Saturation with saline solution provided the opposite effect to the removal of
573 soluble salts, decreasing elasticity at low strains (i.e γ_{LVR}) and retarding microstructure
574 flow (YP). The decrease of γ_{LVR} probably occurred due to reduced thickness of the
575 diffuse double layer. The increase of the cation concentration in electrolyte solution
576 decreases the electric potential of particle surface, reducing repulsion between
577 particles with similar electrical charges (Chorover and Sposito, 1995; Fontes et al.,
578 2001; Shaikh et al., 2017; Sposito, 2008) and increasing the contact between them.

579 The effect of electrolyte concentration on the colloidal behavior of
580 montmorillonite aqueous suspensions was studied by Tombácz e Szekeres (2004).
581 These authors concluded that the large amount of negative charge on the surface of
582 the particles is compensated by exchangeable cations in the diffuse part of the electric
583 double layer, increasing particle flocculation. Flocculation increases the particles
584 contact, and may decrease their ability to move, which would explain the smaller γ_{LVR}
585 on soils saturated with cations. This corroborates the results of Magzoub et al. (2017),
586 who found increased viscosity and reduced linear viscoelastic range in colloidal
587 dispersion of Ca-bentonite treated with addition of sodium carbonate.

588 This greater contact between soil particles due to the reduction of the diffuse
589 double layer in the saline treatments delayed the soil flow, i.e, it increased the
590 deformation range before the flow (γ_{YP}). This type of bond, when compared to
591 polycationic bridges, is less rigid and more elastic, because it allows the sliding of one
592 particle in relation to another while maintaining contact between them. Therefore,
593 greater deformation is required for the soil to flow.

Among the studied cations, K^+ provided the greatest positive effect on the microstructure, especially in the rheological resistance variables. The effect of this cation on soil microstructure was evaluated by Holthusen et al. (2010), who found linear and positive relationship between maximum shear stress and stress at microstructure yield point with increased K^+ concentration. This is probably due to the type of binding of K^+ to clay minerals. The K^+ ion best fits in the interlayer of expandable clay, because of its smaller hydrated radius, causing partial or total collapse of this space and thus reducing the mineral expansiveness (Sparks, 2003).

Furthermore, compared to Ca^{+2} or Mg^{+2}, K^+ is easily hydrolyzable, allowing the formation of internal sphere complex with the siloxane surfaces of 2:1 clay minerals (Essington, 2004). This type of chemical bond decreases the net charge on the surface of the particles (Chorover and Sposito, 1995; Fontes et al., 2001), resulting in less repulsion between them. Less expansiveness and decreased repulsion by inner sphere complex bonds provide greater microstructure rigidity. Nevertheless, Mg^{+2} negatively impacted the microstructure of some soils, which is related to amplified expansion of saturated clays in the presence of this cation, causing breakdown of microaggregates (Bronick and Lal, 2005).

Overall, it is clear that, in salinized soils, leaching of soluble salts or substitution by other cations by soil fertilization may be an alternative to mitigate the dispersive effect on microstructure of tropical saline soils. However, salt leaching advanced the yield point, destabilizing the microstructure of soil when compared to saline saturation. In order to improve microstructural quality by increasing elasticity and strength, it is recommended to apply mineral fertilizers containing K^+ or Ca^{+2}. The choice of fertilizer will depend on their cost and ease of purchase, as well as field operationalization. It is noteworthy that the experiment was carried out in the laboratory under controlled

619 conditions and different results can be found in the field due to the multiplicity of factors
620 that interfere in the physical processes in microscale. In addition, all field salinity
621 remediation techniques must be accompanied by an efficient drainage system and
622 evapotranspiration control, to prevent the return of soluble salts to the soil surface by
623 capillary water rise.
624
625 **5 CONCLUSIONS**
626 Microstructural behavior of four saline alluvial soils submitted to the controlled
627 deformation amplitude sweep test showed great variation in rheological properties
628 between soil profiles and between horizons in the same profile. In addition, the factors
629 and/or processes that condition the microstructural characteristics are not determined
630 by pedogenetic processes, but are sensitive to changes caused by soil chemical
631 management.
632 Simulation of salinization remediation techniques by removing soluble salts or by
633 modifying cation concentration by saturation with saline solution of KCl, $CaCl_2$, and
634 $MgCl_2$ indicate the effect of cations on soil microstructure increases with augmented
635 clay content, being more pronounced on the subsurface horizons of textural-gradient
636 soils.
637 Leaching of soluble salts caused destabilization of the soil microstructure, reducing
638 the soil strain at the yield point and integral z, whereas soil cation saturation, especially
639 with K^+, slowed soil flow and increased shear strength and microstructural stability.
640 This conclusion is an important finding that needs to be addressed by measures
641 accompanying remediation of salinized soils to maintain soil physical quality.
642

Declaration of Competing Interest

The authors declare no conflicts of interest.

Acknowledgments

The authors thank the Coordination for the Improvement of Higher Education Personnel (Capes) – Finance code 001; Brazilian Council for Scientific and Technological Development (CNPq); “Fundação de Amparo à Pesquisa do Estado do Rio Grande do Sul” (Fapergs); and Professor Francisco Ernesto Sobrinho for his help in collecting and identifying the soil used in this study.

REFERENCES

Barbosa, W.R., Romero, R.E., de Souza Júnior, V.S., Cooper, M., Sartor, L.R., de Moya Partiti, C.S., Jorge, F. de O., Cohen, R., de Jesus, S.L., Ferreira, T.O., 2015. Effects of slope orientation on pedogenesis of altimontane soils from the Brazilian semi-arid region (Baturité massif, Ceará). Environ. Earth Sci. 73, 3731–3743. https://doi.org/10.1007/s12665-014-3660-4

Barros, M. de F.C., Fontes, M.P.F., Alvarez V., V.H., Ruiz, H.A., 2004. Recuperação de solos afetados por sais pela aplicação de gesso de jazida e calcário no Nordeste do Brasil. Rev. Bras. Eng. Agríc. E Ambient. 8, 59–64. https://doi.org/10.1590/S1415-43662004000100009

Barros, M. de F.C., Santos, P.M. dos, Silva, A.J. da, 2005. Recuperação de solos afetados por sais usando água de qualidade inferior. Rev. Bras. Eng. Agríc. E Ambient. 9, 310–313. https://doi.org/10.1590/S1415-43662004000100009

666 Baumgarten, W., Dörner, J., Horn, R., 2013. Microstructural development in volcanic
667 ash soils from South Chile. Soil Tillage Res. 129, 48–60.
668 https://doi.org/10.1016/j.still.2013.01.007

669 Baumgarten, W., Neugebauer, T., Fuchs, E., Horn, R., 2012. Structural stability of
670 Marshland soils of the riparian zone of the Tidal Elbe River. Soil Tillage Res.
671 125, 80–88. https://doi.org/10.1016/j.still.2012.06.002

672 Brasil, 1971. Levantamento exploratório - Reconhecimento de solos do Estado de Rio
673 Grande do Norte (Técnico No. 21), (Boletim Técnico, 21). Ministério de
674 Agricultura, Recife.

675 Bronick, C.J., Lal, R., 2005. Soil structure and management: a review. Geoderma 124,
676 3–22. https://doi.org/10.1016/j.geoderma.2004.03.005

677 Cho, G.-C., Dodds, J., Santamarina, J.C., 2006. Particle shape effects on packing
678 density, stiffness, and strength: natural and crushed sands. J. Geotech.
679 Geoenvironmental Eng. 132, 591–602. https://doi.org/10.1061/(ASCE)1090-
680 0241(2006)132:5(591)

681 Chorover, J., Sposito, G., 1995. Surface charge characteristics of kaolinitic tropical
682 soils. Geochim. Cosmochim. Acta 59, 875–884.
683 https://doi.org/10.1016/0016-7037(94)00357-2

684 Cordeiro, G.G., 1988. Aspectos gerais sobre salinidade em áreas irrigadas: origem,
685 diagnóstico e recuperação (No. 50), Documentos. Petrolina.

686 Dias, N. da S., Blanco, F.F., 2010. Efeitos dos sais no solo e na planta, in: Manejo da
687 salinidade na agricultura estudos básicos e aplicados. INCTSal, Fortaleza.

688 EMBRAPA, 2017. Manual de Métodos de Análise de Solo, 3rd ed. Embrapa, Brasília.

689 Essington, M.E., 2004. Soil and water chemistry: an integrative approach. CRC Press,
690 Boca Raton, Fla.

691 FAO, 2014. World reference base for soil resources 2014: international soil
692 classification system for naming soils and creating legends for soil maps.
693 FAO, Rome.

694 Ferreira, E.B., Cavalcanti, P.P., Nogueira, D.A., 2018. ExpDes.pt: Pacote
695 Experimental Designs (Portuguese).

696 Ferreira, J.T.P., Ribeiro Filho, M.R., Ribeiro, M.R., Souza Júnior, V.S. de, Bittar,
697 S.M.B., Santos, R.G. dos, 2016. Planosols developed in different
698 geoenvironmental conditions in Northeastern Brazil. Rev. Bras. Ciênc. Solo
699 40. https://doi.org/10.1590/18069657rbcs20150131

700 Fontes, M.P.F., Camargo, O.A. de, Sposito, G., 2001. Eletroquímica das partículas
701 coloidais e sua relação com a mineralogia de solos altamente
702 intemperizados. Sci. Agric. 58, 627–646. https://doi.org/10.1590/S0103-
703 90162001000300029

704 Freire, M.B.G. dos S., Ruiz, H.A., Ribeiro, M.R., Ferreira, P.A., Alvarez V., V.H., Freire,
705 F.J., 2003. Condutividade hidráulica de solos de Pernambuco em resposta à
706 condutividade elétrica e RAS da água de irrigação. Rev. Bras. Eng. Agríc. E
707 Ambient. 7, 45–52. https://doi.org/10.1590/S1415-43662003000100008

708 Galindo, I.C. de L., Ribeiro, M.R., Santos, M. de F. de A.V., Lima, J.F.W.F., Ferreira,
709 R.F. de A. e L., 2008. Relações solo-vegetação em áreas sob processo de
710 desertificação no município de Jataúba, PE. Rev. Bras. Ciênc. Solo 32,
711 1283–1296. https://doi.org/10.1590/S0100-06832008000300036

712 Ghezzehei, T. a., Or, D., 2001. Rheological properties of wet soils and clays under
713 steady and oscillatory stresses. Soil Sci. Soc. Am. J. 65, 624–624.
714 https://doi.org/10.2136/sssaj2001.653624x

715 Holthusen, D., Pértile, P., Reichert, J.M., Horn, R., 2019. Viscoelasticity and shear
716 resistance at the microscale of naturally structured and homogenized
717 subtropical soils under undefined and defined normal stress conditions. Soil
718 Tillage Res. 191, 282–293. https://doi.org/10.1016/j.still.2019.04.014

719 Holthusen, D., Pértile, P., Reichert, J.M., Horn, R., 2017. Controlled vertical stress in
720 a modified amplitude sweep test (rheometry) for the determination of soil
721 microstructure stability under transient stresses. Geoderma 295, 129–141.
722 https://doi.org/10.1016/j.geoderma.2017.01.034

723 Holthusen, D., Peth, S., Horn, R., 2010. Impact of potassium concentration and matric
724 potential on soil stability derived from rheological parameters. Soil Tillage
725 Res. 111, 75–85. https://doi.org/10.1016/j.still.2010.08.002

726 Holthusen, D., Reeb, D., Horn, R., 2012. Influence of potassium fertilization, water and
727 salt stress, and their interference on rheological soil parameters in planted
728 containers. Soil Tillage Res. 125, 72–79.
729 https://doi.org/10.1016/j.still.2012.05.003

730 ITPS, I.T.P. on S., 2015. Global status of soil salinization and sodification, in: Status of
731 the World's Soil Resources. FAO, Roma.

732 Kämpf, N., Curi, N., Marques, J.J., 2009. Intemperismo e ocorrências de minerais no
733 ambiente do solo, in: Química e Mineralogia Do Solo: Conceitos Básicos.
734 Sociedade Brasileira de Ciência do Solo, Viçosa.

735 Kämpf, N., Marques, J.J., Curi, N., 2012. Mineralogia de solos brasileiros, in:
736 Pedologia: Fundamentos. Sociedade Brasileira de Ciência do Solo, Viçosa.

737 Kegel, W., 1965. A estrutura geológica do Nordeste do Brasil, Brasil. Ministério das
738 Minas e Energia. DNPM. (Boletim técnico, 227). Divisão de Geologia e
739 Mineralogia, Rio de Janeiro.

740 Khaydapova, D., Milanovskiy, E., Shein, E., 2015. Rheological properties of different
741 minerals and clay soils. EURASIAN J. SOIL Sci. EJSS 4, 198–198.
742 https://doi.org/10.18393/ejss.2015.3.198-202

743 Khitrov, N.B., Khaydapova, D.D., 2019. Viscoelastic behavior of Vertic Solonetz in the
744 Kamennaya Steppe. Eurasian Soil Sci. 52, 808–821.
745 https://doi.org/10.1134/S1064229319070056

746 Levene, H., 1960. Robust tests for equality of variances, in: Olkin, I., Ghurye, S.G.,
747 Hoeffding, W., Madow, W.G., Mann, H.B. (Eds.), Contributions to Probability
748 and Statistics: Essays in Honor of Harold Hotelling (Ingram Olkin, Sudhist G.
749 Ghurye, Wassily Hoeffding, William G. Madow, and Henry B. Mann, Eds.).
750 Stanford University Press, Menlo Park, pp. 278–292.
751 https://doi.org/10.1137/1003016

752 Magzoub, M.I., Nasser, M.S., Hussein, I.A., Benamor, A., Onaizi, S.A., Sultan, A.S.,
753 Mahmoud, M.A., 2017. Effects of sodium carbonate addition, heat and
754 agitation on swelling and rheological behavior of Ca-bentonite colloidal
755 dispersions. Appl. Clay Sci. 147, 176–183.
756 https://doi.org/10.1016/j.clay.2017.07.032

Markgraf, W., Horn, R., 2007. Scanning electron microscopy–energy dispersive scan analyses and rheological investigations of South-Brazilian soils. Soil Sci. Soc. Am. J. 71, 851–851. https://doi.org/10.2136/sssaj2006.0231

Markgraf, W., Horn, R., 2006. Rheological-stiffness analysis of K+-treated and CaCO3-rich soils. J. Plant Nutr. Soil Sci. 169, 411–419. https://doi.org/10.1002/jpln.200521934

Markgraf, W., Horn, R., Peth, S., 2006. An approach to rheometry in soil mechanics—Structural changes in bentonite, clayey and silty soils. Soil Tillage Res. 91, 1–14. https://doi.org/10.1016/j.still.2006.01.007

Markgraf, W., Watts, C.W., Whalley, W.R., Hrkac, T., Horn, R., 2012. Influence of organic matter on rheological properties of soil. Appl. Clay Sci. 64, 25–33. https://doi.org/10.1016/j.clay.2011.04.009

Matos, A.T. de, Almeida Neto, O.B., Matos, M.P. de, 2014. Saturação do complexo de troca de solos oxídicos com sódio. Rev. Bras. Eng. Agríc. E Ambient. 18, 501–506. https://doi.org/10.1590/S1415-43662014000500006

Melo, R.M., Barros, M. de F.C., Santos, P.M. dos, Rolim, M.M., 2008. Correção de solos salino-sódicos pela aplicação de gesso mineral. Rev. Bras. Eng. Agríc. E Ambient. 12, 376–380. https://doi.org/10.1590/S1415-43662008000400007

Melo, V.F., Wypych, F., 2009. Caulinita e Haloisita, in: Química e Mineralogia Do Solo: Conceitos Básicos. Sociedade Brasileira de Ciência do Solo, Viçosa.

Mezger, T.G., 2014. The Rheology Handbook, 4th ed. Vincentz Network, Hanover.

779 Mitchell, J.K., Soga, K., 2005. Fundamentals of soil behavior, 3. ed. ed. Wiley,
780 Hoboken, NJ.

781 Molina Junior, W.F., 2017. Comportamento mecânico do solo em operações agrícolas.
782 Universidade de São Paulo. Escola Superior de Agricultura Luiz de Queiroz.
783 https://doi.org/10.11606/9788592238407

784 Moreira, L.C.J., Teixeira, A. dos S., Galvão, L.S., 2014. Laboratory Salinization of
785 Brazilian Alluvial Soils and the spectral effects of gypsum. Remote Sens. 6,
786 2647–2663. https://doi.org/10.3390/rs6042647

787 Oliveira, J.B.D., 2011. Pedologia aplicada, 4th ed. FEALQ, Piracicaba.

788 Oliveira, L.B., Ribeiro, M.R., Ferraz, F.B., Ferreira, M.G.V.X., Mermut, A.R., 2004.
789 Mineralogia, micromorfologia e gênese de solos planossólicos do Sertão do
790 Araripe, estado de Pernambuco. Rev. Bras. Ciênc. Solo 28, 665–678.
791 https://doi.org/10.1590/S0100-06832004000400009

792 Pedrotti, A., Chagas, R.M., Ramos, V.C., Prata, A.P. do N., Tadeu Lucas, Santos, P.B.
793 dos, 2015. Causas e consequências do processo de salinização dos solos.
794 Rev. Eletrônica Em Gest. Educ. E Tecnol. Ambient. 19, 1308–1324.
795 https://doi.org/105902/2236117016544

796 Pértile, P., Holthusen, D., Gubiani, P.I., Reichert, J.M., 2018. Microstructural strength
797 of four subtropical soils evaluated by rheometry: properties, difficulties and
798 opportunities. Sci. Agric. 75, 154–162. https://doi.org/10.1590/1678-992x-
799 2016-0267

Pértile, P., Reichert, J.M., Gubiani, P.I., Holthusen, D., Costa, A. da, 2016. Rheological parameters as affected by water tension in subtropical soils. Rev. Bras. Ciênc. Solo 40, 1–14. https://doi.org/10.1590/18069657rbcs20150286

Pfaltzgraff, P.A. dos S., Torres, F.S. de M., 2010. Geodiversidade do estado do Rio Grande do Norte. Serviço Geológico do Brasil, Recife.

R Development Core Team, 2017. R: A Language and Environment for Statistical Computing.

Reichert, J.M., Reinert, D.J., Suzuki, L.E.A.S., Horn, R., 2010. Mecânica do solo, in: Física Do Solo. Sociedade Brasileira de Ciência do solo, p. 298.

Rengasamy, P., Olsson, K., 1991. Sodicity and soil structure. Soil Res. 29, 935. https://doi.org/10.1071/SR9910935

Ribeiro, M.R., Freire, F.J., Montenegro, A., 2003. Solos halomórficos no Brasil: ocorrência, gênese, classificação, uso e manejo sustentável., in: Tópicos Em Ciência Do Solo. Sociedade Brasileira de Ciência do Solo, Viçosa, pp. 165–208.

Santamarina, J.C., 2003. Soil behavior at the microscale: particle forces, in: Soil Behavior and Soft Ground Construction. Presented at the Symposium on Soil Behavior and Soft Ground Construction Honoring Charles C. “Chuck” Ladd, American Society of Civil Engineers, Cambridge, Massachusetts, United States, pp. 25–56. https://doi.org/10.1061/40659(2003)2

Santamarina, J.C., Cho, G.C., 2004. Soil behaviour: The role of particle shape, in: Advances in Geotechnical Engineering: The Skempton Conference. Thomas Telford, Londres, pp. 604–617. https://doi.org/10.1680/aigev1.32644.0035

Santamarina, J.C., Klein, K.A., Wang, Y.H., Prencke, E., 2002. Specific surface: determination and relevance. Can. Geotech. J. 39, 233–241. https://doi.org/10.1139/t01-077

Santos, R.D. dos, Lemos, R.C. de, Santos, H.G. dos, Ker, J.C., Anjos, L.H.C. dos, Shimizu, S.H., 2013. Manual de descrição e coletas de solo no campo, 6th ed. Sociedade Brasileira de Ciência do Solo, Viçosa.

Schramm, G., 2006. Rheology and Rheometry: theoretical and practical fundamentals. Artliber.

Shaikh, S.M.R., Nasser, M.S., Hussein, I., Benamor, A., Onaizi, S.A., Qiblawey, H., 2017. Influence of polyelectrolytes and other polymer complexes on the flocculation and rheological behaviors of clay minerals: A comprehensive review. Sep. Purif. Technol. 187, 137–161. https://doi.org/10.1016/j.seppur.2017.06.050

Shapiro, S.S., Wilk, M.B., 1965. An analysis of variance test for normality (Complete Samples). Biometrika 52, 591. https://doi.org/10.2307/2333709

Sparks, D.L., 2003. Environmental soil chemistry, 2nd ed. Academic Press, California.

Sposito, G., 2008. The chemistry of soils, 2nd ed. Oxford University Press, NewYork.

Stoppe, N., Horn, R., 2018. Microstructural strength of tidal soils – a rheometric approach to develop pedotransfer functions. J. Hydrol. Hydromech. 66, 87–96. https://doi.org/10.1515/johh-2017-0031

Suzuki, L.E.A.S., Reichert, J.M., Albuquerque, J.A., Reinert, D.J., Kaiser, D.R., 2015. Dispersion and flocculation of Vertisols, Alfisols and Oxisols in Southern

845 Brazil. Geoderma Reg. 5, 64–70.
846 https://doi.org/10.1016/j.geodrs.2015.03.005

847 Tombácz, E., Szekeres, M., 2004. Colloidal behavior of aqueous montmorillonite
848 suspensions: the specific role of pH in the presence of indifferent electrolytes.
849 Appl. Clay Sci. 27, 75–94. https://doi.org/10.1016/j.clay.2004.01.001

850 Vallejo, L.E., Mawby, R., 2000. Porosity influence on the shear strength of granular
851 material–clay mixtures. Eng. Geol. 58, 125–136.
852 https://doi.org/10.1016/S0013-7952(00)00051-X

853 Vasconcelos, R.R.A. de, Barros, M. de F.C., Silva, Ê.F. de F., Graciano, E.S.A.,
854 Fontenele, A.J.P.B., Silva, N.M.L. da, 2013. Características físicas de solos
855 salino-sódicos do semiárido pernambucano em função de diferentes níveis
856 de gesso. Rev. Bras. Eng. Agríc. E Ambient. 17, 1318–1325.
857 http://dx.doi.org/10.1590/S1415-43662013001200010

858 Vepraskas, M.J., Cassell, D.K., 1987. Sphericity and roundness of sand in Coastal
859 Plain soils and elationships with soil physical properties. Soil Sci. Soc. Am. J.
860 51, 1108–1112.

861 Vyalov, S.S., 1986. Summary for policymakers, in: Intergovernmental Panel on Climate
862 Change (Ed.), Reological Fundamentals of Soil Mechanics. Cambridge
863 University Press, Cambridge, pp. 564–564.
864 https://doi.org/10.1017/CBO9781107415324.004

865 Wicke, B., Smeets, E., Dornburg, V., Vashev, B., Gaiser, T., Turkenburg, W., Faaij, A.,
866 2011. The global technical and economic potential of bioenergy from salt-

affected soils. Energy Environ. Sci. 4, 2669. https://doi.org/10.1039/c1ee01029h

Zhukova, Yu.A., Khaydapova, D.D., Kovda, I.V., Morgun, E.G., 2015. Rheological properties of Vertisol complexes formed under different climate conditions. Mosc. Univ. Soil Sci. Bull. 70, 110–115. https://doi.org/10.3103/S0147687415030084

FIGURES

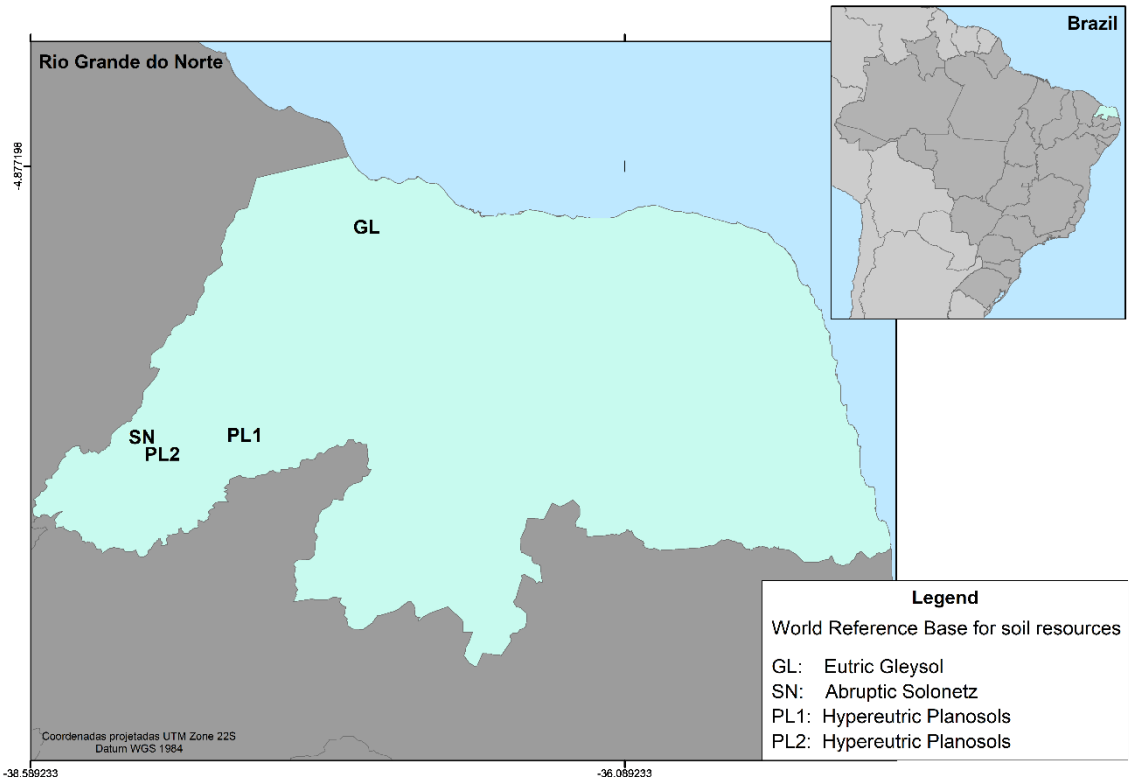

Figure 1. Location of sampled saline alluvial soil profiles.

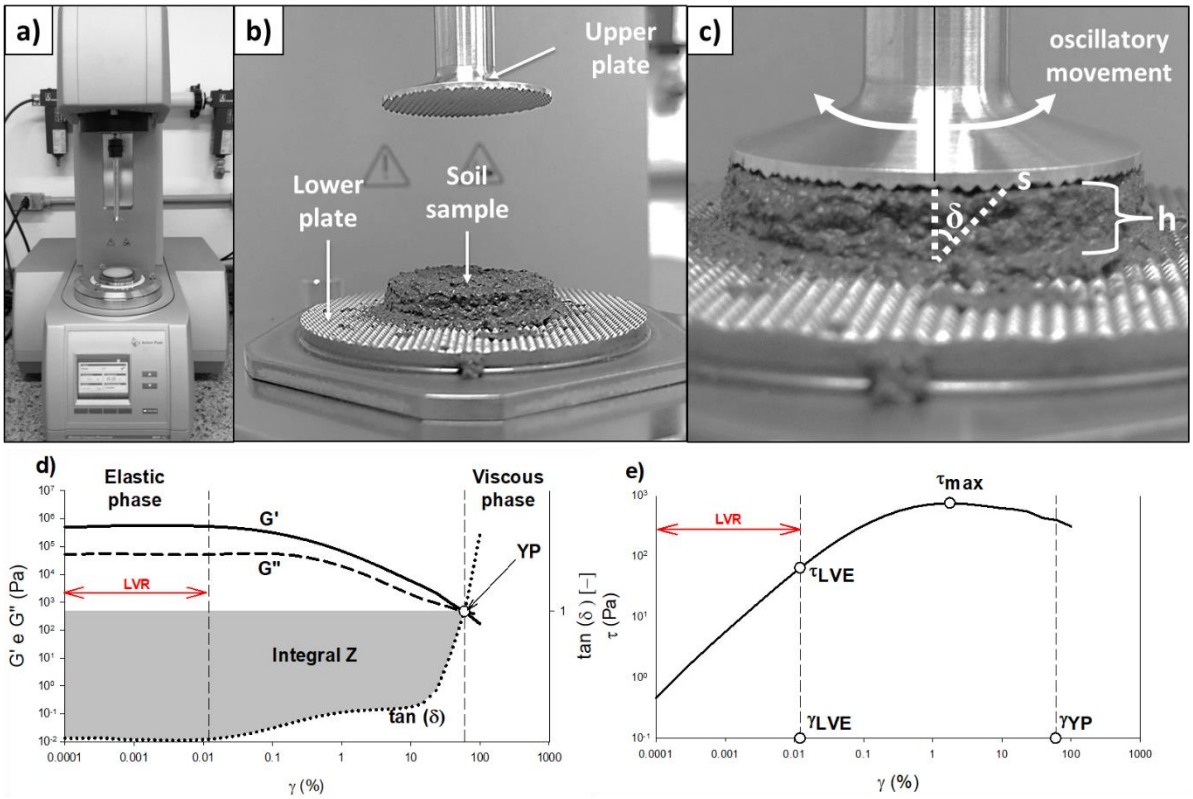

878

879 Figure 2. Representation of the equipment and the test used. a) Compact modular
880 rheometer (Anton Paar MCR 102). b) Model PP25 / P2 parallel plate measuring
881 system. c) Deflection (s), sample height or gap (h) and phase loss angle (δ). d) Results
882 obtained from the amplitude sweep test: storage module (G'), loss module (G") and
883 phase loss (tan δ) curves as a function of deformation (γ) from the start of the test to
884 the yield point (YP). e) Rheological variables obtained from the relationship between
885 stress (τ) and strain (γ): stress (τ_{LVR}) and strain (γ_{LVR}) at the end of the linear viscoelastic
886 interval; maximum shear stress (τ_{max}) and yield point deformation (γ_{YP}).

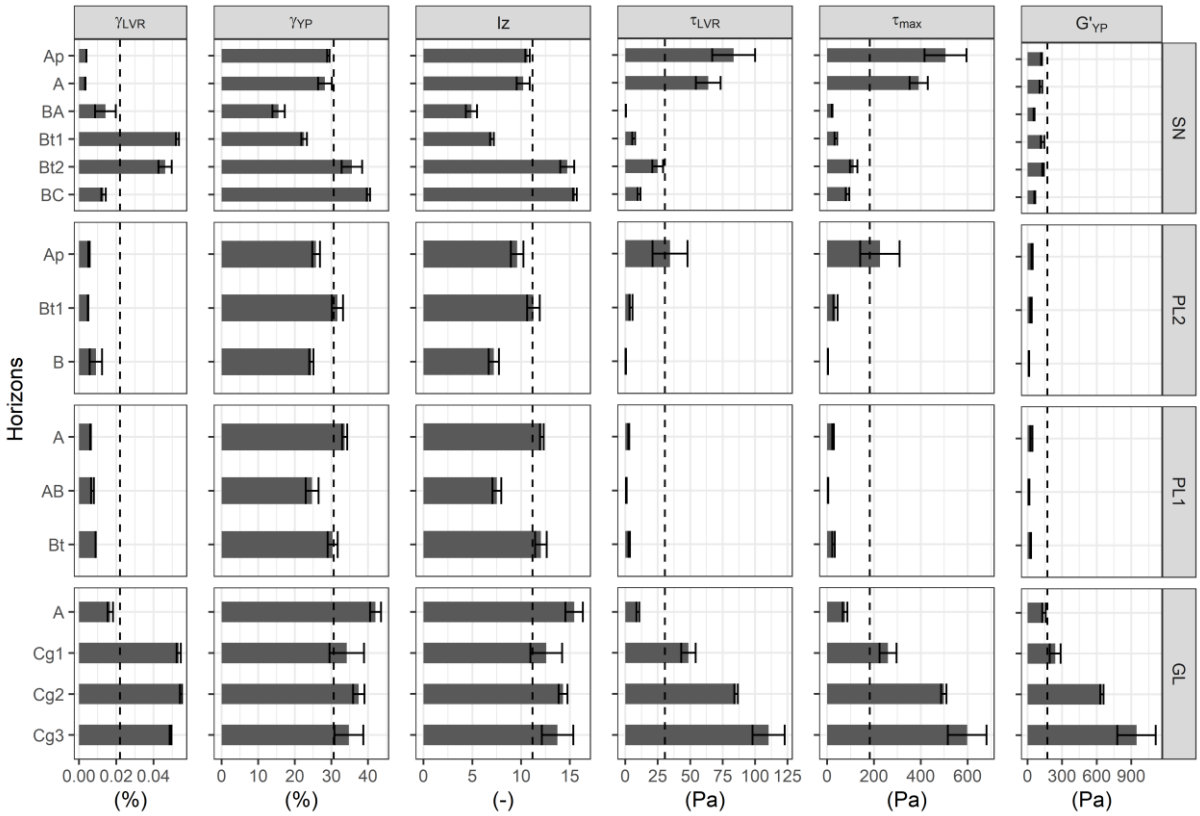

887

888 Figure 3. Mean values of strain at the end of the linear viscoelastic range (γ_{LVR}), strain
889 at the yield point deformation (γ_{YP}), integral z (Iz), stress at the end of the linear
890 viscoelastic range (τ_{LVR}), maximum shear stress (τ_{max}), and storage modulus at the
891 yield point (G'_{YP}) of Abruptic Solonetz (Epiarenic, Differentic, Ochric, Hypernatric) –
892 (SN), Eutric Gleysol (Abruptc, Clayic, Ochric, Protosodic) – (GL),Hypereutric Planosols
893 (Ochric) – (PL1) and Hypereutric Planosols (Ochric, Hypermagnesic) – (PL2) and their
894 corresponding horizons. Error bars denote standard deviation, dotted line represents
895 the overall mean of each rheological variable.

896

897 Figure 4. Saturation of cations in the cation exchange complex of each horizon of an
898 Abruptic Solonetz (Epiarenic, Differentic, Ochric, Hypernatric) – (SN), Eutric Gleysol
899 (Abruptc, Clayic, Ochric, Protosodic) – (GL), Hypereutric Planosols (Ochric) – (PL1)
900 and Hypereutric Planosols (Ochric, Hypermagnesic) – (PL2) in each treatment. The
901 +Ca, +K and +Mg represents saturation by capillarity in saline solution in the
902 concentration of 0.1 mol L^{-1} of $CaCl_2$, KCl and $MgCl_2$, respectively, and Ds represents
903 removal of soluble salts and control the untreated soil.

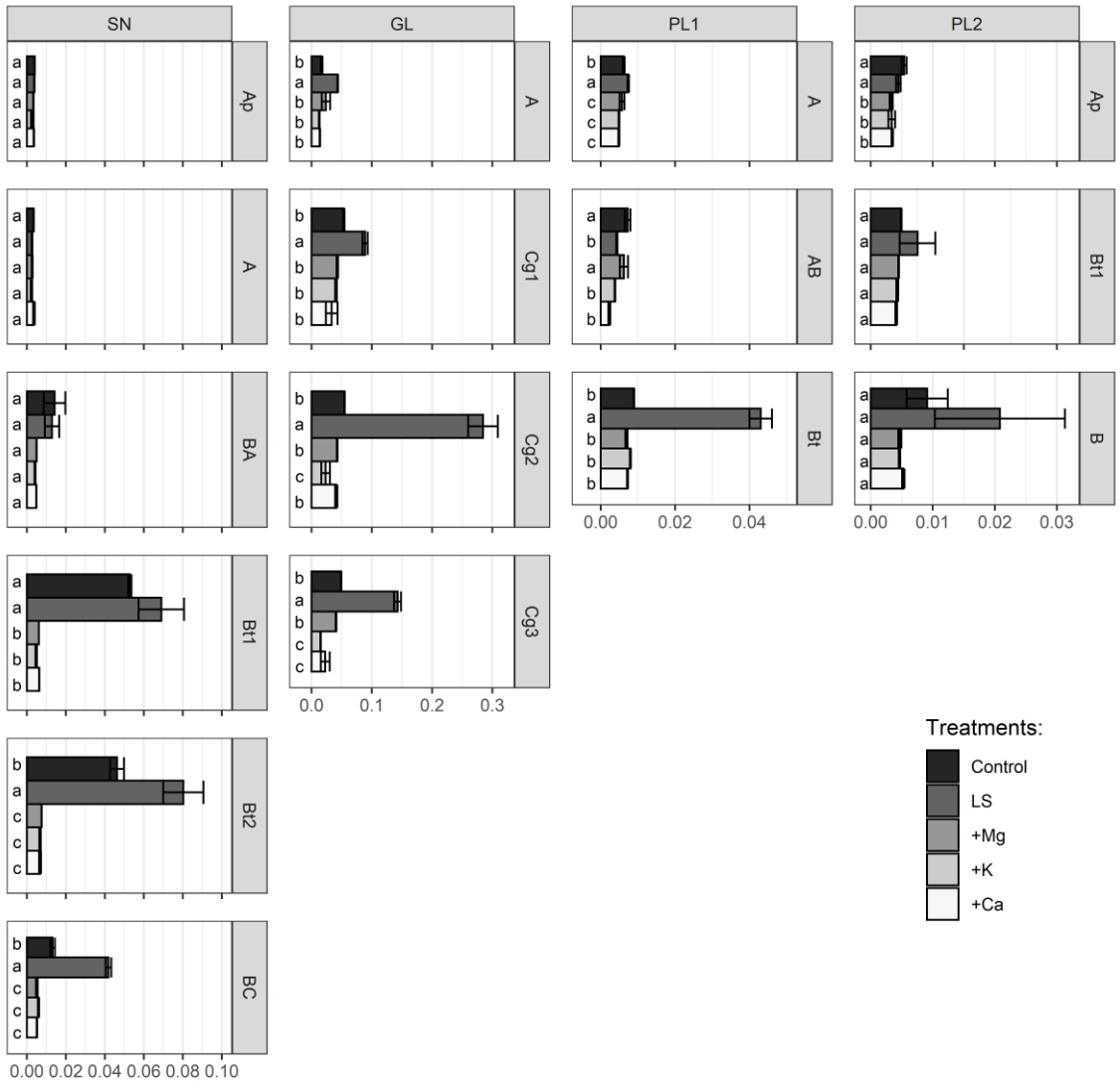

Figure 5. Strain (γ_{LVR}) at the end of linear viscoelastic range Abruptic Solonetz (Epiarenic, Differentic, Ochric, Hypernatric) – (SN), Eutric Gleysol (Abruptc, Clayic, Ochric, Protosodic) – (GL), Hypereutric Planosols (Ochric) – (PL1) and Hypereutric Planosols (Ochric, Hypermagnesic) – (PL2) saturated by capillarity in saline solution in the concentration of 0.1 mol L^{-1} of $CaCl_2$ (+Ca), KCl (+K) and $MgCl_2$ (+Mg), of the leached soil (LS) and untreated soil (control). Treatments followed by the same lowercase letter on each soil horizon (column) do not differ from each other by the Scott Knott test at 5% significance. Horizontal bars represent the standard error.

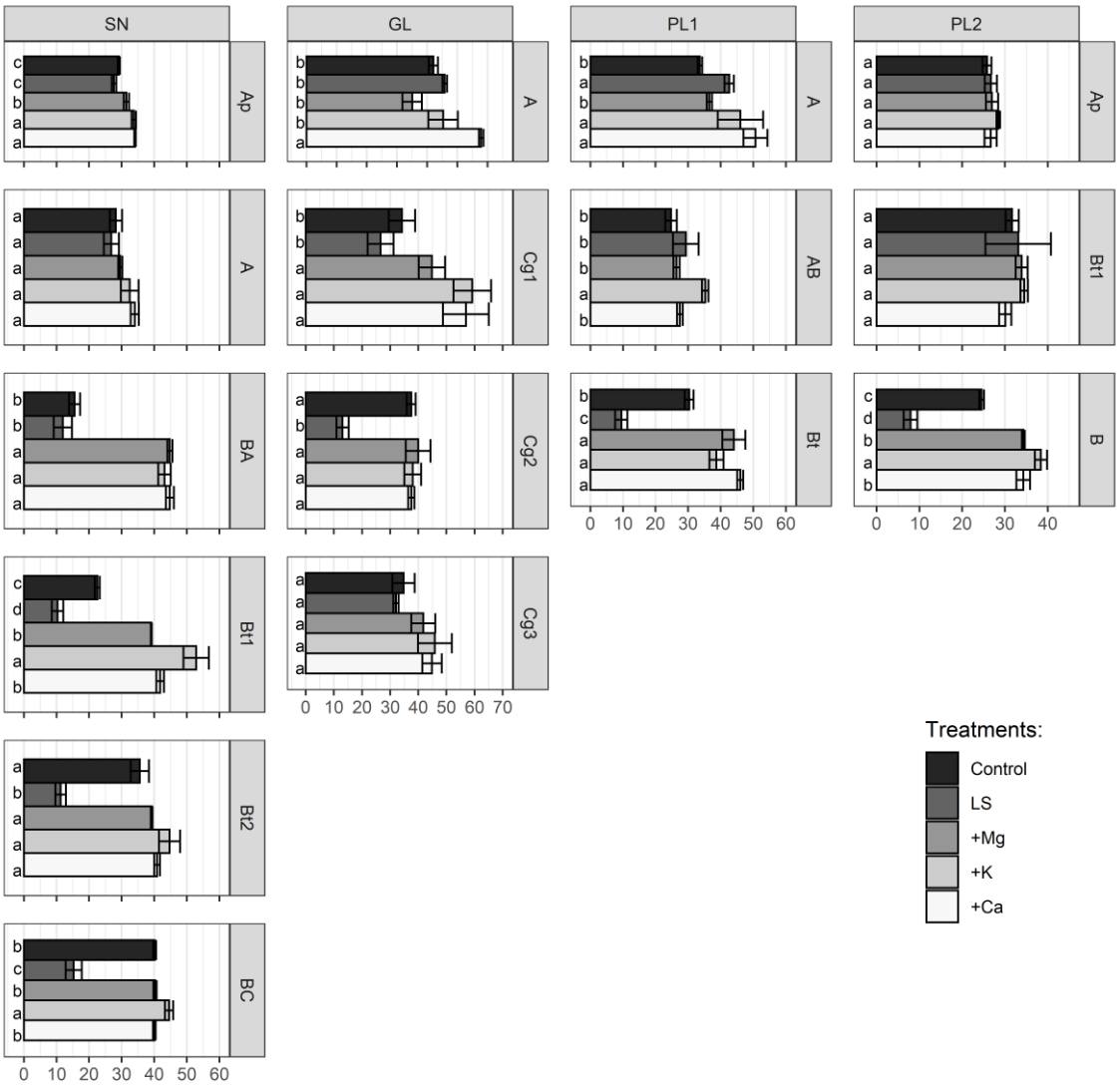

913

914 Figure 6. Strain (γ_{YP}) at the yield point of Abruptic Solonetz (Epiarenic, Differentic,
915 Ochric, Hypernatric) – (SN), Eutric Gleysol (Abruptc, Clayic, Ochric, Protosodic) –
916 (GL), Hypereutric Planosols (Ochric) – (PL1) and Hypereutric Planosols (Ochric,
917 Hypermagnesic) – (PL2) saturated by capillarity in saline solution in the concentration
918 of 0.1 mol L^{-1} of $CaCl_2$ (+Ca), KCl (+K) and $MgCl_2$ (+Mg), of the leached soil (LS) and
919 untreated soil (control). Treatments followed by the same lowercase letter on each soil
920 horizon (column) do not differ from each other by the Scott Knott test at 5%
921 significance. Horizontal bars represent the standard error.

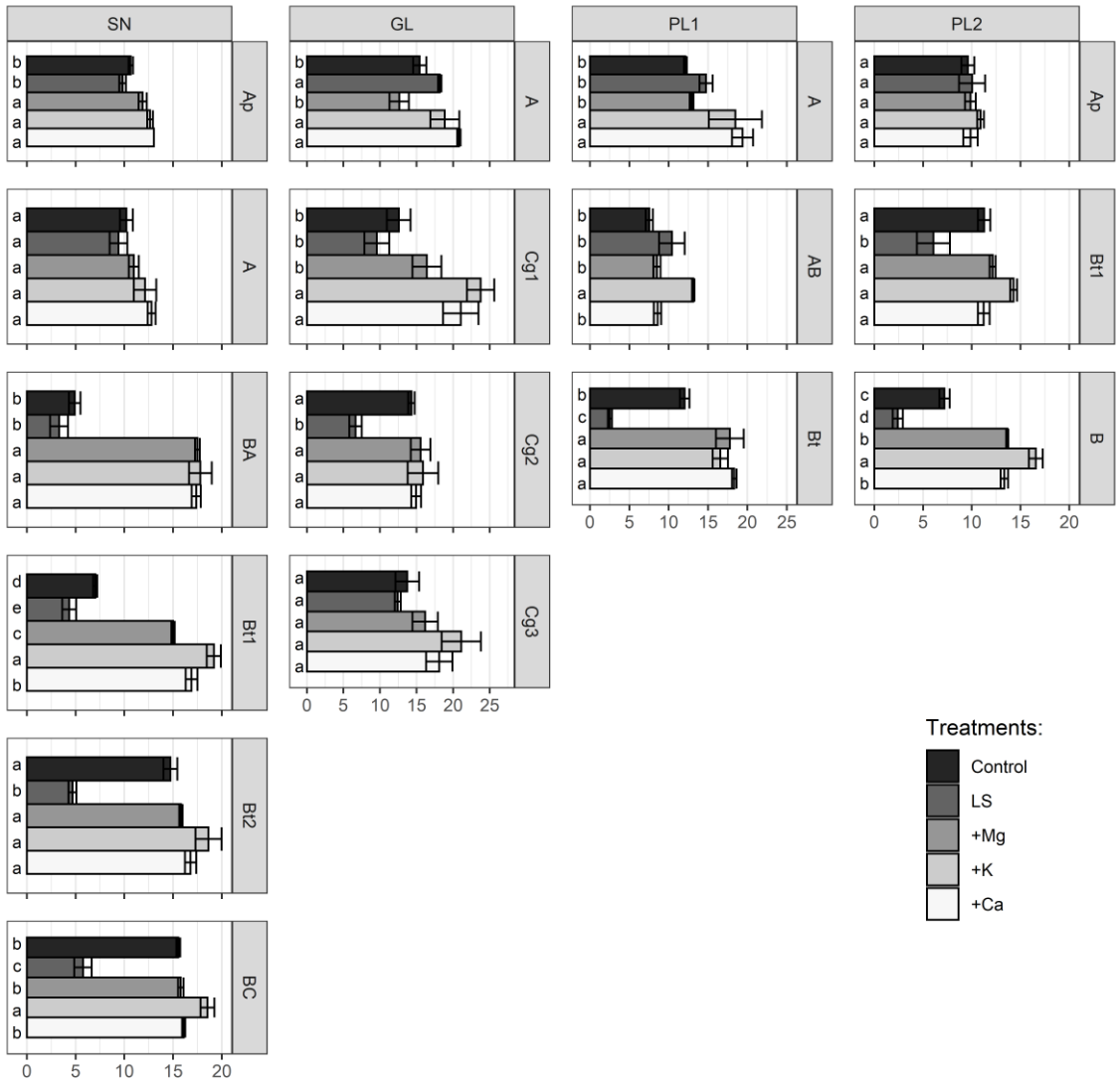

Figure 7. Integral Z (Iz) of Abruptic Solonetz (Epiarenic, Differentic, Ochric, Hypernatric) (SN), Eutric Gleysol (Abruptc, Clayic, Ochric, Protosodic) – (GL), Hypereutric Planosols (Ochric) – (PL1) and Hypereutric Planosols (Ochric, Hypermagnesic) – (PL2) saturated by capillarity in saline solution in the concentration of 0.1 mol L^{-1} of $CaCl_2$ (+Ca), KCl (+K) and $MgCl_2$ (+Mg), of the leached soil (LS) and untreated soil (control). Treatments followed by the same lowercase letter on each soil horizon (column) do not differ from each other by the Scott Knott test at 5% significance. Horizontal bars represent the standard error.

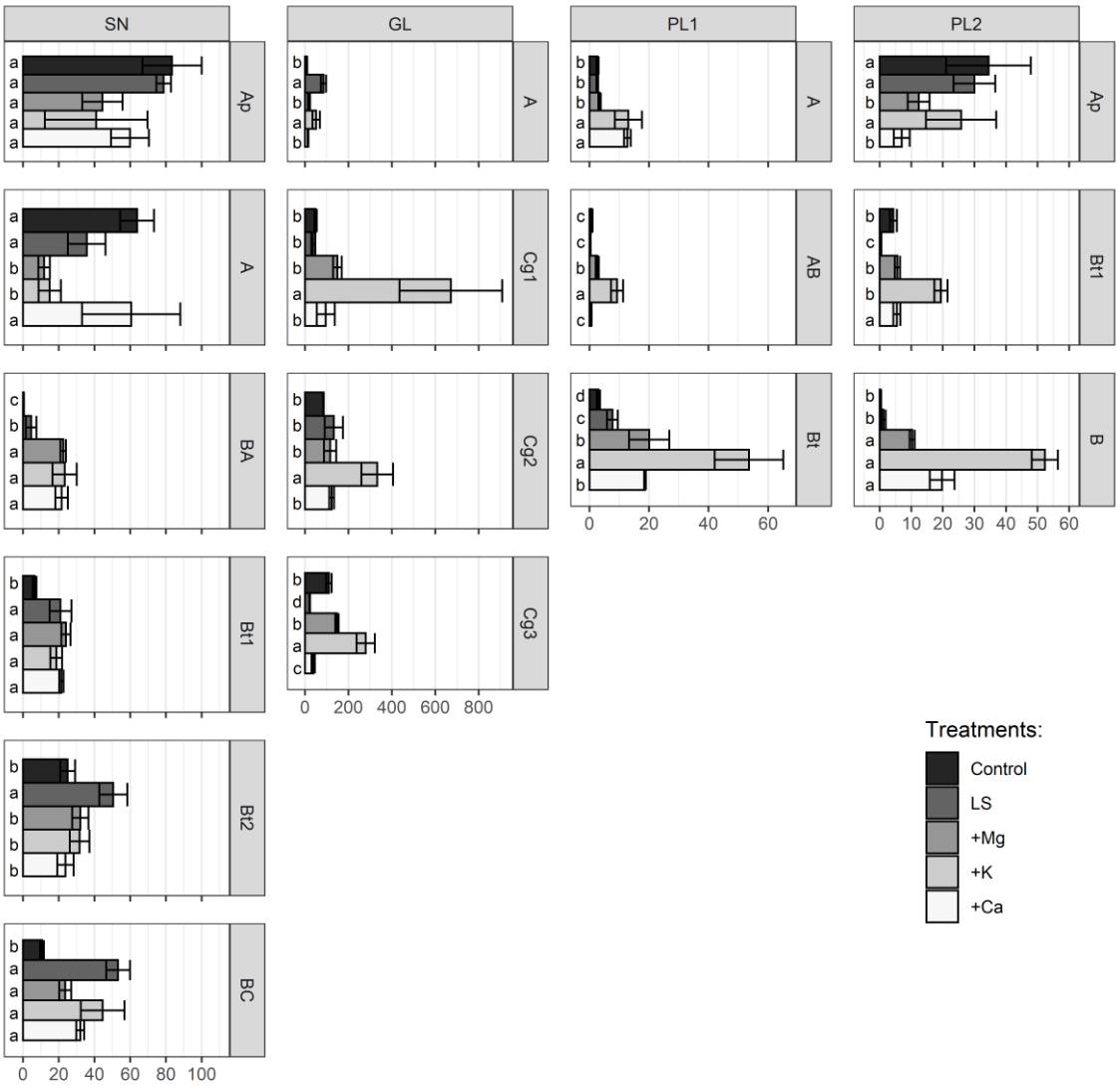

931

932 Figure 8. Stress (τ_{LVR}) at the end of linear viscoelastic range of Abruptic Solonetz
933 (Epiarenic, Differentic, Ochric, Hypernatric) – (SN), Eutric Gleysol (Abruptc, Clayic,
934 Ochric, Protosodic) – (GL), Hypereutric Planosols (Ochric) – (PL1) and Hypereutric
935 Planosols (Ochric, Hypermagnesic) – (PL2) saturated by capillarity in saline solution
936 in the concentration of 0.1 mol L^{-1} of $CaCl_2$ (+Ca), KCl (+K) and $MgCl_2$ (+Mg), of the
937 leached soil (LS) and untreated soil (control). Treatments followed by the same
938 lowercase letter on each soil horizon (column) do not differ from each other by the
939 Scott Knott test at 5% significance. Horizontal bars represent the standard error.

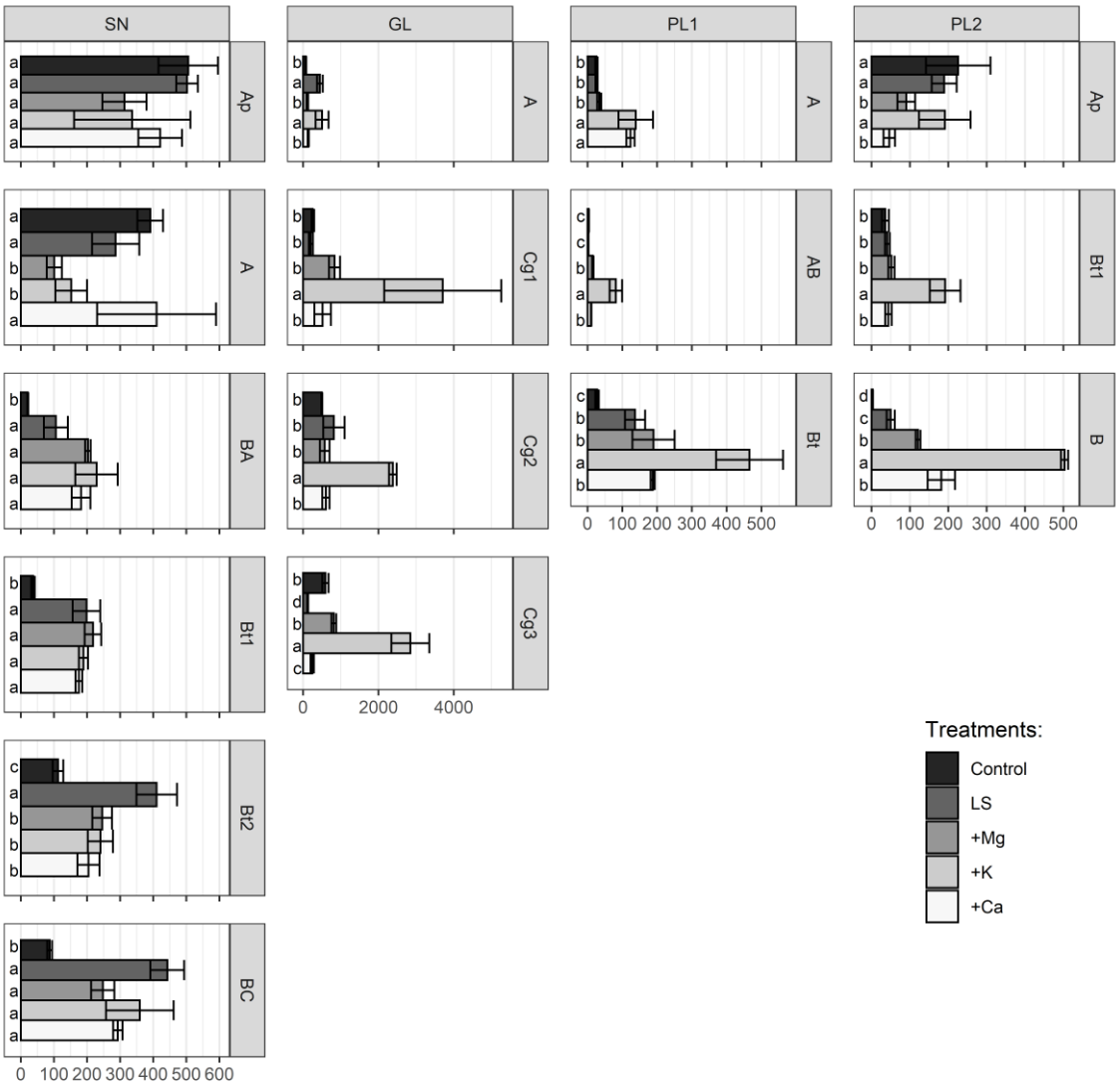

940

941 Figure 9. Maximum shear stress (τ_{max}) of Abruptic Solonetz (Epiarenic, Differentic,
942 Ochric, Hypernatric) – (SN), Eutric Gleysol (Abruptc, Clayic, Ochric, Protosodic) –
943 (GL), Hypereutric Planosols (Ochric) – (PL1) and Hypereutric Planosols (Ochric,
944 Hypermagnesic) – (PL2) saturated by capillarity in saline solution in the concentration
945 of 0.1 mol L^{-1} of $CaCl_2$ (+Ca), KCl (+K) and $MgCl_2$ (+Mg), of the leached soil (LS) and
946 untreated soil (control). Treatments followed by the same lowercase letter on each soil
947 horizon (column) do not differ from each other by the Scott Knott test at 5%
948 significance. Horizontal bars represent the standard error.

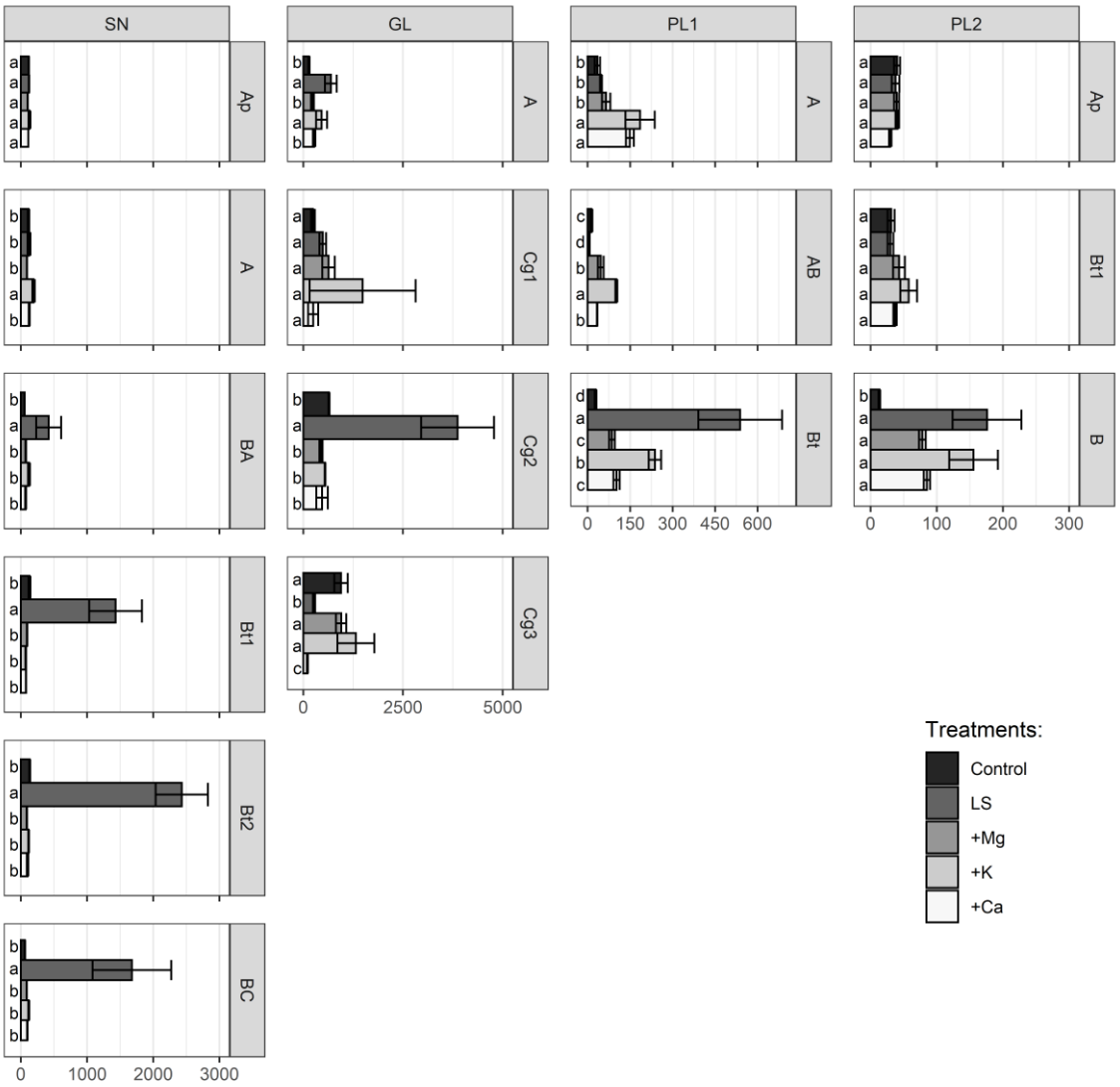

Figure 10. Storage modulus value (G'_{YP}) of Abruptic Solonetz (Epiarenic, Differentic, Ochric, Hypernatric) – (SN), Eutric Gleysol (Abruptc, Clayic, Ochric, Protosodic) – (GL), Hypereutric Planosols (Ochric) – (PL1) and Hypereutric Planosols (Ochric, Hypermagnesic) – (PL2) saturated by capillarity in saline solution in the concentration of 0.1 mol L^{-1} of $CaCl_2$ (+Ca), KCl (+K) and $MgCl_2$ (+Mg), of the leached soil (LS) and untreated soil (control). Treatments followed by the same lowercase letter on each soil horizon (column) do not differ from each other by the Scott Knott test at 5% significance. Horizontal bars represent the standard error.

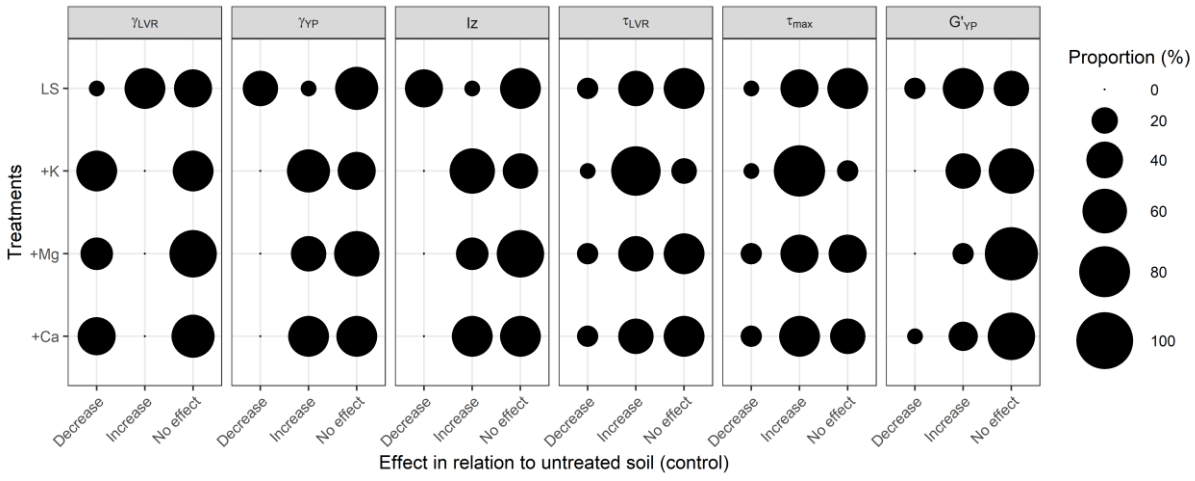

958

959 Figure 11. Contingency analysis of the effect of treatments on rheological variables.

960

961

3 DISCUSSÃO GERAL

O comportamento mecânico da microestrutura é influenciado pelas propriedades físico-químicas do solo, pela organização das partículas e pelos processos atuantes nos contatos entre as mesmas (BAUMGARTEN; HORN, 2009). Isto depende da distribuição de tamanho de partículas, do conteúdo de MO, do tipo de minerais de argila (BRONICK; LAL, 2005; SIX et al., 2004; TISDALL; OADES, 1982), do conteúdo de água (GHEZZEHEI; OR, 2001; PÉRTILE et al., 2016), do tipo e concentração de cátions (HOLTHUSEN et al., 2012a; HOLTHUSEN; PETH; HORN, 2010) e da força de compressão sobre as partículas (HOLTHUSEN et al., 2017). A atuação destes fatores, em diferentes tipos e intensidades, determina elasticidade e a resistência da microestrutural do solo.

A rigidez microestrutural pode ser definida como a capacidade da microestrutura em suportar a tensão e a flexão. Desta forma, uma microestrutura rígida, apresentará maior resistência, ou seja, maior força contrária à deformação. Ao mesmo tempo, terá mais flexibilidade, isto é, suportará maiores deformações para entrar em colapso ou cisalhar. As propriedades reológicas obtidas por teste de varredura de amplitude, de acordo com suas características e determinação, podem indicar diferentes condições na rigidez microestrutural dentro de um mesmo solo (PÉRTILE et al., 2018).

As variáveis τ_{LVE}, τ_{max} e τ_{YP} expressam, nessa ordem, a força necessária para causar deformação na microestrutura no final do intervalo viscoelástico linear, no ponto de cisalhamento máximo e no ponto de escoamento. Já o γ_L e a γ_{YP} informa a amplitude de deformação suportada pela microestrutura, para atingir o limite de deformação viscoelástico e o ponto de escoamento respectivamente. A Iz é calculada pela soma da área delimitada pela *tan* (δ), da menor deformação aplicada até o ponto de escoamento (HOLTHUSEN; PETH; HORN, 2010; MARKGRAF; HORN; PETH, 2006; PÉRTILE et al., 2018; STOPPE; HORN, 2018), sendo altamente correlacionada com o γ_{YP}.

Um processo ou fator de ligação entre partículas poder causar efeitos diversos sobre a microestrutura do solo, influenciando a resistência e a flexibilidade de diferentes formas, conduzindo a interpretações errôneas sobre a rigidez microestrutural. Os diferentes efeitos das propriedades do solo sobre a microestrutura

são mais perceptíveis quando se analisa as propriedades reológicas do solo agrupadas em propriedades que representam a elasticidade (γ_{LVR}, γ_{YP} e Iz) e a resistência (τ_{LVR}, τ_{max} e G'_{YP}).

Uma propriedade pode afetar as variáveis de elasticidade e resistência de um determinado solo de três maneiras: i) no mesmo sentido ou convergentemente (aumentar [↑↑] ou diminuir [↓↓] ambos grupos de variáveis); ii) em sentido oposto ou divergentemente (aumentar um grupo de variável e diminuir o outro [↑↓]); ou iii) afetar somente um grupo de variáveis, enquanto o outro permanece quase inafetado (↑Ø ou ↓Ø).

O carbono orgânico do solo (COS) afetou as variáveis reológicas das terras pretas arqueológicas (TPAs) no mesmo sentido. No estudo I, verificamos que a perda de COS de apenas 1 g kg^{-1} de solo (0,1%) reduziu significativamente a resistência e flexibilidade da microestrutural das TPAs. Esses resultados corroboram com os encontrados por Baumgarten et al. (2013), que verificaram que a modificação do uso da terra de floresta nativa para pastagem, proporcionou redução do conteúdo de MO, e que as alterações antrópicas induziram degradação da estrutura e rearranjo das partículas, diminuindo a estabilidade microestrutural dos solos. Também estão de acordo com os encontrados por Fedotov et al. (2014), que avaliaram a influência da MO na estrutura e nas características mecânicas de horizonte chernozêmico siltosos e verificaram que as substâncias húmicas estão cobrindo e ligando as partículas do solo, sendo o fator principal na formação da estrutura nesse tipo de solo.

O COS proporciona grande elasticidade à microestrutura. Isso porque a estrutura molecular do COS é bastante flexível, apresentando elevada capacidade de modificar sua conformação geométrica durante a deformação do solo. O COS também atua na resistência da microestrutura por causa da elevada superfície específica e grande quantidade de radicais orgânicos. Estes radicais interagem com a superfície de partículas minerais por pontes de cátions, ligações eletrostáticas e de coordenação, pontes de hidrogênio e forças de van der Waals (KLEBER; SOLLINS; SUTTON, 2007), formando ligações bastante estáveis e contribuindo para a microagregação do solo (TISDALL; OADES, 1982). Ainda influencia no processo de agregação pela aproximação das partículas do solo favorecida pela atividade microbiana, e pelo efeito cimentante sobre componentes minerais (SIX et al., 2004).

Contudo, no estudo II foi verificada correlação negativa entre teor de COS a resistência no início do teste em amostras não saturadas, indicando que o efeito do COS sobre as variáveis reológicas também dependem da distribuição do tamanho de partícula do solo. Em solos argilosos (maior ASE), o COS influencia a elasticidade e resistência da microestrutura no mesmo sentido, como relatado anteriormente. Em solos arenosos (menor ASE), a redução do teor de COS pode aumentar a resistência e diminuir a elasticidade da microestrutura. Isso porque o carbono orgânico particulado atua como lubrificante, diminuindo o atrito entre as partículas grandes (VALLEJO; MAWBY, 2000). Além disso, devido à grande capacidade de retenção de água, o COS aumenta as forças de meniscos em solos arenosos onde as forças capilares são reduzidas (BACHMANN; ZHANG, 1991), aumentando a resistência da microestrutura em potenciais matriciais mais negativos.

O aumento da ASE está relacionado com elasticidade da microestrutura. Independente do teor de COS do solo, o aumento da ASE provocou aumento da γ_{LVR}, γ_{YP} e da integral Z. Em solos com elevada ASE, há grande proporção de partículas na fração argila. Essas partículas apresentam formato laminar (VEPRASKAS; CASSELL, 1987), o que facilita o movimento de cisalhamento (CHO; DODDS; SANTAMARINA, 2006), proporcionando maior elasticidade à microestrutura.

Entretanto, a ação cimentante dos óxidos de Fe e de outros compostos inorgânicos em solos com elevada ASE favorece a formação de microagregados muito estáveis. Esses microagregados exibem comportamento semelhante ao das partículas de areia (pseudoareias) e de silte (pseudossilte), diminuindo a elasticidade da microestrutura do solo. Em solos com baixa ASE ou com presença de pseudoareias, o contato entre as partículas grandes é bastante frágil devido à baixa quantidade de agentes de ligação, como a argila e COS. Assim uma pequena deformação pode causar separação das partículas.

Não foi observado relação entre ASE e a resistência da microestrutura avaliada pelas variáveis reológicas τ_{LVR}, τ_{max} e G'_{YP} no estudo II, indicando que a ASE exerce grande influência sobre a elasticidade e pequena ou quase nenhuma influência sobre a resistência da microestrutura. Isso porque, a resistência da microestrutura também apresenta relação com fatores externos ao solo, como a força normal incidente sobre a amostra no início do teste de varredura de amplitude (HOLTHUSEN et al., 2017, 2019). Porém, ao analisar o efeito da distribuição do tamanho de partículas sobre as

variáveis reológicas das TPAs no estudo I, verificou-se que a maior proporção entre silte e argila (silte/argila) apresentou relação com resistência da microestrutura ao cisalhamento.

Em relação às diferenças na distribuição do tamanho de partículas, Markgraf e Horn (2006) concluíram que solos arenosos e siltosos apresentam comportamento mecânico semelhante. Contudo, maior resistência estrutural inicial é encontrada em solos da classe areia franca em relação a solo franco-siltoso. Entretanto, a elasticidade avaliada pelo γ_{YP} dos solso franco-siltosos foi maiores do que os franco-arenosos. Solos constituído predominantemente por areia e silte, exibem maior área de contato real entre as partículas (REICHERT et al., 2010), o que aumenta o atrito e restringe o movimento entre elas. Assim, para cisalhar, as partículas precisam rolar uma sobre as outras (CHO; DODDS; SANTAMARINA, 2006), exigindo grande tensão de cisalhamento.

Um processo ou fator de ligação entre as partículas do solo, além de causar efeitos divergentes na resistência e na elasticidade da microestrutura, também influencia as variáveis dentro do mesmo grupo (elasticidade ou resistência) em sentidos opostos. Isso foi verificado o estudo III, no qual a lixiviação dos sais solúveis aumentou a elasticidade no final do intervalo viscoelástico linear (γ_{LVR}), ou seja, em baixa intensidade de deformação, e reduziu a elasticidade no ponto de escoamento (γ_{YP}), isto é, em altas intensidade de deformação. Por outro lado, a saturação com solução salina, independentemente do tipo de cátion, provocou efeito contrário, diminuindo a γ_{LVR} e aumentando a γ_{YP}. Ainda, tanto a lixiviação dos sais, como a saturação com solução salina tenderam a aumentar a resistência da microestrutura.

Quanto à concentração e ao tipo de cátion na solução do solo, verificou-se a estabilização da microestrutura pelo Ca^{+2} no estudo III, pelo aumento da elasticidade anterior ao escoamento (γ_{YP} e Iz) e da resistência da microestrutura avaliada pela τ_{max}. Também ocorreu aumento resistência microestrutural com o aumento da relação Ca/Mg nos estudos I e II. Baumgarten et al. (2012) estudando o comportamento reológico de solos salinos e calcários ocorrentes no norte da Alemanha também observaram aumento da agregação e da resistência da estrutura com o aumento do teor de Ca^{2+}. O efeito estabilizador do Ca^{+2} na floculação de partículas e na estrutura também foi evidenciado por Chorom e Rengasamy (1995), Holthusen et al. (2012), Lee et al. (2012) Paradelo et al. (2013).

Esta estabilização provocada pelo Ca^{+2} pode ocorrer pela formação de complexos organometálicos, atuando como pontes policatiônicas entre moléculas orgânicas, melhorando a estabilidade de microagregados (BRONICK; LAL, 2005; TISDALL; OADES, 1982). Também, pode ter atuado na redução da dupla camada difusa, diminuindo as forças repulsivas de partículas com cargas elétricas semelhantes (HILLEL, 2004; MAHANTA; MISHRA; KANSAL, 2012), aumentando as associações estáveis entre as partículas (BRANDENBURG; LAGALY, 1988).

Em alguns horizontes dos solos salinos, a saturação com Mg^{+2} aumentou elasticidade e a resistência da microestrutura. Em solos com elevados teores de sais solúveis como os estudados no estudo III, ocorre a dispersão das partículas principalmente pela presença de Na^{+}. O aumento da concentração de íons bivalentes, como o Mg^{+2}, pode aumentar a floculação das partículas pela redução da espessura da dupla camada difusa (FONTES; CAMARGO; SPOSITO, 2001; SPOSITO, 2008) e pela formação de pontes catiônicas com moléculas orgânicas e argilominerais com cargas elétricas negativas (BRONICK; LAL, 2005), principalmente em solos com presença de minerais 2:1.

Contudo, a maior proporção de Mg^{+2} em detrimento à Ca^{+2} se relacionou negativamente com γ_{YP} e Iz nas TPAs analisadas no estudo I, indicando a desestabilização da microestrutura. Comparado ao Ca, o Mg tem menor eletronegatividade e menor preferência de adsorção eletrostática (SPOSITO, 2008), Consequentemente, menor será sua interação com os grupos funcionais de superfície dos coloides inorgânicos e orgânicos, dispersando às partículas e causando ruptura dos microagregados.

Resultados divergentes também foram observados para o K^{+}. A maior proporção de K^{+} em relação ao Ca e/ou Mg teve correlação negativa com γ_{YP} e Iz, indicando uma desestabilização da microestrutura das TPAs no estudo I. Já para alguns solos salinizados, observou-se maior elasticidade e resistência em solos saturados K^{+}. Holthusen et al. (2012) estudando o efeito da adubação potássica, estresse salino e hídrico sobre o comportamento reológico do solo em experimentos de longa duração, verificaram o efeito dispersivo do sódio, diminuindo a rigidez da microestrutura do solo. Entretanto, observaram que, com a adubação potássica, ocorre o fortalecimento da estrutura. Ainda, Holthusen et al. (2010), estudando o impacto da poro pressão e da força iônica sobre os parâmetros reológicos, concluíram

que o aumento da concentração de K^+ na solução, provoca incremento da resistência da microestrutural dos solos.

Os efeitos divergentes do K^+ sobre a microestrutura podem estar relacionados à composição mineralógica da fração argila destes solos. Em solos compostos predominantemente por caulinita, hematita e goethita , como as TPAs (AQUINO et al., 2016; LIMA et al., 2002; SANTOS et al., 2018; SILVA et al., 2011), há grande quantidade de cargas elétricas positivas na condição de pH natural (AZEVEDO; BONUMÁ, 2004; CHOROVER; SPOSITO, 1995). Assim, o K^+ atuaria na dispersão das partículas por aumentar a espessura da dupla camada difusa e pela incapacidade de formar pontes catiônicas entre partículas com mesma carga elétrica. Por outro lado, os solos salinos da região nordeste apresentam predominância de caulinita e argilominerais 2:1 do grupo das smectitas, ilitas e montmorilonitas, (PFALTZGRAFF; TORRES, 2010), com grande quantidade de cargas elétricas negativas permanentes (KÄMPF; MARQUES; CURI, 2012), Nestes solos, além de reduzir a dupla camada elétrica, o K^+ pode ser adsorvido especificamente na cavidade siloxana, reduzindo o potencial elétrico de superfície e diminuindo a expansividade do mineral (SPARKS, 2003; SPOSITO, 2008), proporcionando maior estabilidade ao solo.

O efeito da concentração e do tipo de cátions é dependente da ASE, uma vez que os efeitos da remediação sobre a microestrutura dos solos salinizados no estudo III foi maior nos horizontes subsuperficiais, onde há incremento do teor de argila, e consequentemente maior ASE.

Em solos com predomínio de partículas de maior diâmetro (baixa ASE), a atuação das forças elétricas no contato entre partículas é pequena, o contato entre as partículas maiores dependeria somente da força gravitacional devido ao peso das partículas. Essa força dificilmente é alterada pela mudança da concentração eletrolítica da solução do solo (SANTAMARINA, 2003). A medida que ocorre aumento na ASE, o diâmetro das partículas diminui e a importância do peso é reduzida, e a influência das forças elétricas no contato entre as partículas aumenta (SANTAMARINA et al., 2002) bem como dos fenômenos de adsorção de íons que modificam o campo elétrico na superfície dos coloides do solo (Essington, 2004; Sposito, 2008).

4 CONCLUSÕES

Um processo ou fator de união de partículas pode afetar as propriedades reológicas de três formas básicas: *i*) convergentemente, aumentando ou diminuindo a elasticidade e a resistência da microestrutura; *ii*) divergentemente: aumentando a elasticidade e diminuindo a resistência, ou vice-versa e *iii*) aumentando ou diminuindo a elasticidade, enquanto a resistência é pouco afeta, ou

A resistência e a elasticidade da microestrutura de Terras Pretas Arqueológicas são bastante dependentes do teor de carbono orgânico do solo (COS). A redução do teor de COS pela oxidação com peróxido de hidrogênio afetou as propriedades reológicas das TPAs no mesmo sentido, diminuindo a resistência e a elasticidade da microestrutura. O efeito da redução do COS sobre a microestrutura depende da quantidade e da qualidade do COS.

O aumento da área superficial específica (ASE) aumenta a elasticidade da microestrutura. Entretanto, a formação de microagregados muito estáveis (pseudoareias) em solos com elevada ASE e alto teor de óxidos de Fe diminuem a elasticidade do solo. A rigidez na microestrutura não apresentou correlação com a ASE, mas foi dependente da distribuição do tamanho de partículas, da força normal atuante sobre a superfície da amostra e da concentração de cátions.

A resistência e a elasticidade da microestrutura de solos aluviais salinos apresentaram grande variação entre os tipos de solos e em profundidade no perfil, devido principalmente a diferenças no teor de sais solúveis e na distribuição do tamanho de partículas. A saturação com solução salina aumentou a elasticidade e a resistência microestrutural, enquanto a lixiviação dos sais solúveis desestabilizou a microestrutura, adiantando o comportamento de fluxo do solo. A saturação com potássio proporcionou maior elasticidade e resistência à microestrutura quando comparado ao cálcio e magnésio. Além disso os efeitos do tipo de cátions sobre a microestrutura aumentaram em profundidade devido ao maior teor de argila em solos com gradiente textural.

5 REFERÊNCIAS BIBLIOGRÁFICAS

ABIVEN, S.; MENASSERI, S.; CHENU, C. The effects of organic inputs over time on soil aggregate stability – A literature analysis. **Soil Biology and Biochemistry**, v. 41, n. 1, p. 1–12, jan. 2009.

ANDERSON, S. J.; SPOSITO, G. Proton surface-charge density in soils with structural and ph-dependent charge. **Soil Science Society of America Journal**, v. 56, n. 5, p. 1437, 1992.

AQUINO, R. E. DE et al. Characteristics of color and iron oxides of clay fraction in Archeological Dark Earth in Apuí region, southern Amazonas. **Geoderma**, v. 262, p. 35–44, jan. 2016.

AZEVEDO, A. C. DE; BONUMÁ, A. S. Partículas coloidais, dispersão e agregação em Latossolos. **Ciência Rural**, v. 34, n. 2, p. 609–617, abr. 2004.

BALESDENT, J.; CHENU, C.; BALABANE, M. Relationship of soil organic matter dynamics to physical protection and tillage. **Soil and Tillage Research**, v. 53, n. 3–4, p. 215–230, fev. 2000.

BARNES, H. A. **A Handbook of Elementary Rheology**. Aberystwyth: University of Wales Institute of Non-Newtonian Fluid, 2000. v. 331

BASTOS, R. S. et al. Soil aggregate formation and stabilization as influenced by wetting drying cycles and organic compounds with different hydrophobic characteristics. **Revista Brasileira de Ciência do Solo**, v. 29, n. 1, p. 21–31, 2005.

BAUMGARTEN, W. et al. Structural stability of Marshland soils of the riparian zone of the Tidal Elbe River. **Soil and Tillage Research**, v. 125, p. 80–88, set. 2012.

BAUMGARTEN, W.; DÖRNER, J.; HORN, R. Microstructural development in volcanic ash soils from South Chile. **Soil and Tillage Research**, v. 129, p. 48–60, 2013.

BAUMGARTEN, W.; HORN, R. Rheological Investigations in Soil Micro Mechanics: Measuring Stiffness Degradation and Structural Stability on a Particle Scale. In: GRAGG, L. P.; CASSELL, J. M. (Eds.). . **Progress in management engineering**. New York: Nova Science Publishers, 2009. p. 237–279.

BRADY, N. C.; WEIL, R. R. **Elements of Nature and Soil Properties**. 3. ed. Porto Alegre: Bookman, 2013.

BRAIDA, J. et al. **Organic matter and its effect on soil physics**. [s.l: s.n.].

BRANDENBURG, U.; LAGALY, G. Rheological properties of sodium montmorillonite dispersions. **Applied Clay Science**, v. 3, n. 3, p. 263–279, ago. 1988.

BRONICK, C. J.; LAL, R. Soil structure and management: a review. **Geoderma**, v. 124, n. 1–2, p. 3–22, jan. 2005.

CASTRO, C.; LOGAN, T. J. Liming Effects on the Stability and Erodibility of Some Brazilian Oxisols. **Soil Science Society of America Journal**, v. 55, n. 5, p. 1407, 1991.

CHO, G.-C.; DODDS, J.; SANTAMARINA, J. C. Particle shape effects on packing density, stiffness, and strength: natural and crushed sands. **Journal of Geotechnical and Geoenvironmental Engineering**, v. 132, n. 5, p. 591–602, maio 2006.

CHOROM, M.; RENGASAMY, P. Dispersion and zeta potential of pure clays as related to net particle charge under varying pH, electrolyte concentration and cation type. **European Journal of Soil Science**, v. 46, n. 4, p. 657–665, dez. 1995.

CHOROVER, J.; SPOSITO, G. Surface charge characteristics of kaolinitic tropical soils. **Geochimica et Cosmochimica Acta**, v. 59, n. 5, p. 875–884, mar. 1995.

DEXTER, A. R. Advances in characterization of soil structure. **Soil and Tillage Research**, v. 11, n. 3, p. 199–238, 1988.

DIAS, N. DA S.; BLANCO, F. F. Efeitos dos sais no solo e na planta. In: GUEYE, H. R.; DIAS, N. DA S.; LACEDERDA, C. F. (Eds.). . **Manejo da salinidade na agricultura estudos básicos e aplicados.** Fortaleza: INCTSal, 2010.

DIMOYIANNIS, D. G.; TSADILAS, C. D.; VALMIS, S. Factors affecting aggregate instability of Greek agricultural soils. **Communications in Soil Science and Plant Analysis**, v. 29, n. 9–10, p. 1239–1251, maio 1998.

EDWARDS, A. P.; BREMNER, J. M. MICROAGGREGATES IN SOILS1. **Journal of Soil Science**, v. 18, n. 1, p. 64–73, mar. 1967.

FEDOTOV, G. N.; SHOBA, S. A.; KHAYDAPOVA, D. D. The mechanism of influence of the organic matter on the soil structure and mechanical properties. **Doklady Biological Sciences**, v. 456, n. 1, p. 177–181, maio 2014.

FONTES, M. P. F.; CAMARGO, O. A. DE; SPOSITO, G. Eletroquímica das partículas coloidais e sua relação com a mineralogia de solos altamente intemperizados. **Scientia Agricola**, v. 58, n. 3, p. 627–646, set. 2001.

FRAZÃO, L. A. et al. Estoques de carbono e nitrogênio e fração leve da matéria orgânica em Neossolo Quartzarênico sob uso agrícola. **Pesquisa Agropecuária Brasileira**, v. 45, n. 10, p. 1198–1204, out. 2010.

GHEZZEHEI, T. A; OR, D. Dynamics of soil aggregate coalescence and theological processes. **Water Resources Research**, v. 36, n. 2, p. 367–379, 2000.

GHEZZEHEI, T. A.; OR, D. Rheological properties of wet soils and clays under steady and oscillatory stresses. **Soil Science Society of America Journal**, v. 65, n. 3, p. 624–624, 2001.

HILLEL, D. **Introdution to environmental soil physics**. San Diego: Academic Press, 2004.

HOLTHUSEN, D. et al. Physical properties of a Luvisol for different long-term fertilization treatments: II. Microscale behavior and its relation to the mesoscale. **Journal of Plant Nutrition and Soil Science**, v. 175, n. 1, p. 14–23, fev. 2012a.

HOLTHUSEN, D. et al. Physical properties of a Luvisol for different long-term fertilization treatments: I. Mesoscale capacity and intensity parameters. **Journal of Plant Nutrition and Soil Science**, v. 175, n. 1, p. 4–13, fev. 2012b.

HOLTHUSEN, D. et al. Flow and deformation behavior at the microscale of soils from several long-term potassium fertilization trials in Germany. **Journal of Plant Nutrition and Soil Science**, v. 175, n. 4, p. 535–547, ago. 2012c.

HOLTHUSEN, D. et al. Controlled vertical stress in a modified amplitude sweep test (rheometry) for the determination of soil microstructure stability under transient stresses. **Geoderma**, v. 295, p. 129–141, jun. 2017.

HOLTHUSEN, D. et al. Viscoelasticity and shear resistance at the microscale of naturally structured and homogenized subtropical soils under undefined and defined normal stress conditions. **Soil and Tillage Research**, v. 191, p. 282–293, ago. 2019.

HOLTHUSEN, D.; PETH, S.; HORN, R. Impact of potassium concentration and matric potential on soil stability derived from rheological parameters. **Soil and Tillage Research**, v. 111, n. 1, p. 75–85, dez. 2010.

HOLTHUSEN, D.; REEB, D.; HORN, R. Influence of potassium fertilization, water and salt stress, and their interference on rheological soil parameters in planted containers. **Soil and Tillage Research**, v. 125, p. 72–79, set. 2012.

JOHNSTON, C. T.; TOMBACZ, E. Surface Chemistry of Soil Minerals. In: DIXON, J. B.; SCHULZE, D. G. (Eds.). . **SSSA Book Series**. [s.l.] Soil Science Society of America, 2002. p. 37–65.

KÄMPF, N.; MARQUES, J. J.; CURI, N. Mineralogia de solos brasileiros. In: KER, J. C. et al. (Eds.). . **Pedologia: Fundamentos**. 1. ed. Viçosa: Sociedade Brasileira de Ciência do Solo, 2012.

KÄMPF, N.; SCHWERTMANN, U. Avaliação da estimativa de substituição de Fe por Al em hematitas de solos. **Revista Brasileira de Ciência do Solo**, v. 22, p. 209–213, 1998.

KLEBER, M.; SOLLINS, P.; SUTTON, R. A conceptual model of organo-mineral interactions in soils: self-assembly of organic molecular fragments into zonal structures on mineral surfaces. **Biogeochemistry**, v. 85, n. 1, p. 9–24, 4 jul. 2007.

LAGALY, G. Principles of flow of kaolin and bentonite dispersions. **Applied Clay Science**, v. 4, n. 2, p. 105–123, jun. 1989.

LEE, B. J. et al. Competition between kaolinite flocculation and stabilization in divalent cation solutions dosed with anionic polyacrylamides. **Water Research**, v. 46, n. 17, p. 5696–5706, nov. 2012.

LEPSCH, I. F.; SILVA, N. M. DA; ESPIRONELO, A. Relação entre matéria orgânica e textura de solos sob cultivo de algodão e cana-de-açúcar, no estado de São Paulo. **Bragantia**, v. 41, n. 1, p. 231–236, 1982.

LIMA, H. N. et al. Pedogenesis and pre-Colombian land use of “Terra Preta Anthrosols” (“Indian black earth”) of Western Amazonia. **Geoderma**, v. 110, n. 1–2, p. 1–17, nov. 2002.

MAHANTA, K. K.; MISHRA, G. C.; KANSAL, M. L. Estimation of electric double layer thickness from linearized and nonlinear solutions of Poisson–Boltzman equation for single type of ions. **Applied Clay Science**, v. 59–60, p. 1–7, maio 2012.

MARKGRAF, W. et al. Influence of organic matter on rheological properties of soil. **Applied Clay Science**, v. 64, p. 25–33, ago. 2012.

MARKGRAF, W.; HORN, R. Rheological-stiffness analysis of K+-treated and CaCO3-rich soils. **Journal of Plant Nutrition and Soil Science**, v. 169, n. 3, p. 411–419, jun. 2006.

MARKGRAF, W.; HORN, R.; PETH, S. An approach to rheometry in soil mechanics—Structural changes in bentonite, clayey and silty soils. **Soil and Tillage Research**, v. 91, n. 1–2, p. 1–14, dez. 2006.

MEZGER, T. G. **The Rheology Handbook**. 4. ed. Hanover: Vincentz Network, 2014.

OADES, J. M. Soil organic matter and structural stability: mechanisms and implications for management. **Plant and Soil**, v. 76, p. 319–337, 1984.

OADES, J.; WATERS, A. Aggregate hierarchy in soils. **Australian Journal of Soil Research**, v. 29, n. 6, p. 815, 1991.

PARADELO, R.; VAN OORT, F.; CHENU, C. Water-dispersible clay in bare fallow soils after 80years of continuous fertilizer addition. **Geoderma**, v. 200–201, p. 40–44, jun. 2013.

PÉRTILE, P. et al. Rheological parameters as affected by water tension in subtropical soils. **Revista Brasileira de Ciência do Solo**, v. 40, n. September, p. 1–14, 2016.

PÉRTILE, P. et al. Microstructural strength of four subtropical soils evaluated by rheometry: properties, difficulties and opportunities. **Scientia Agricola**, v. 75, n. 2, p. 154–162, abr. 2018.

PFALTZGRAFF, P. A. DOS S.; TORRES, F. S. DE M. **Geodiversidade do estado do Rio Grande do Norte**. Recife: Serviço Geológico do Brasil, 2010.

PICCOLO, A.; PIETRAMELLARA, G.; MBAGWU, J. S. C. Use of humic substances as soil conditioners to increase aggregate stability. **Geoderma**, v. 75, n. 3–4, p. 267–277, fev. 1997.

REICHERT, J. M. et al. Mecânica do solo. In: VAN LIER, Q. DE J. (Ed.). . **Física do solo**. [s.l.] Sociedade Brasileira de Ciência do solo, 2010. p. 298.

ROSSI, C. Q. et al. Frações orgânicas e índice de manejo de carbono do solo em Latossolo Vermelho sob plantio de soja no cerrado goiano. **Revista Brasileira de Ciências Agrárias**, v. 7, n. 2, p. 233–241, 20 jul. 2012.

SANTAMARINA, J. C. et al. Specific surface: determination and relevance. **Canadian Geotechnical Journal**, v. 39, n. 1, p. 233–241, fev. 2002.

SANTAMARINA, J. C. **Soil behavior at the microscale: particle forces**. Soil Behavior and Soft Ground Construction. **Anais**... In: SYMPOSIUM ON SOIL BEHAVIOR AND SOFT GROUND CONSTRUCTION HONORING CHARLES C. "CHUCK" LADD. Cambridge, Massachusetts, United States: American Society of Civil Engineers, 13 jan. 2003Disponível em: <http://ascelibrary.org/doi/abs/10.1061/40659%282003%292>. Acesso em: 20 ago. 2018

SANTOS, L. A. C. DOS et al. Pedogenesis in an archaeological Dark Earth – Mulatto Earth Catena over Volcanic Rocks in Western Amazonia, Brazil. **Revista Brasileira de Ciência do Solo**, v. 42, p. 1–18, 2018.

SCHRAMM, G. **Rheology and Rheometry: theoretical and practical fundamentals**. [s.l.] Artliber, 2006.

SCHULTEN, H.-R.; LEINWEBER, P. Dithionite-Citrate-Bicarbonate-Extractable Organic Matter in Particle-Size Fractions of a Haplaquoll. **Soil Science Society of America Journal**, v. 59, n. 4, p. 1019, 1995.

SILVA, F. W. R. et al. Chemical and mineralogical characterization of anthropic soils (Amazonian Dark Earths) in the central Amazon. **Revista Brasileira de Ciência do Solo**, v. 35, n. 3, p. 673–681, jun. 2011.

SIX, J. et al. A history of research on the link between (micro)aggregates, soil biota, and soil organic matter dynamics. **Soil and Tillage Research**, v. 79, n. 1, p. 7–31, set. 2004.

SIX, J.; ELLIOTT, E. T.; PAUSTIAN, K. Soil macroaggregate turnover and microaggregate formation: a mechanism for C sequestration under no-tillage agriculture. **Soil Biology and Biochemistry**, v. 32, n. 14, p. 2099–2103, dez. 2000.

SOLLINS, P.; HOMANN, P.; CALDWELL, B. A. Stabilization and destabilization of soil organic matter: mechanisms and controls. **Geoderma**, v. 74, n. 1–2, p. 65–105, nov. 1996.

SPARKS, D. L. **Environmental soil chemistry**. 2. ed. California: Academic Press, 2003.

SPOSITO, G. **The chemistry of soils**. 2. ed. NewYork: Oxford University Press, 2008.

STOPPE, N.; HORN, R. Microstructural strength of tidal soils – a rheometric approach to develop pedotransfer functions. **Journal of Hydrology and Hydromechanics**, v. 66, n. 1, p. 87–96, mar. 2018.

TAVARES FILHO, J. **Física e conservação do solo e da água**. Londrina: EDUEL, 2013.

TISDALL, J. M.; OADES, J. M. Organic matter and water-stable aggregates in soils. **Journal of Soil Science**, v. 33, n. 2, p. 141–163, jun. 1982.

VALLEJO, L. E.; MAWBY, R. Porosity influence on the shear strength of granular material–clay mixtures. **Engineering Geology**, v. 58, n. 2, p. 125–136, nov. 2000.

VEPRASKAS, M. J.; CASSELL, D. K. Sphericity and roundness of sand in Coastal Plain soils and elationships with soil physical properties. **Soil Science Society of America Journal**, v. 51, p. 1108–1112, 1987.

VEZZANI, F. M.; MIELNICZUK, J. Soil aggregation and carbon stock of a paleudult under different agricultural managaments. **Revista Brasileira de Ciência do Solo**, v. 35, n. 1, p. 213–223, fev. 2011.

VRDOLJAK, G.; SPOSITO, G. Soil aggregate hierarchy in a Brazilian oxisol. In: **Developments in Soil Science**. [s.l.] Elsevier, 2002. v. 28p. 197–217.

ZHANG, X. C.; NORTON, L. D. Effect of exchangeable Mg on saturated hydraulic conductivity, disaggregation and clay dispersion of disturbed soils. **Journal of Hydrology**, v. 260, n. 1–4, p. 194–205, mar. 2002.